

Bangor University

DOCTOR OF PHILOSOPHY

Microwave I.F Signal Processing Strategies For Coherent Optical Communications

Choudhry, Mohammed

Award date:
2019

Awarding institution:
Bangor University

[Link to publication](#)

General rights

Copyright and moral rights for the publications made accessible in the public portal are retained by the authors and/or other copyright owners and it is a condition of accessing publications that users recognise and abide by the legal requirements associated with these rights.

- Users may download and print one copy of any publication from the public portal for the purpose of private study or research.
- You may not further distribute the material or use it for any profit-making activity or commercial gain
- You may freely distribute the URL identifying the publication in the public portal ?

Take down policy

If you believe that this document breaches copyright please contact us providing details, and we will remove access to the work immediately and investigate your claim.

Download date: 16. May. 2022

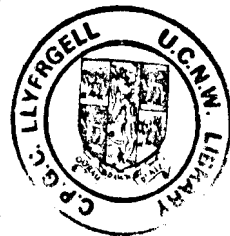
Microwave I.F Signal Processing Strategies For Coherent Optical Communications

**Thesis Submitted in Candidature for the Degree of
Doctor of Philosophy**

August 1993

Mohammed Sabih Chaudhry

**School of Electronic Engineering and Computer Systems
University College of North Wales
Bangor
United Kingdom**



Acknowledgments

I wish to extend my sincerest thanks to Professor John O'Reilly for his guidance and continuous encouragement for the duration of this research programme. I am also indebted to him for his help in the preparation of this thesis.

I am also grateful for the help extended by all my colleagues, in particular, Ms. Carmo Medeiros, Phil Lane, Ed Warner, Bian Yi, Paulo Moreira, Henrique Salgado, Tom Crummey, Neale Hall and Izzat Darwazeh. A special mention has to be made to Andy Popplewell, Warren Jones and Chris Hancock for their continual support, encouragement and friendship.

Thanks are also due to John Tame for the fabrication of the microstrip equalisers, Myles Woolfenden for the construction of the test jigs, Rutherford Appleton Labs. for fabrication of the GaAs MMIC equaliser and Paul Birdsall and David Newson of BT for testing the GaAs MMIC equaliser.

Financial support for this research has been provided by the U.K. Science and Engineering Research Council together with Dr. Mike Brain of BT, for which I am very grateful.

I wish to thank my parents and family for their continual support and inspiration during my years in academia.

Finally, I wish to offer my sincerest gratitude and appreciation to Kal for believing in me, motivating me and above all putting up with me - thank you.

Summary

This thesis is concerned with the realisation of microwave phase correcting networks for implementation in high bit-rate coherent optical systems to alleviate the impairments caused by fibre chromatic dispersion. This research has focused on three main areas: further investigation of microstrip equalisation strategies, design and realisation of gallium arsenide (GaAs) monolithic microwave integrated circuit (MMIC) group delay equalisers and the system implications of equalisation.

The most common and well reported models describing the dispersive characteristics of microstrip were assessed and compared to practical realisations, thereby enabling accurate modelling of the dispersive behaviour of the microstrip equaliser. The possibility of effecting a variation in the group delay characteristic of microstrip equalisers was explored by means of investigating the influences of the constituent material and physical geometry. Particular attention was given to the implications of the residual delay error resulting from the cascading of microstrip equalisers in a transparent optically amplified system.

Attention is focused, for the first time, on the design and realisation of microwave pseudo-lumped-element GaAs MMIC group delay equalisers. Based on simple bridged-T networks derived from second order lattice arrangements, GaAs MMIC equalisers compensating for high bit-rate transmission over various fibre lengths have been investigated. Higher order network configurations have also been explored with reference to extending both the equalised bandwidth and fibre spans.

The implications of equalised systems have been assessed, noting specifically the performance of the equalisers for linear and non-linear modulation formats. The GaAs MMIC equalisers are shown to be extremely flexible and robust to variations in the fibre spans. Additionally, the tolerance of GaAs MMIC equalisers has been investigated for slightly chirped systems with a view to implementation, ultimately in a practical system.

Contents

1	Introduction	1
1.1	Lightwave Communication Systems	1
1.2	Structure of Thesis	2
1.3	Summary of Main Contributions	4
1.4	Summary	6
2	Coherent Optical Transmission Systems	7
2.1	Introduction	7
2.2	Coherent Systems	8
2.2.1	Merits and technical prerequisites of coherent detection	9
2.3	Homodyne Detection	19
2.4	Heterodyne Detection	22
2.5	Fibre Chromatic Dispersion	22
2.5.1	Group delay	25
2.5.2	Dispersion mapping in the electrical domain	26

2.5.3	Dispersion variation with local oscillator frequency	27
2.6	Summary	30
3	Review of Current Equalisation Strategies	31
3.1	Introduction	31
3.2	Optical Domain Equalisation	32
3.2.1	Pre-transmission equalisation	32
3.2.2	In-line equalisation	38
3.2.3	Pre-detection equalisation	41
3.3	Electrical Domain Equalisation	43
3.3.1	Waveguide Equalisers	43
3.3.2	Microstrip Equalisers	46
3.4	Summary	49
4	Microstrip Equalisation Strategies	50
4.1	Introduction	50
4.2	Aspects of Microstrip Technology	50
4.2.1	Microstrip Wave Propagation	52
4.3	Phase Equalisation Characteristics of Microstrip lines	56
4.3.1	Microstrip Dispersion model	57

4.3.2	Influence of Substrate Material	69
4.3.3	Influence of Track Thickness and Substrate Height	70
4.4	Illustrative Practical Equalisers	74
4.4.1	Compensated Fibre Span and Bandwidth Available With Variations in Substrate Type	75
4.4.2	Compensated Fibre Span and Bandwidth Available With Variations in Both Track Thickness and Substrate Height	76
4.4.3	Implication of In-Line Amplification on The Tolerable Residual Delay Dispersion	78
4.5	Summary	82
5	GaAs Phase Equalisation	83
5.1	Introduction	83
5.2	GaAs Technology	84
5.2.1	GaAs Lumped Element Models	86
5.3	Lumped Element Phase Equaliser Networks	95
5.3.1	First order all-pass transfer function	96
5.3.2	Second order all-pass transfer function	97
5.3.3	All-pass networks	98
5.4	Single Section GaAs Phase Equaliser	100
5.4.1	Modelling the bridged-T	102

5.4.2	Design method of a single section equaliser	104
5.5	Cascaded Staggered Section Equaliser	108
5.5.1	Realisation of a staggered GaAs MMIC equaliser	109
5.6	Summary	113
6	System Performance Implications of Equalisation	115
6.1	Introduction	115
6.2	Modulation Formats	116
6.2.1	Amplitude Shift Keying (ASK)	116
6.2.2	Continuous-Phase FSK (CPFSK) and Minimum Shift Keying (MSK)	119
6.3	System Modelling	124
6.4	Performance Assessment of Equalised Systems	128
6.4.1	Performance of the single section equaliser	129
6.4.2	Performance of the cascaded staggered section equaliser	135
6.4.3	Performance of higher order equaliser	140
6.4.4	Equalisation of chirped systems	143
6.5	Summary	145
7	Conclusions	146
7.1	Research Outcomes	146

7.1.1	Microstrip Technology	147
7.1.2	GaAs MMIC Realisation	148
7.1.3	System Implications of Equalisation	149
7.2	Summary of Thesis	150
7.3	Suggestions for Further Work	152
References		153

List of Figures

2.1	<i>Intensity modulated direct detection scheme</i>	8
2.2	<i>Coherent balanced receivers; Heterodyne (a) and Homodyne (b)</i>	9
2.3	<i>Frequency division multiplexing (FDM) [11]</i>	12
2.4	<i>FDM heterodyne receiver</i>	15
2.5	<i>Two-arm phase diversity receiver for homodyne detection</i>	20
2.6	<i>Pulse broadening due to fibre dispersion[38]</i>	23
2.7	<i>Relative delay of a standard single mode fibre</i>	25
2.8	<i>Signal and dispersion mapping when local oscillator < signal frequency</i>	28
2.9	<i>Signal and dispersion mapping when local oscillator > signal frequency</i>	29
3.1	<i>Dispersion limited bit-rate distance product for Gaussian and super - Gaussian pulses as a function of the chirp factor C [42]</i>	33
3.2	<i>Broadening factor of a Gaussian pulse against distance for a range of chirp factors with $\tilde{\beta} > 0$. The dispersion length L_D is defined as the propagation length over which the dispersive effects become important $L_D = \frac{T_2^2}{ \tilde{D} }$ [42]</i>	34

3.3	<i>Optical pre-chirping transmission system illustrating propagation of pre-chirped pulse; A) before transmission, B) in transmission and C) received optical pulse [44]</i>	35
3.4	<i>Soliton transmission system comprising of many repeaters of L separation. The pump lasers inject cw light in both directions through wavelength-dependent directional couplers [42]</i>	37
3.5	<i>Dispersion characteristics for various fibres</i>	38
3.6	<i>Dispersion-supported transmission [58]; I - laser drive current, λ - transmitter wavelength, P_{dir} and P_{ext} - optical power with direct and external modulation and V_{dec} - voltage after decision circuit</i>	40
3.7	<i>Transmission system with optical equalisation</i>	41
3.8	<i>Transmissive equaliser</i>	41
3.9	<i>Delay characteristics of the optical equaliser</i>	42
3.10	<i>Heterodyne detection system with electrical equaliser</i>	43
3.11	<i>Waveguide delay equalisers. (a) Folded-tape meander-line type and (b) comb-type</i>	44
3.12	<i>Normalised time delay versus frequency (α) for various values of B/f_c [63]</i>	45
3.13	<i>Microstrip line equaliser</i>	46
3.14	<i>Delay characteristics for various microstrip equalisers. Dashed lines show the delay produced by a given fibre span</i>	47
4.1	<i>Some transmission line MIC structures [68]</i>	51

4.2	<i>Hybrid modes in microstrip [69]</i>	53
4.3	<i>Static model of the electric and magnetic fields in the microstrip transmission line [69]</i>	54
4.4	<i>Dynamic model of the magnetic field in the microstrip transmission line of length $\lambda/2$ [69]</i>	55
4.5	<i>Dynamic model of the electrical field in the microstrip transmission line of length $\lambda/2$ [69]</i>	55
4.6	<i>Equivalent model for strip of finite width</i>	58
4.7	<i>Equivalent model for strip of finite thickness</i>	59
4.8	<i>Various models for $\epsilon_{r,eff}(f)$</i>	65
4.9	<i>Comparison of $\epsilon_{r,eff}(f)$ obtained practically and the best matched model, that of Yamashita et al.</i>	66
4.10	<i>Relative delay obtained with various reported models and a practically realised microstrip transmission line on a ceramic Al_2O_3 substrate</i> . . .	67
4.11	<i>Relative delay obtained with various reported models and a practically realised microstrip transmission line on RT/duroid.</i>	68
4.12	<i>Relative delay obtained with various reported models and a practically realised microstrip transmission line on Cuclad</i>	69
4.13	<i>$\epsilon_{r,eff}(f)$ for a 10.5cm microstrip transmission line fabricated on various substrate types with a substrate height of $625\mu m$</i>	70
4.14	<i>Group delay characteristics for a 10.5cm microstrip transmission line fabricated on various substrate types with a substrate height of $625\mu m$</i>	71

4.15	Influence of variations in the track thickness on the $\epsilon_{r,eff(f)}$ of a 10.5cm microstrip transmission line ($h = 625\mu\text{m}$ - constant). Note: The excessively large track thickness ($500\mu\text{m}$) is impractical and is used here to illustrate the effect only.	71
4.16	Influence of variations in the track thickness on the group delay characteristics of a 10.5cm microstrip transmission line ($h = 625\mu\text{m}$ - constant)	72
4.17	Influence of variations in the substrate height on the $\epsilon_{r,eff(f)}$ of a 10.5cm microstrip transmission line ($t = 35\mu\text{m}$ - constant)	73
4.18	Influence of variations in the substrate height on the group delay characteristics of a 10.5cm microstrip transmission line ($t = 35\mu\text{m}$ - constant)	73
4.19	Group delay characteristics showing an equaliser fabricated on RT/duroid substrate to correct for given length of fibre (top) and the equalised bandwidth defined by $\pm 1\text{ps}$ of residual delay (bottom)	75
4.20	The residual group delay error, accumulative with the number of repeaters	79
4.21	Dispersion power penalty resulting from the accumulation of the residual error from each of the cascaded equalisers	80
4.22	Impact of equalisation on long haul repeated transmission; a) with 5 repeaters, b) with 10 repeaters and c) 60 repeaters	81
5.1	GaAs MMIC cross section	84
5.2	GaAs resistor structure	87
5.3	GaAs resistor equivalent circuit	87
5.4	GaAs spiral inductor	88

5.5	<i>GaAs spiral inductor equivalent circuit</i>	89
5.6	<i>GaAs polyimide parallel plate capacitor</i>	90
5.7	<i>GaAs polyimide capacitor equivalent circuit</i>	90
5.8	<i>GaAs silicon nitride parallel plate capacitor</i>	91
5.9	<i>GaAs interdigital capacitor</i>	92
5.10	<i>GaAs interdigital capacitor equivalent circuit</i>	92
5.11	<i>GaAs MMIC multi-dielectric microstrip line</i>	93
5.12	<i>Equivalent circuit of the physical GaAs/alumina transition</i>	94
5.13	<i>All-Pass pole-zero locations for (a) first order and (b) second order transfer functions</i>	96
5.14	<i>Effect of varying Q on the group delay profile of a second order transfer function</i>	99
5.15	<i>Lattice networks for (a) first order and (b) second order transfer functions</i>	99
5.16	<i>Cascade of constant resistance networks</i>	99
5.17	<i>Bridged-T equivalents for the (a) first order and (b) second order lattice networks</i>	100
5.18	<i>ABCD matrix for a series impedance two port network</i>	102
5.19	<i>ABCD matrix for a shunt impedance two port network</i>	102
5.20	<i>Analytically predicted (a) group delay and (b) magnitude responses of the equaliser</i>	105

5.21	<i>CAD layout of single section bridged-T equaliser</i>	106
5.22	<i>Photomicrograph of single section bridged-T equaliser</i>	106
5.23	<i>Measured (a) group delay and (b) magnitude responses of the GaAs MMIC equaliser</i>	107
5.24	<i>Realisation of wideband equalisers by cascading single sections with staggered delay responses</i>	108
5.25	<i>Realisation of GaAs MMIC wideband equaliser by cascading single sections with staggered delay responses; (top) magnitude (bottom) group delay</i>	110
5.26	<i>Photomicrograph of cascaded bridged-T equalisers</i>	111
5.27	<i>Group delay responses of four ideal element equalisers designed to correct for fibre spans of 150, 200, 250 and 300km</i>	112
5.28	<i>Magnitude (top) and group delay (bottom) responses of an optimised GaAs MMIC equaliser to compensate for the dispersion produced by 200km of single mode fibre</i>	112
6.1	<i>ASK waveform</i>	116
6.2	<i>ASK power spectrum for 5 & 8Gbit/s signalling rates</i>	118
6.3	<i>Data sequence and corresponding FSK waveform</i>	119
6.4	<i>MSK power spectrum for 5 & 8Gbit/s signalling rates</i>	121
6.5	<i>MSK waveform generation</i>	123
6.6	<i>MSK transmitter</i>	124

6.7	<i>Block diagram of an ASK transmission system</i>	125
6.8	<i>Block diagram of a MSK transmission system</i>	125
6.9	<i>Dispersion power penalty improvement with single section equaliser for a 5Gbit/s ASK modulated system</i>	130
6.10	<i>Eye patterns for a) unequalised and b) equalised ASK modulated signals at 5Gbit/s over 350km</i>	131
6.11	<i>Dispersion limitations for ASK,MSK and CPFSK modulated systems operating at 1.55μm with 15-17ps/km-nm of chromatic dispersion . . .</i>	131
6.12	<i>Dispersion power penalty improvement with single sectioned equaliser for a 5Gbit/s MSK modulated system</i>	132
6.13	<i>Eye patterns for a) unequalised and b) equalised MSK modulated signals at 5Gbit/s over 250km</i>	133
6.14	<i>Dispersion power penalty improvement with single sectioned equaliser for a 5Gbit/s CPFSK modulated system</i>	133
6.15	<i>Eye patterns for a) unequalised and b) equalised CPFSK modulated signals at 5Gbit/s over 160km</i>	134
6.16	<i>Dispersion power penalty for ASK, MSK and CPFSK systems for a 5Gbit/s modulation rate</i>	134
6.17	<i>Performance assessment of the wideband equaliser at 8Gbit/s for an ASK system; a) dispersion power penalty with variation in distance, b) eye without equalisation at 200km and c) eye of equalised system at 200km</i>	136

6.18	Performance assessment of the wideband equaliser at 8Gbit/s for a MSK system; a) dispersion power penalty with variation in distance, b) eye without equalisation at 100km and c) eye of equalised system at 100km	137
6.19	Performance assessment of the wideband equaliser at 8Gbit/s for a CPFSK system; a) dispersion power penalty with variation in distance, b) eye without equalisation at 50km and c) eye of equalised system at 50km	138
6.20	Comparison of performances between the single section equaliser and the cascaded staggered section wideband equaliser	139
6.21	Performance evaluation of the higher order equalisers	141
6.22	Equaliser performance for a chirped ASK system	144

List of Tables

2.1	<i>Theoretical receiver sensitivity limits for various modulation formats given as the no. of photons per “one” bit</i>	11
2.2	<i>Non-linear effects and their characteristics relevant to FDM systems [18]. N is the number of channels for a fibre length in excess of 100km, operation in the 1550nm window, an attenuation of 0.2dB/km and a 10GHz channel separation frequency</i>	14
2.3	<i>FDM/WDM experiments</i>	15
2.4	<i>Linewidths of various laser types</i>	17
2.5	<i>Linewidth requirements for different modulation formats, assuming a 1dB receiver sensitivity penalty</i>	18
2.6	<i>(bit-rate)² - distance product for various modulation formats</i>	24
3.1	<i>Characteristics of waveguide equalisers with B=8Gbit/s and L=68km [63]</i>	45
4.1	<i>Some key microstrip substrates</i>	52
4.2	<i>Influence of substrate type on the maximum attainable equalised fibre length and bandwidth for a 10cm microstrip line length of $Z_o = 50\Omega$.</i>	76

4.3	<i>Influence of the track thickness on the maximum attainable equalised fibre length and bandwidth for a 10cm microstrip line length of $Z_0 = 50\Omega$</i>	77
4.4	<i>Influence of the substrate height on the maximum attainable equalised fibre length and bandwidth for a 10cm length of microstrip line of $Z_0 = 50\Omega$</i>	77
5.1	<i>GaAs layer dimensional tolerances</i>	86
5.2	<i>GaAs inductor types</i>	89
5.3	<i>Tolerance and range of various GaAs capacitors</i>	93
5.4	<i>Expressions for the element values of the lattice and the equivalent bridged-T networks</i>	101
5.5	<i>Percentage change in the component values after optimisation</i>	107
5.6	<i>Percentage change in the component values after optimisation of the two-section cascaded equaliser</i>	113
6.1	<i>System performance of the single section equaliser for various modulation formats</i>	129
6.2	<i>System performance of the cascaded staggered section equaliser for various modulation formats</i>	135
6.3	<i>Comparison in performance of microstrip and cascaded staggered section equaliser types</i>	142

Abbreviations

APD	Avalanche Photo Diode
ASK	Amplitude Shift Keying
CAD	Computer Aided Design
CPFSK	Continuous Phase Frequency Shift Keying
DBR	Distributed Bragg Reflector
DF	Dispersion Flattened
DFB	Distributed Feedback
DPFSK	Differential Phase Frequency Shift Keying
EDFA	Erbium Doped Fibre Amplifier
FDM	Frequency Division Multiplexing
FSK	Frequency Shift Keying
FWM	Four Wave Mixing
FWHM	Full Width Half Maximum
GaAs	Gallium Arsenide
\Im	Imaginary part
IC	Integrated Circuit
IF	Intermediate Frequency
IM/DD	Intensity Modulated - Direct Detection
ISI	Inter Symbol Interference
LD	Laser Diode
LP	Linearly Polarised
MIC	Microwave Integrated Circuit
MIM	Metal Insulator Metal

MMIC	Monolithic Microwave Integrated Circuit
MQW	Multi Quantum Well
MSK	Minimum Shift Keying
NRZ	Non Return-to-Zero
OPLL	Optical Phase Locked Loop
OQPSK	Offset Quadrature Phase Shift Keying
PSK	Phase Shift Keying
QPSK	Quadrature Phase Shift Keying
\Re	Real part
RACE	Research into Advanced Communications for Europe
SBS	Stimulated Brillouin Scattering
SDH	Synchronous Digital Hierarchy
SI	Semi - Insulating
SLA	Semiconductor Laser Amplifier
SOP	State Of Polarisation
SPM	Self Phase Modulation
SRS	Stimulated Raman Scattering
TE	Transverse Electric
TM	Transverse Magnetic
TEM	Transverse Electromagnetic
WDM	Wavelength Division Multiplexing

Chapter 1

Introduction

1.1 Lightwave Communication Systems

The ever increasing consumer demands on the present communication infrastructure have led to an interest in high bit-rate multi-channel long haul transmission systems. Of the vast amount of bandwidth available with optical fibres, some 30,000GHz, only upto 10GHz is currently used in practice. To increase the present channel capacity techniques such as wavelength division multiplexing (WDM) are being explored while optical amplifiers are used to extend the maximum attainable fibre reach[1]. Such is the interest in utilising the available optical bandwidth that a consortium of six European institutes involved in the RACE (Research into Advanced Communications for Europe) programme have successfully demonstrated a coherent multi-channel system for broadband signal distribution in preparation for fibre-to-the-home systems of the future[2, 3].

Direct detection systems employing preamplifiers have generally been used to achieve multi bit-rate transmission over large distances. However, with growing interest in WDM multi-carrier systems coherent transmission represents a plausible alternative. Such systems have been demonstrated to be flexible in supporting synchronous multiplexed signal transport; synchronous digital hierarchy (SDH)[4].

The availability of the rare earth doped fibre amplifiers based on erbium in silica fi-

bre, the erbium doped fibre amplifier (EDFA), has had a profound effect on long haul transmission systems. EDFAs unlike the first generation semiconductor laser amplifiers (SLAs) offer high gain, low noise, large bandwidth and are transparent to modulation schemes and bit-rates. Realisation of long haul transmission is now normally effected with cascaded optical amplifiers, but this can be significantly impaired by fibre chromatic dispersion and nonlinear effects. Dispersion is particularly problematic for standard monomode fibre - originally designed primarily for operation at 1300nm - when used in the 1550nm window appropriate to EDFAs. As device technology matures and transmission rates and distances increase, the effects of the transmission impairments will be exacerbated. To obtain any substantial increase in systems performance these impairments will need to be suppressed[5].

A variety of methods have been developed to correct for the fibre chromatic dispersion, applicable to direct detection and coherent systems. Optical domain equalisation techniques are generally applied to direct detection systems whereas post detection equalisation in the electrical domain is possible for coherent heterodyne systems. Heterodyne detection allows for mapping of the dispersion from the optical domain directly into the electrical domain while preserving the phase information. The work reported in this thesis is mainly concerned with devising a practical approach for electrical domain equalisation.

1.2 Structure of Thesis

The following chapter provides an introductory review of coherent optical transmission systems, detailing the principles and potential of such systems while effecting a comparison between direct and coherent detection schemes. The device requirements for coherent systems are also addressed together with the issue of fibre chromatic dispersion.

Chapter 3 is concerned with defining the present state-of-the-art for pre-transmission, in-line, pre- and post detection equalisation strategies. These techniques are assessed

in terms of their merits when applied to long haul transmission. The various optical domain and electrical domain equalisation techniques are discussed and the chapter concludes by drawing a comparison between all the strategies considered.

The use of microstrip circuits for post detection electrical domain equalisation is considered in chapter 4. Some of the more common models defining the microstrip dispersion characteristics are compared with each other and with practical microstrip realisations. The model which is found to be most consistent with practical realisations is used in an evaluation of the microstrip group delay behaviour with respect to variations in the microstrip constituent material and physical geometry. Implications of multi-section in-line amplification on the tolerable residual delay dispersion resulting from long haul transmission are considered and illustrated by means of eye simulations.

Chapter 5 reviews and examines for the first time an alternative technology, gallium arsenide (GaAs) monolithic microwave integrated circuits (MMICs), for realising phase correction networks for optical fibre systems. The planar microstrip equalisers have a major drawback in that they are limited by their size. With GaAs technology compact complex monolithic microwave integrated circuit (MMIC) equalisers are realised based on pseudo-lumped-element components. A single section equaliser based on a second order all-pass network is designed to correct for the fibre dispersion produced by 100km of standard monomode fibre when operating in the 1550nm window. The fabricated equaliser response is compared to the theoretical predictions. This design is extended further to realise equalisers of wider equalised bandwidths correcting for larger fibre spans. These equalisers are realised by means of cascading single sections of staggered individual delay characteristics.

The benefits of using GaAs MMIC equalisers for long haul coherent optical transmission are assessed in chapter 6. The single section and the wideband cascaded staggered section equalisers are evaluated with linear (ASK) and non-linear (CPFSK/MSK) modulation schemes. A comparison is effected between the potential of the GaAs MMIC and microstrip equalisers in terms of the bit-rate distance product. The performance and robustness of the GaAs MMIC equalisers is further assessed for optically chirped

signals and for distances larger than the original design fibre lengths. Finally, chapter 7 concludes the thesis by summarising the main findings and provides suggestions for further work.

1.3 Summary of Main Contributions

The research presented in this thesis examines the possibility of correcting for fibre chromatic dispersion using state-of-the-art strategies for application in very high bit-rate long haul optical heterodyne systems. The major contributions stemming from this work can be summarised as follows:

- The models reported in the literature, describing the dispersion characteristics of microstrip lines, are inconsistent from one to the next when the parameters are varied widely. Some of the more commonly used models were evaluated and a comparison effected between them. The models were also compared with practical microstrip realisations on various substrates and a model was identified that offered a very good match with the practical results.
 - The influence of the microstrip constituent material and physical geometry on the group delay characteristics were evaluated.
 - The implications of using microstrip equalisers for multi-section optically amplified transmission systems were determined noting specifically the influence of the residual dispersion on the maximum attainable transmission lengths.
 - A single section pseudo-lumped-element equaliser of 5GHz bandwidth was designed and fabricated as a GaAs MMIC to correct for the dispersion produced by a fibre length of 100km.
 - Higher order wideband (10GHz bandwidth) equalisers were designed demonstrating the potential for achieving wideband equalisation by means of cascading staggered single section equalisers.
-

- System implications of equalisation were evaluated for linear (ASK) and non-linear (CPFSK) modulation formats offering a marked improvement in the dispersion power penalty for the non-linear schemes.
- The wideband equaliser has been evaluated for a slightly chirped system employing an unbalanced external modulator of the Mach-Zehnder type, showing the equaliser to be tolerant to the slight residual chirp from such external modulators.
- The equalisers have been shown to be robust and flexible in correcting for fibre spans greater than that for which they were originally designed.

The contributions made during the course of this research have led to the following publications:

1. "Microwave Technology for Coherent Optical Communication". M.S. Chaudhry and J.J. O'Reilly, Digest Second IEE Bangor Communications Symposium, pages 215-218, May 1990.
 2. "Microstrip Compensation of Fibre Chromatic Dispersion in Optically Amplified Coherent Systems". J.J. O'Reilly and M.S. Chaudhry, Digest IEE Colloquium on Microwave Optoelectronics, Savoy Place, London, October 1990.
 3. "Chromatic Dispersion Compensation in Heterodyne Optical Systems Using Monolithic Microwave Intergrated Circuits". M.S. Chaudhry and J.J. O'Reilly, OSA/IEEE Digest of Optical Fibre Communications Conference, OFC '92, San Jose, USA, page 179, January 1992.
 4. "Evaluation of a GaAs MMIC Fibre Chromatic Dispersion Equaliser for Heterodyne Optical Systems". M.S. Chaudhry and J.J. O'Reilly, Digest Fourth IEE Bangor Communications Symposium, pages 192-195, May 1992.
 5. "Equalisation of Fibre Chromatic Dispersion For Very High Bit Rate Transmission Using Monolithic Microwave Integrated Circuits". M.S. Chaudhry and J.J. O'Reilly, OSA/IEEE Digest of Optical Fibre Communications Conference, OFC '93, San Jose, USA, pages 132-133, February 1993.
-

6. "Fibre Chromatic Dispersion Equalisation For Coherent Lightwave Systems Using GaAs MMIC Networks". M.S. Chaudhry and J.J. O'Reilly, SPIE International Symposium on Fibre Optic Networks and Video Communications, Berlin, April 1993.
7. "Post-Detection Chromatic Dispersion Equalisation Using GaAs MMICs in Heterodyne Detection Systems". M.S. Chaudhry and J.J. O'Reilly, Digest IEE Colloquium on Optical Detectors and Receivers, London, April 1993.
8. "Multi-Section GaAs MMIC Group Delay Equaliser for Dispersion-Compensated 8Gbit/s Heterodyne transmission". M.S. Chaudhry and J.J. O'Reilly, SPIE International Symposium on Multigigabit Fibre Communication Systems, California, July 1993.

1.4 Summary

This chapter has indicated the motivation for research on coherent heterodyne system equalisation and has identified the main areas of contribution. With this background we now proceed, in the following chapter, to a review of coherent optical transmission systems.

Chapter 2

Coherent Optical Transmission Systems

2.1 Introduction

Coherent detection techniques for radios were first proposed by Fessenden[6] in 1905. Some twenty years elapsed before these ideas were implemented as during this interval the technology for realising the essential components was refined. With optical transmission systems, it was shown[7] in the early 1960's that coherent detection offered a substantial improvement in the signal to noise (S/N) ratio over intensity modulated direct detection systems. However, device limitations have hindered the widespread practical realisation of coherent systems. Field demonstrations of modest bit-rate coherent transmission[8, 9] through conventional single-mode fibre has proved that these systems could become commercially significant in the future and offer an attractive alternative to direct detection systems.

This chapter details coherent system principles and effects a comparison between direct detection and coherent detection schemes.

Device requirements for homodyne/heterodyne detection are outlined and the issue of fibre chromatic dispersion is addressed.

2.2 Coherent Systems

Optical receivers may be categorised as either direct detection receivers or coherent receivers. Direct detection receivers directly convert the modulated optical signal (f_s) to the baseband signal, whereas with coherent detection, the incoming modulated optical signal is mixed with an optical local oscillator signal (f_{lo}). The mixing process theoretically generates the sum and difference of the two optical frequencies with the difference in frequencies, ($f_s \pm f_{lo}$) known as the *Intermediate Frequencies (IF)* being of interest and detected by the photodiode. Figure 2.1 shows a conventional direct detection system where a post-detection baseband amplifier is used prior to the signal processing circuitry.

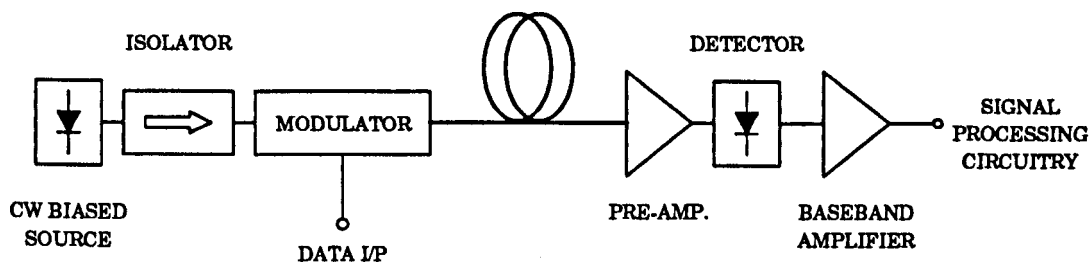
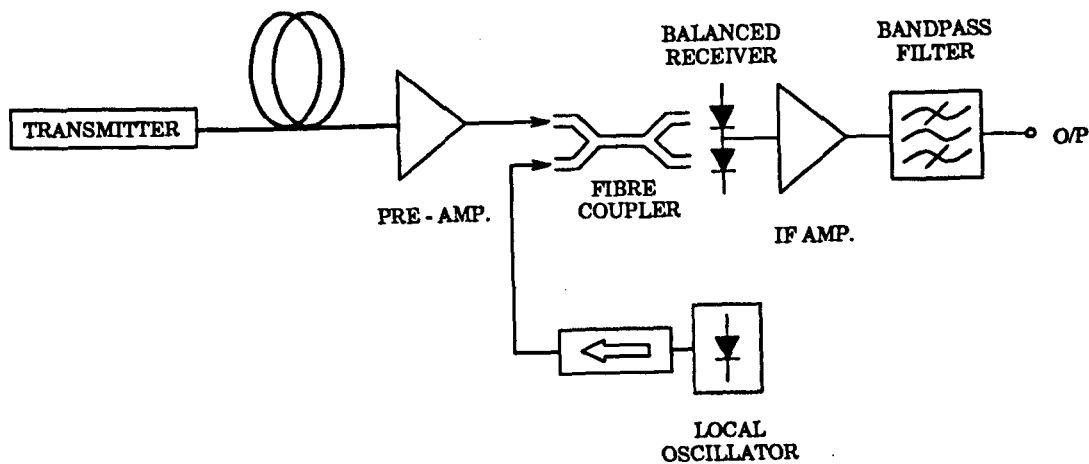


Figure 2.1: *Intensity modulated direct detection scheme*

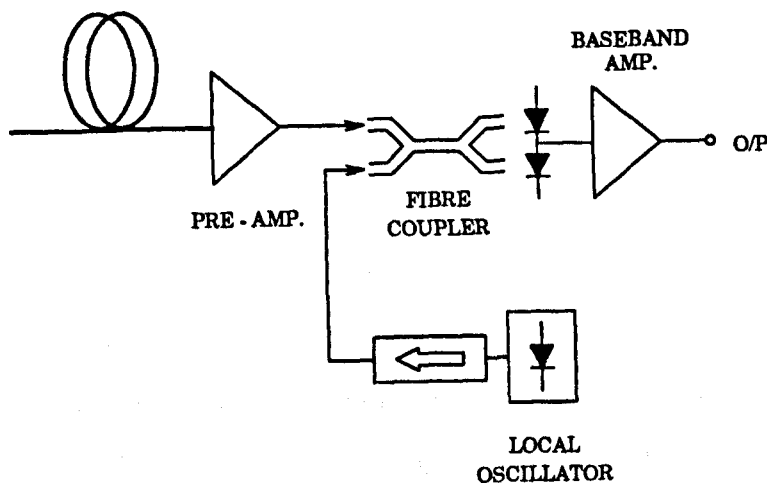
A coherent detection system is illustrated by figure 2.2. The combining of the received and the local oscillator signals is implemented using a high ratio coupler where the output is taken from one of the coupler output arms and illuminates the detector. This means that any power in the other output arm is simply disregarded. To capitalise on the available power and in turn improve the receiver sensitivity a balanced detector regime is employed as shown in figure 2.2. This detector network eliminates the need for high pass filtering as the matched frequency responses of the photodiodes cause cancellation of the dc current terms. The local oscillator laser intensity noise and adjacent channel interference for multichannel systems are reduced with balanced detection[10].

Mixing results in the generation of the message signal at the IF. Should the local oscillator frequency be matched to that of the incoming signal then the IF is at zero frequency and the message signal gets mapped down at the baseband, this being termed

Homodyne detection. On the other hand if the local oscillator is offset then the message signal is mapped to the IF, giving *Heterodyne detection*.



(a)



(b)

Figure 2.2: Coherent balanced receivers; Heterodyne (a) and Homodyne (b)

2.2.1 Merits and technical prerequisites of coherent detection

The interest in coherent systems is attributed to the advantages that this scheme offers over the conventional direct detection systems. The two distinctive features of this system that make it attractive are the

- improvement in sensitivity of $\approx 20\text{dB}$
- the possibility of finer optical frequency-division-multiplexing (FDM).

The trend towards the adoption of coherent systems has been somewhat hampered by the refinement needed for some underlying optoelectronic devices, mainly;

- frequency stable lasers
- narrow linewidth laser sources
- polarisation controllers

All of the above topics will be briefly addressed before dealing with heterodyne/homodyne reception.

Sensitivity improvement

Coherent detection schemes have been shown to offer improvements in sensitivity of the order of 20dB [11] compared with direct detection, assuming the latter does not employ an optical preamplifier. Direct detection system sensitivity is governed by the circuit noise (due to the electronic devices in the amplifying stage, mainly the FETs) when using a PIN or by the dark current and avalanche enhanced signal shot noise when using APDs (due to multiplication process). These noise components inhibit direct detection receivers from achieving the shot-noise limit, but with pre-amplification (figure 2.1) by means of optical amplifiers, the optical signal is boosted immediately before detection resulting in an increase in the receiver sensitivity[12]. With the aid of pre-amplification, direct detection receivers can be made to emulate their coherent counterparts in terms of obtainable receiver sensitivity.

With coherent detection the shot-noise limit may be approached by increasing the local oscillator intensity. The extent to which the local oscillator power may be increased is determined by the limitations of the detector. Table 2.1 effects a comparison

Receiver type	Modulation format	Number of photons per bit for $\text{BER} = 10^{-9}$
Heterodyne	ASK	72
	FSK	36
	PSK	18
Homodyne	ASK	36
	PSK	9
Direct detection	ASK	21

Table 2.1: Theoretical receiver sensitivity limits for various modulation formats given as the no. of photons per "one" bit

of the receiver sensitivity for coherent (heterodyne/homodyne) and direct detection receivers[13]. PSK detection by either a heterodyne or homodyne receiver yields a sensitivity greater than the direct detection limit. To date, the best sensitivity achieved with homodyne PSK[14] is 20 photon/bit at 565 Mbit/s.

Frequency division multiplexing (FDM)

Requirements for enhanced telecommunication network capacity has led to techniques in frequency-division-multiplexing. These techniques, already employed for radio broadcast systems allow each broadcasting station to transmit on a particular frequency. At the receiver the local oscillator can be used to select a specific station by means of heterodyning (FDMA - Frequency division Multiple Access). This principle has been applied to optical wideband local networks drawing on the immense unused bandwidth potential of the fibre already installed, thus allowing the consumer a wide range of services and television channels without the need of satellite dishes[15]. The advantage of FDM in coherent heterodyne systems is that very fine frequency separation can be accommodated. In figure 2.3 three optical carriers are illustrated, each modulated with five sub-carrier multiplexed signals of 100GHz separation. Over the $1.3\mu\text{m}$ to $1.6\mu\text{m}$

wavelength thousands of channels can be accommodated at spacings of $\approx 10\text{GHz}$ [16].

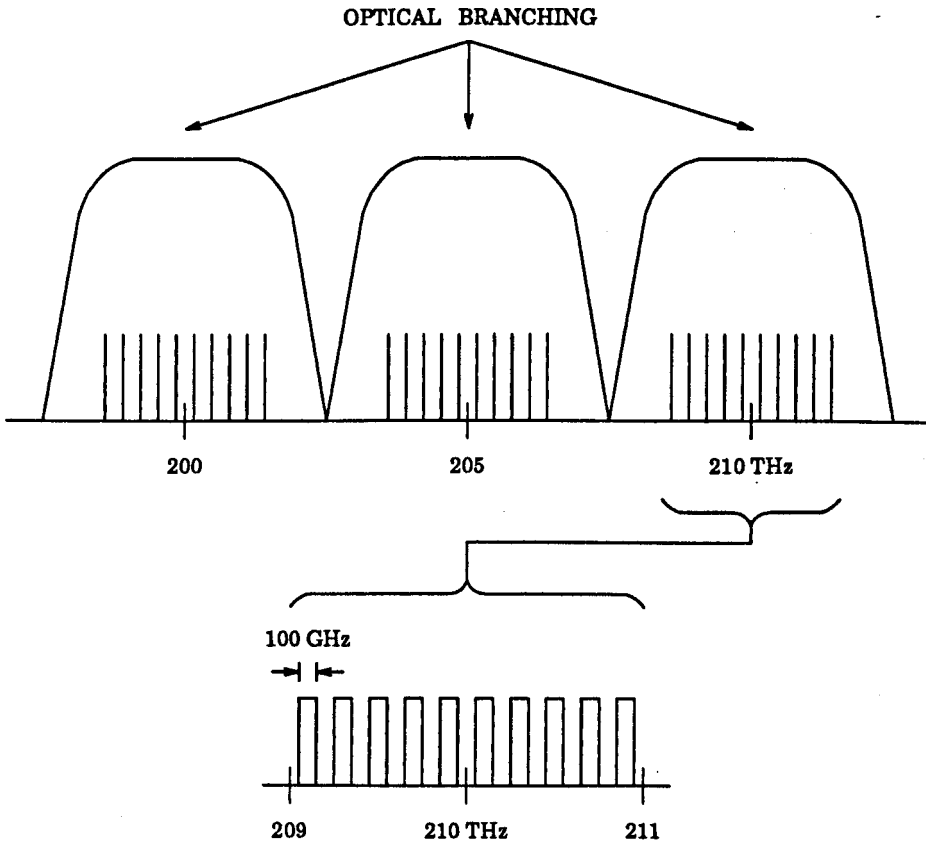


Figure 2.3: Frequency division multiplexing (FDM) [11]

The sharp electronic filter characteristics available offer a high degree of selectivity and dense channel spacing. Optical domain filters cannot achieve the selectivity offered by their electrical domain counterparts, thus limiting the channel capacity available with direct detection systems.

The nonlinear interactions occurring within the single mode fibre pose an upper bound on the transmitter power and number of channels which may be employed. Nonlinear effects such as four wave mixing (FWM), stimulated Brillouin scattering (SBS) and stimulated Raman scattering (SRS) generally dictate the channel capacity.

FWM - arises as a consequence of the intensity dependent variations in the refractive index of the optical fibre (Kerr effect), resulting in the generation of new frequency

components. At least two co-propagating modes are needed for the manifestation of this nonlinear effect, which is more pronounced in dispersion shifted fibres than with conventional fibres. This is attributed to the better phase matching obtained in the dispersion shifted fibres[17].

SBS - can be regarded as the modulation of light by means of molecular vibrations within the fibre producing scattered optical light, which appears as sidebands about the incident frequency, the separation between the sidebands being equal to the modulation frequency of the nonlinear effect. The scattering process produces an acoustic phonon and an optical frequency shift in the backward direction such that the optical frequency is down shifted in frequency by the acoustic frequency. This effect is only present when the optical power is above a certain level given by:

$$P_{SBS} = 4.4 \times 10^{-3} d^2 \lambda^2 \alpha_{dB} \nu \text{ (watts)} \quad (2.1)$$

where d is the fibre core diameter, λ is the operating wavelength, α is the fibre attenuation in decibels and ν is the source bandwidth in gigahertz.

SRS - is similar to *SBS* except that an optical photon is generated instead of an acoustic phonon. *SRS* is a bidirectional effect having optical power threshold many orders of magnitude larger than that of *SBS*. The optical power threshold needed to initiate *SRS* is given by:

$$P_{SRS} = 5.9 \times 10^{-2} d^2 \lambda \alpha_{dB} \nu \text{ (watts)} \quad (2.2)$$

The magnitude of the sidebands produced by the nonlinear *SBS* or *SRS* processes are dependent on the optical power level over and above the respective thresholds and the length of fibre for which the threshold is exceeded.

For a modest number of channels *FWM* is more dominant, but as the number of channels increases to a few hundred then *SRS* becomes dominant[18, 19]. The influence of the nonlinear effects of *FDM* systems may be suppressed as illustrated in table 2.2. With *FDM* many signals, with individual carriers, are multiplexed together electrically

Non-linearity	Effects	P_{max} (dBm)	Comments	Suppression
FWM	Crosstalk through intermodulation products	0 to -10	Decreases with N	Large dispersion; large channel spacing
SBS	Crosstalk	-10	Narrow bandwidth	Suitable channel allocation
SRS	Crosstalk	30 to -20	Decreases with N	Increase channel separation
Kerr effect	Phase noise	10 to -5	Decreases with N	Reduce power fluctuations

Table 2.2: Non-linear effects and their characteristics relevant to FDM systems [18]. N is the number of channels for a fibre length in excess of 100km, operation in the 1550nm window, an attenuation of 0.2dB/km and a 10GHz channel separation frequency

and modulated onto an optical carrier. However if a number of optical carriers operating at different wavelengths are multiplexed onto a single fibre, then the technique is referred to as wavelength-division-multiplexing (WDM). In figure 2.3, many channels are electrically multiplexed onto a single carrier which in turn is optically multiplexed with other optical carriers by means of a star coupler and transmitted through a single fibre. For each optical branch there is a dedicated heterodyne receiver which maps the channels down to the IF, prior to IF amplification and band-pass filtering as shown in figure 2.4. Field experiments (eg. STARNET [20, 21]) have already demonstrated the advantages of denser channel spacing and higher data capacity at the expense of added complexity of WDM/FDM coherent heterodyne systems, supported by table 2.3.

The theoretical optical channel spacing for multichannel FDM systems is given by[22]:

$$D_{opt} = D_{ele} + 2f_{IF} \quad (2.3)$$

where D_{ele} is the channel spacing in the electrical domain. For negligible cross-talk the

	TERNET	RAINBOW	UCOL	STARNET	CPFSK [21]
Modulation format	ASK	ASK	DPFSK	PSK	CPFSK
Bit rate (br)	1Gbit/s	200Mbit/s	155Mbit/s	3Gbit/s	1.244Gbit/s
Channel separation	187 br	1040 br	23 br	2.7 br	8 br
Receiver	Direct detection	Direct detection	Coherent	Coherent	Coherent

Table 2.3: FDM/WDM experiments

minimum D_{ele} and f_{IF} must be twice the bit-rate. Thus for optimal carrier spacing narrow linewidth and frequency stability of the laser source are very important.

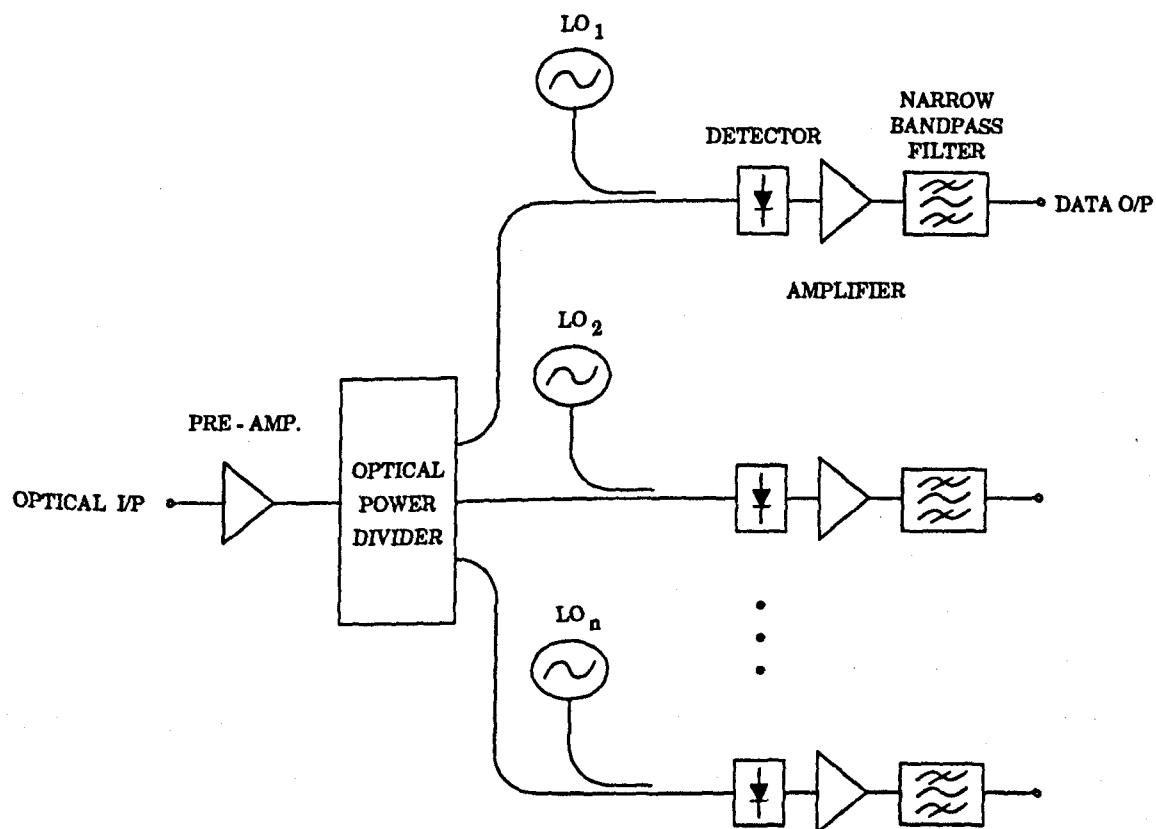


Figure 2.4: FDM heterodyne receiver

Laser frequency stability

A frequency stable single mode laser is essential for future multichannel FDM networks. Single mode lasers tend to suffer from frequency fluctuations. The reasons for this may be attributed to:

ambient - temperature variations which cause mode hopping;

electrical - drive current fluctuations from within supply circuitry;

optical - back reflections which may be eliminated with the use of isolators;

intrinsic - interplay between the charge carriers in the cavity.

Some of the more commonly used lasers for single mode operation are the DFB (Distributed Feedback), DBR (Distributed Bragg Reflector) and Er-doped fibre ring-laser[23]. The Er-doped fibre ring-laser has been demonstrated to be both stable and tunable.

Both the DFB and DBR lasers exhibit wavelength shifts of about 0.1nm at 1550nm with DBR lasers more inclined to mode hopping with temperature changes. The frequency stability of DFB lasers for use in FDM systems has been demonstrated[24] using only temperature and current control techniques.

Laser linewidth

The spectral linewidth of a single mode laser is a manifestation of phase fluctuations occurring inside the laser. Two mechanisms contribute to phase fluctuations; spontaneous emission and fluctuations in the carrier population. The spontaneously emitted photons result from the transitions of the carriers between energy levels. As the energy levels comprise of a band of energies then the carrier transition may be from any level within the higher energy band to a lower state energy level. This undeterministic random process results in spontaneously emitted photons of various frequencies,

Laser type	Linewidth
MQW DFB	70kHz [26]
MQW DBR	85kHz [27]
External cavity	10kHz [28]
Stimulated Brillouin fibre ring laser	2kHz [29]
Er-doped fibre ring laser	1.4kHz [23]

Table 2.4: Linewidths of various laser types

termed phase noise[25], which contributes to the broadening of the linewidth spectrum degrading system performance and consequently leading to a deterioration of the bit-error-rate. Direct modulation of the laser subjects the laser cavity to fluctuations in the carrier density causing substantial variations in the cavity refractive index, thereby resulting in wavelength shifts (chirp). Below a certain threshold current the laser output is very low as it is operating in the spontaneous emission region giving rise to a wide spectrum (linewidth). Above the threshold current the laser operates in the stimulated emission region amplifying the light. The higher photon densities generated by the stimulated emission reduce the influence of spontaneous emission and subsequently reduce the laser spectrum. Biasing the laser above the threshold current has the effect of reducing the chirp. Increasing the cavity length of the laser causes a reduction in the linewidth as the effective mirror losses[22] are reduced. Frequency chirp can be reduced by using multi-quantum well laser structures (MQW) consisting of alternating ultra thin layers of low bandgap (well) and high bandgap (barrier) materials. These structures improve the laser's dynamic response[30]. Alternatively, the signal can be externally modulated or the profile of the laser drive current altered from a step to gentle staircase shape in an attempt to reduce the effects of chirp.

Some of the best achievements in obtaining narrow laser linewidths are given in table 2.4. The effects of the non-zero linewidth are more serious for homodyne receivers than with heterodyne detection. This is best illustrated in table 2.5, which relates the required linewidth as a percentage of the transmission bit-rate[31]. The less sensitive

Receiver type	Modulation format	Laser linewidth (% of bit-rate)
Heterodyne	FSK	9
	DPSK	0.16
	ASK	0.1 - 0.3
Homodyne (phase locked)	PSK	0.03

Table 2.5: *Linewidth requirements for different modulation formats, assuming a 1dB receiver sensitivity penalty*

heterodyne receiver can accommodate a more relaxed linewidth requirement with FSK modulation format.

The implications of using wide linewidth lasers have been studied by various authors[32, 33] for FDM and weakly coherent optical systems.

With FDM systems wide laser linewidths may be tolerated at the expense of more wider spaced and a reduced number of channels. The laser linewidth requirements with weakly coherent systems can also be relaxed. In weakly coherent systems only the optical signal power contained within the IF passband is measured by the receiver and the phase information is neglected.

Polarisation control

The signal component after mixing is governed by the state of polarisation (SOP) of the received and local oscillator signals. Should the two optical signals SOP be orthogonal then the mixer output component will be zero. The SOP of signals in installed fibres is not preserved but varies slowly along the length of the fibre.

Two degenerate orthogonally polarised modes are supported in a standard monomode fibre. Theoretically there should be no coupling between the modes traveling in a perfectly cylindrical waveguide, but imperfections in the waveguide material composition

and geometry give rise to coupling between the modes. The mixing of the polarisation modes alters the propagation constant (β) of the modes propagating in the x and y directions, resulting in a periodic change of power between the modes.

The time varying SOP of the incoming signal needs to be matched continuously, as momentary mismatches can lead to a loss of data. The continuous matching of the SOP is referred to as *endless control*.

One of the apparently simplest solutions is to employ polarisation maintaining fibre but excessive manufacturing cost has limited the use of this fibre type. Also uprooting the conventional single mode fibre network to replace it with the polarisation maintaining fibre would not be feasible. However new local networks based on polarisation maintaining fibre could certainly be an alternative in principle.

Other methods relying on mechanical fibre squeezing techniques to make the fibre birefringent have been used in field demonstrations of coherent systems[8]. Refined endless polarisation methods using algorithms to control individual polarisation correcting devices have also been reported[34].

State-of-the-art integrated optic devices [35] and complex control methods [36] including polarisation diversity schemes[37], auger well for comprehensive confinement of the problem of polarisation.

2.3 Homodyne Detection

A homodyne receiver (figure 2.2a) is one which requires the local oscillator to track both the frequency and the phase of the received signal, recovering the information down at the baseband. The bandwidth requirement of the homodyne baseband amplifier is halved in comparison to the IF bandpass amplifier needed for heterodyne detection. This implies that in comparison with heterodyne receivers, homodyne receivers have their noise power reduced in half and consequently a receiver sensitivity improvement of 3dB, assuming only additive white noise. With such receivers the signal bandwidth

can be extended to that of the receiver.

However for real systems, assuming white additive noise for signals at baseband and at the IF is too simplistic as the $1/f$ noise and the f^2 noise, depending on the bit-rates, become significant and needs to be considered together with the additive white noise.

A serious drawback of homodyne receivers is that very tight tracking of the frequency and phase is needed. A phase difference of 90° between the local oscillator and the received signal will result in zero output signal, thus optical phase locked loops (OPLL) are employed to track the phase of the received signal. Even with strict control of the phase, the non-zero laser linewidth contributes a phase noise and degrades the receiver sensitivity. As shown previously in table 2.5, homodyne receivers are more sensitive than heterodyne receivers and therefore demand a very tight control of the phase. Even with the advantages that homodyne receivers have over heterodyne receivers, phase matching between the local oscillator and the signal is very difficult.

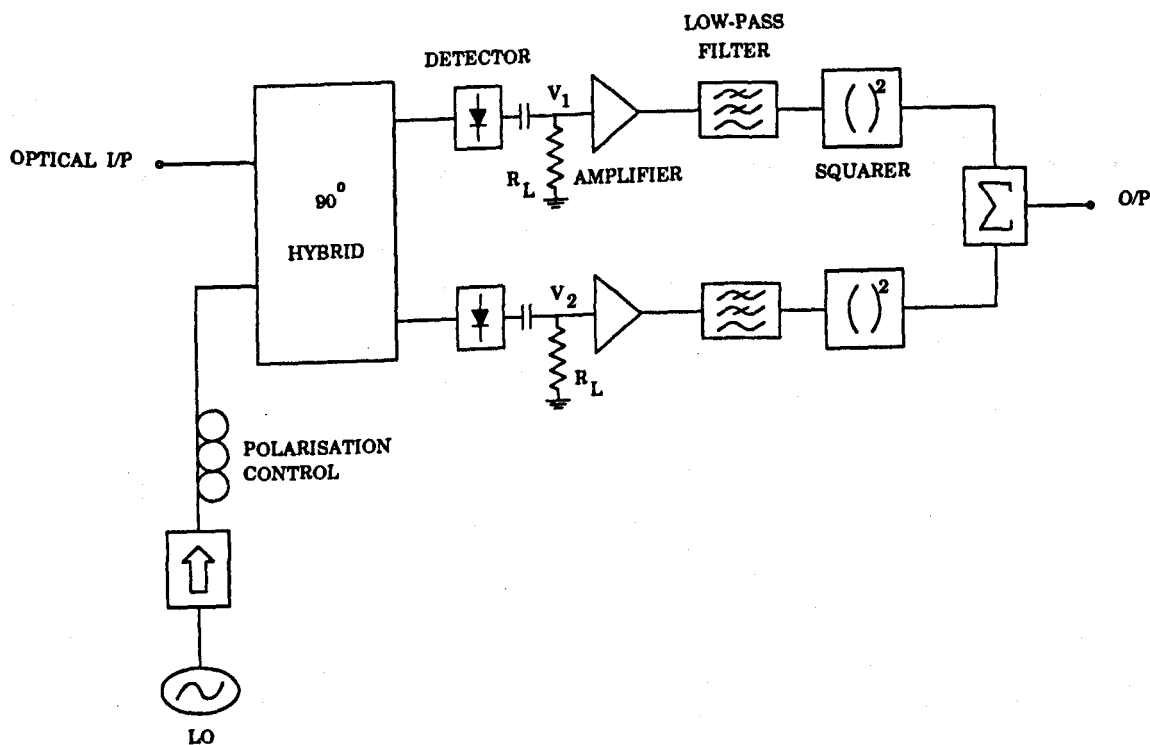


Figure 2.5: Two-arm phase diversity receiver for homodyne detection

However, a receiver type that provides baseband operation and is tolerant to phase

noise at the same time is the *phase-diversity homodyne receiver* illustrated in fig 2.5. The coupler mixes the local oscillator signal with the received signal in such a manner that for a two-phase phase diversity scheme, the 90° hybrid fields are[37]:

$$E_1 = \sqrt{\frac{L}{2}} \cdot (E_s + E_{lo}) \quad (2.4)$$

$$E_2 = \sqrt{\frac{L}{2}} \cdot (E_s + jE_{lo}) \quad (2.5)$$

where $-10\log(L)$ is the power loss (dB), $L=0.5$ for the two branch case of 3dB intrinsic loss, E_s and E_{lo} are the received signal and the local oscillator electric fields respectively. The voltages produced by the photodetectors are then

$$V_1 = A_s d \cos \phi \quad (2.6)$$

$$V_2 = A_s d \sin \phi \quad (2.7)$$

Here ϕ is the total phase noise, d is the data sequence of 1's or 0's and A_s is the signal amplitude given by

$$A_s = RR_L \sqrt{P_s \cdot P_{lo}} \quad (2.8)$$

The signal and local oscillator powers at the two output ports are given by P_s and P_{lo} respectively. R is the detector responsivity and R_L is the load resistance, as shown in figure 2.5. The output voltages from the two filters are squared and summed resulting in a final output voltage independent of phase noise:

$$V_T = V_1^2 + V_2^2 = A_s^2 d \quad (2.9)$$

This scheme can be extended to three or four-branched phase diversity receivers to reduce the intensity noise penalty and the polarisation sensitivity. Increasing the number of branches further is not practical since it involves both increased electronic circuit complexity and reduced overall sensitivity due to the loss associated with the additional hybrid ports[16]. The total voltages obtained after the summing stage is inversely proportional to the number of branches. Thus to sustain a moderate S/N for a large number of branches, a larger local oscillator power will be needed.

2.4 Heterodyne Detection

A heterodyne receiver (figure 2.2b) employs a local oscillator offset from the received signal carrier frequency. As with the homodyne case the two signals are coupled together before illuminating the detector. The optical mixing generates the difference frequency, (IF); this generally falls in the giga-hertz region for high bit-rates.

A heterodyne receiver needs only to track the carrier frequency, not the phase, of the received signal. The bandwidth needed for heterodyne reception can be as large as five times the signal bandwidth if a nonlinear modulation format is used. Provided that the bandwidth is obtainable, the difficulties associated with OPLL's make heterodyne receivers an attractive option.

Heterodyne techniques have an added advantage of allowing the mapping of any fibre chromatic dispersion directly into the electrical domain, such that electrical phase correction techniques may be adopted to avoid dispersion-induced distortions.

2.5 Fibre Chromatic Dispersion

Pulse broadening in monomode fibre arises from interaction between the fibre chromatic dispersion and the finite spectral linewidth of the optical source. Optical sources be they lasers or LED's, do not emit a single frequency but a band of frequencies. Thus the individual spectral components of a single light pulse transmitted through a fibre will experience different delays causing broadening of the pulse. The total fibre chromatic dispersion is comprised of components resulting from the fibre material (material dispersion), the fibre structure (waveguide dispersion) and also the refractive index profile (profile dispersion).

Waveguide dispersion results from variations in the group velocity with wavelength for a particular propagation mode. Loosely, we can think of this as the angle between the ray and the fibre axis varying with wavelength, whence the transmission time for

the ray varies leading to dispersion. For single mode fibres waveguide dispersion is exhibited when $(d^2\beta/d\lambda^2) \neq 0$, where β is the propagation constant. This dispersion mechanism is of significance when dealing with single mode fibres.

Material dispersion corresponds to nonlinear variation of the phase velocity of the propagating wave with wavelength as a result of the material properties themselves (the refractive index) rather than the waveguide structure.

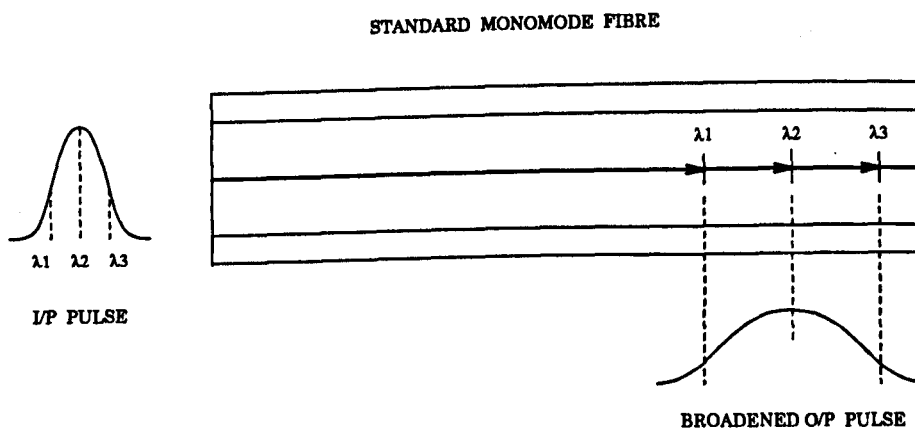


Figure 2.6: Pulse broadening due to fibre dispersion[38]

The effect of pulse spreading is demonstrated in Figure 2.6. The pulse spreading due to material dispersion may be defined as:

$$\Delta T = \frac{L\lambda}{c} \left| \frac{d^2n}{d\lambda^2} \right| \Delta\lambda \quad (2.10)$$

The dispersion (units: ps/nm/km) is a function of the change in refractive index with respect to the wavelength ($dn/d\lambda$), the fibre length (L), the wavelength(λ) and the source linewidth ($\Delta\lambda$). A material is said to exhibit material dispersion when $(d^2n/d\lambda^2) \neq 0$.

Conventional single mode fibres, based on silica, have near zero dispersion at $1.3\mu\text{m}$ but on operating in the lower loss $1.55\mu\text{m}$ window the dispersion increases to some 15-20ps/nm/km. By appropriately re-designing the waveguide, however, it can be arranged that the material and waveguide dispersions cancel at the desired wavelength. Hence the dispersion zero can be shifted to the $1.55\mu\text{m}$ low loss window, a typical

Modulation format	Chromatic dispersion index (γ)		B^2L (Gbit/s) ² .km	
	1dB	2dB	1dB	2dB
ASK	0.220	0.275	≈ 5000	≈ 7000
MSK	0.150	0.183	≈ 4000	≈ 4700
CPFSK	0.096	0.121	≈ 2500	≈ 3000

Table 2.6: (bit-rate)² - distance product for various modulation formats

residual dispersion value is 3.5ps/nm/km [38]. Fibres designed in this manner are referred to as dispersion shifted fibres.

Fibre chromatic dispersion is a major obstacle in achieving long haul high bit-rate transmission over standard monomode fibres, degrading both receiver sensitivity and system performance. In order to alleviate the problem of fibre chromatic dispersion, constraining the linewidth of the optical source is imperative for transparent multi-gigabit systems. However, even with a narrow linewidth source, when the source is modulated the modulation sidebands in combination with fibre dispersion will impose a limit. A figure of merit commonly used to characterise the overall performance of a digital system operating over standard fibre is the (bit-rate)² - distance product[39]. The B^2L varies according to the modulation format used and the maximum allowable eye degradation given by the expression[40]

$$B^2L = \frac{\gamma \pi c}{D(\lambda) \lambda^2} \quad (2.11)$$

(units: (Gbit/s)².km) where B is the bit-rate, L is the fibre length, $D(\lambda) = 15\text{ps/km.nm}$, $\lambda = 1550\text{nm}$ and γ is the chromatic dispersion index. The (bit-rate)² - distance product for the chromatic dispersion index[40] corresponding to 1dB and 2dB eye closures is given in table 2.6 for various modulation formats.

The fibre length that satisfies equation 2.11 for a given bit-rate and modulation format is referred to as the dispersion limited maximum transmission distance.

The fibre chromatic dispersion is the slope of the delay experienced by each frequency component of the transmitted optical signal and defined in the following section.

2.5.1 Group delay

The transfer function of a single mode fibre, neglecting pure delay, is given by [41]:

$$h_{fibre}(f) = \exp \left\{ j2\pi^2 \ddot{\beta} (f - f_s)^2 L + j1.3\pi^3 \dddot{\beta} (f - f_s)^3 L + \dots \right\} \quad (2.12)$$

$\ddot{\beta}$ and $\dddot{\beta}$ are the second and third derivatives of the propagation constant $\beta(f)$ respectively ($\ddot{\beta} = -1.9 \times 10^{-26} \text{ s}^2/\text{m}$ [15ps/nm/km] and $\dddot{\beta} = 8.1 \times 10^{-40} \text{ s}^3/\text{m}$ [0.08ps/km/nm/nm]), where $\beta = \frac{2\pi}{\lambda}$ evaluated when $f = f_s$. L is the fibre length and f_s is the transmitter frequency.

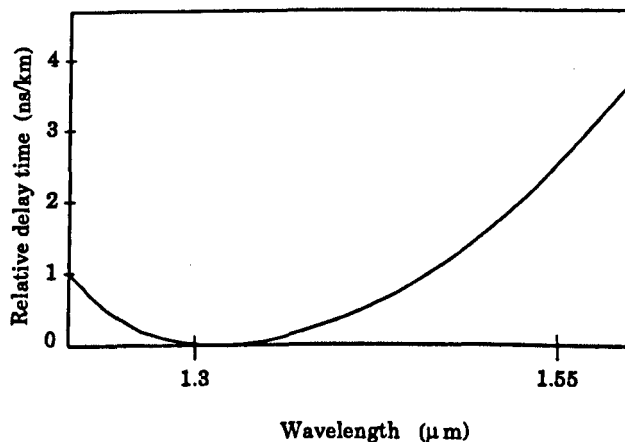


Figure 2.7: Relative delay of a standard single mode fibre

The variation in the relative delay (τ_f) with wavelength, for a standard 1.3μm zero dispersion fibre is shown in figure 2.7, and may be expressed as;

$$\tau_f = 2\pi \ddot{\beta} (f - f_s)L + 2\pi^2 \dddot{\beta} (f - f_s)^2 L + \dots \quad (2.13)$$

The first term of 2.13 defines the linear delay distortion and the second refers to the quadratic delay distortion.

The chromatic dispersion can then be expressed as the slope of the delay:

$$\frac{d\tau_f}{df} = 2\pi \ddot{\beta} L + 4\pi^2 \dddot{\beta} (f - f_s)L + \dots \quad (2.14)$$

2.5.2 Dispersion mapping in the electrical domain

A feature of a coherent receiver is that any dispersion in the optical domain is linearly translated into the electrical domain upon detection. Dispersion mapping with direct detection is a nonlinear process. This is illustrated in the following simple analysis.

Consider the electric field of the message signal (e_s) modulated onto a spectrally pure optical carrier ($\cos\omega_c t$) to be represented as

$$E_s = e_s \cos \omega_c t \quad (2.15)$$

On detection, a photodiode produces a current given by

$$i_p = RP \quad (2.16)$$

where R is the detector responsivity (photocurrent per unit incident optical power) and P is the optical power. The optical power is proportional to the square of the electric field. Thus 2.16 then becomes

$$i_p = R\{E_s^2\} \quad (2.17)$$

It is evident from 2.17 that the photodiode current and the received signal electric field are not linearly related thus any dispersion in the optical domain will not be linearly mapped into the electrical domain with direct detection. However if we consider coherent detection, we have a local oscillator field of the form

$$E_{lo} = e_{lo} \cos \omega_{lo} t \quad (2.18)$$

After the mixing, the resultant electric field of the optical signal incident on the detector will be

$$E_{mix} = E_s + E_{lo} \quad (2.19)$$

Considering the heterodyne scheme where $\omega_c \neq \omega_{lo}$ then substitution of 2.15, 2.18 and 2.19 into 2.17 gives rise to

$$i_p = R(e_s^2 \cos^2 \omega_c t + e_{lo}^2 \cos^2 \omega_{lo} t)$$

The high frequency and dc components may be omitted to represent the signal at the intermediate frequency (I.F):

$$i_d = R\sqrt{P_{lo}}e_s \cos(\omega_c - \omega_{lo})t \quad (2.20)$$

Equation 2.20 reflects the linear relationship between the photodiode current and the electric field of the received signal, implying a direct translation of the dispersion into the electrical domain. Additionally equation 2.20 suggests that the detector photocurrent and receiver sensitivity can be increased by increasing the local oscillator power. Unfortunately the local oscillator intensity may not be increased indefinitely to increase the receiver sensitivity as the diode shot noise is increased proportionally. The S/N ratio reaches a limit known as the quantum limit for coherent detection[13].

With heterodyne detection the mixing process maps the signal at the IF preserving the complex envelope of the message signal unlike homodyne detection where the phase information is not retained with the mapping of the signal at baseband. The preservation of the phase information associated with heterodyne detection allows for the implementation of electrical IF phase equalisation strategies to correct for the fibre chromatic dispersion.

2.5.3 Dispersion variation with local oscillator frequency¹

Transmission in the low loss $1.55\mu\text{m}$ window over conventional $1.3\mu\text{m}$ zero dispersion fibre results in a faster propagation of the high frequency (short wavelength) components. The choice of local oscillator frequency on heterodyning determines the in-band relative group delay characteristics of the signal mapped at the IF. Consider the following cases:

Local oscillator frequency < signal frequency

If we assume that a signal of bandwidth BW is centred about the optical carrier frequency f_s and the local oscillator (ideal) is at f_{lo} , then mixing of these signals (convolution in the frequency domain) results in the direct mapping of the signal down at

¹It should be noted that the relationship between the relative delay time and choice of the local oscillator frequency has been wrongly quoted by the authors in reference [41].

the IF as shown in figure 2.8. The signal spectrum about f_s is then translated down to the IF retaining its original spectral shape and group delay characteristics. To simplify matters let us assume that the local oscillator can remain fixed and that increasing f_s will increase the IF. Increasing the IF relates to a shift in f_s towards the shorter wavelengths and a decrease in the relative group delay. This may be expressed as

$$IF \uparrow = f_s \uparrow = \lambda \downarrow = \tau_f \downarrow$$

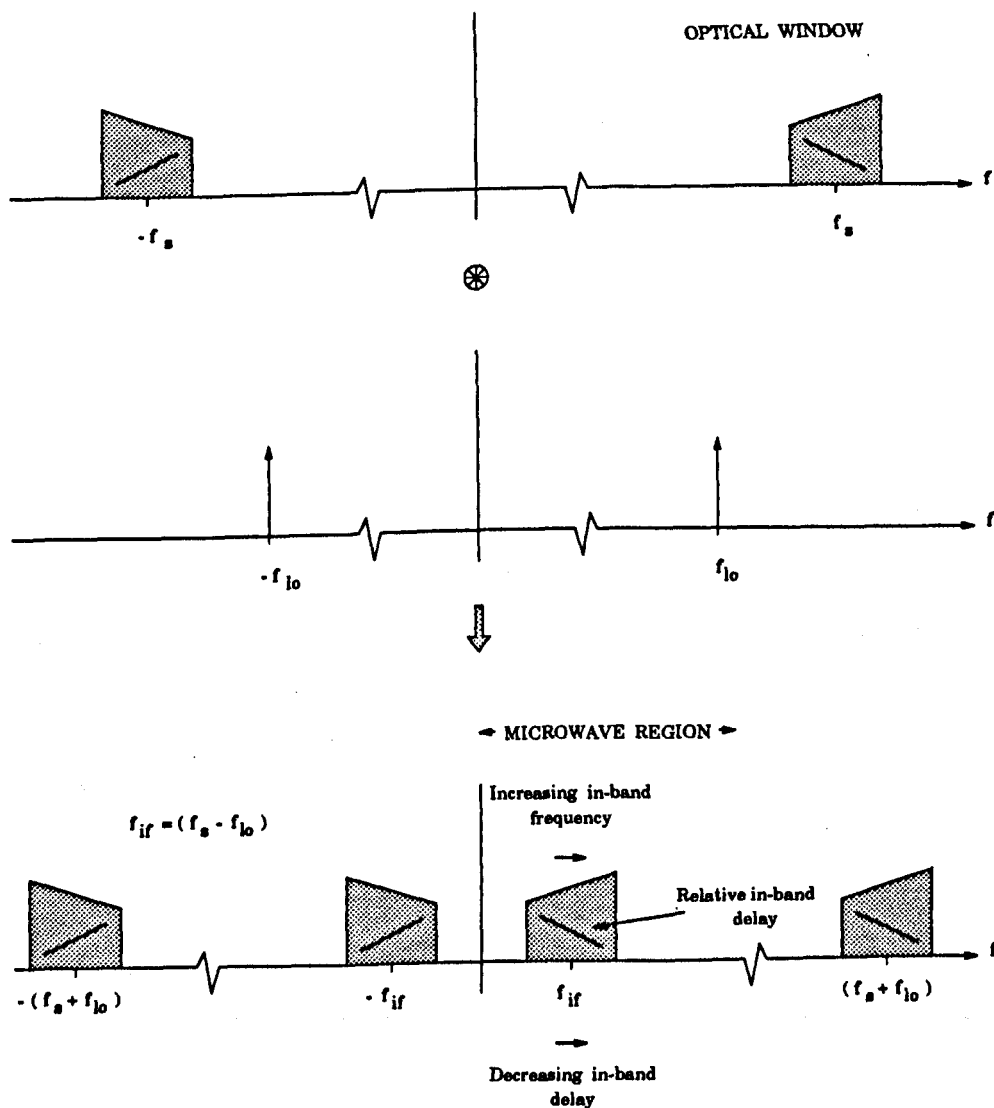


Figure 2.8: Signal and dispersion mapping when local oscillator < signal frequency

Local oscillator frequency > signal frequency

In this case when the local oscillator frequency is set higher than the signal, as shown in figure 2.9 the frequency spectrum and the group delay characteristics at the IF are reversed as a consequence of the mapping. Therefore to increase the IF, a shift in the signal frequency f_s towards the longer wavelengths is required which implies an increase in the relative group delay. This may again be expressed by

$$IF \uparrow = f_s \downarrow = \lambda \uparrow = \tau_f \uparrow$$

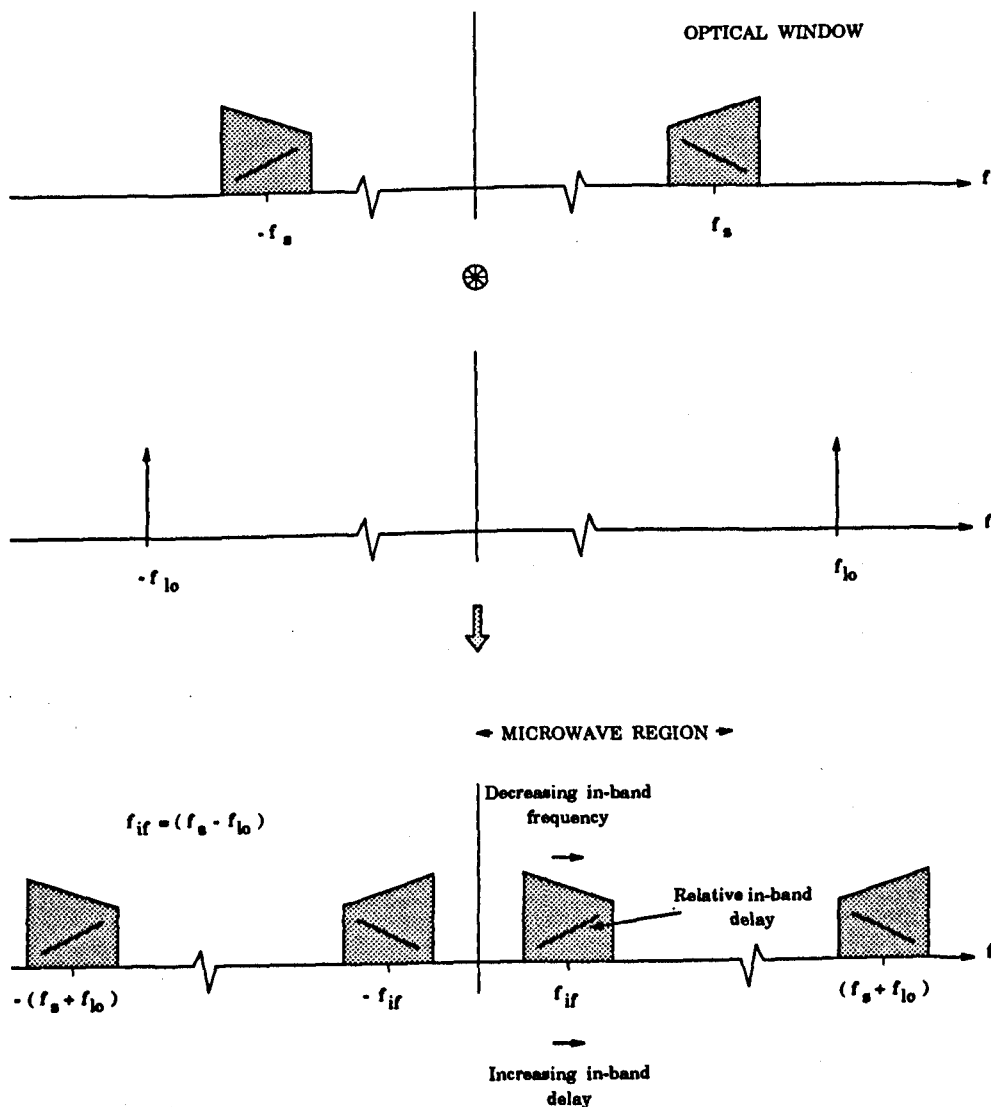


Figure 2.9: Signal and dispersion mapping when local oscillator > signal frequency

2.6 Summary

In this chapter the relative merits of coherent detection and conventional intensity modulated direct detection systems have been discussed, noting specifically on the increase in receiver sensitivity and denser FDM channel spacing attainable with coherent detection. The device requirements for both heterodyne and homodyne detection have been outlined and the impact of fibre chromatic dispersion addressed. The underlying principle of linear dispersion mapping from the optical to the electrical domain has been illustrated with a view to addressing, in the following chapter, state-of-the-art strategies for compensation of the fibre dispersion in both the electrical and optical domains.

Chapter 3

Review of Current Equalisation Strategies

3.1 Introduction

In the previous chapter the attributes of coherent receivers were outlined, noting specifically the improvement in the receiver sensitivity and denser FDM channel spacing obtainable with coherent systems. The problems and limitations imposed on the attainable bit-rate and transmission length by fibre chromatic dispersion were addressed with a view to applying optical and electrical equalisation techniques to correct for any dispersion effects.

The term “optical domain equalisation” is used to encompass equalisation techniques that may be performed before transmission at the transmitter, in-line or immediately prior to detection. Electrical domain equalisation implies the application of post-detection correction methods. The linear mapping of the dispersion from the optical to the electrical domain associated with coherent detection allows for the application of post-detection equalisation.

This chapter reviews some current state-of-the-art optical and electrical domain fibre chromatic dispersion equalisation techniques.

3.2 Optical Domain Equalisation

The complex post-detection signal processing and signal shaping circuitry required to electrically correct for any fibre chromatic dispersion in a direct detection system have led to the adoption of optical domain equalisation techniques. The methods adopted for optical equalisation range from pre-distorting the modulated signals before transmission to using interferometric devices prior to detection.

As optical equalisation can be performed either on transmission, in-line or prior to detection, then this suggests that this form of equalisation can readily be applied to coherent systems.

3.2.1 Pre-transmission equalisation

Optical pulses propagating along a length of fibre are subjected to pulse broadening. Pre-transmission equalisation methods exploit in a constructive manner the effect of fibre chromatic dispersion. This may be done by either

- pre-chirping methods or
- exploiting the fibre nonlinear effects.

Pre-chirping techniques

With direct modulation of a laser diode rapid changes in the carrier densities give rise to fluctuations in the refractive index of the active region resulting in frequency shifts of the laser emission, known as chirp. For modest bit-rates, biasing the laser source above threshold and externally modulating it to reduce the drastic carrier density fluctuations lessens the effect of chirp.

The bit-rate distance (BL) product limit due to chirp is illustrated for Gaussian and

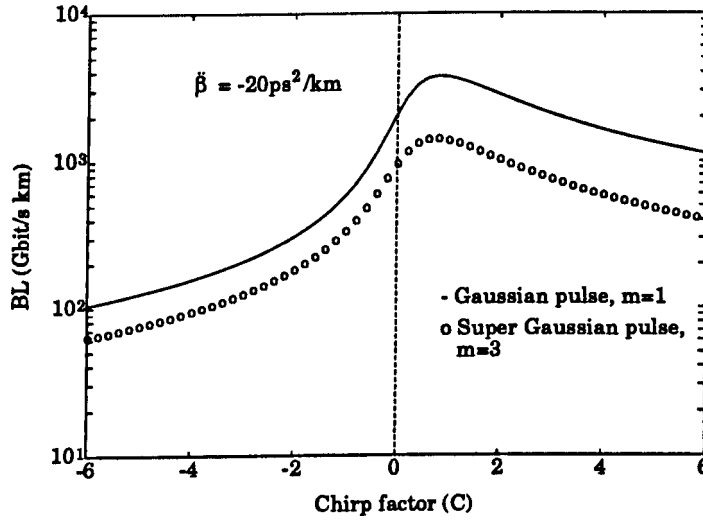


Figure 3.1: Dispersion limited bit-rate distance product for Gaussian and super - Gaussian pulses as a function of the chirp factor C [42]

super-Gaussian pulse shapes in figure 3.1 where a Gaussian/super-Gaussian pulse is given by the expression

$$G(0, T) = \exp \left[-\frac{1 + iC}{2} \left\{ \frac{T}{T_0} \right\}^{2m} \right] \quad (3.1)$$

T_0 is the pulse half-width at $1/e$ - intensity point, T is the pulse half-width after broadening, C is the chirp factor and m defines the sharpness of the edges of a super-Gaussian pulse. If $m=1$ then the pulse is of a Gaussian shape while for any other integer value of m the pulse is referred to as a super-Gaussian. As m increases then the super-Gaussian pulse profile approximates that of an ideal square pulse. The steeper leading edges of the super-Gaussian pulse give rise to a wider frequency spectrum which results in a faster rate of broadening [42], and consequently a lower bit-rate distance product as compared to the Gaussian pulse. The maximum bit-rate distance product is obtained when C is positive ($C \approx 1$) and when the product βC is negative. As conventional semiconductor lasers have a chirp factor which is negative this suggests that a slightly positive value of the dispersion parameter (β) is required to attain the maximum BL product. This is best illustrated in figure 3.2 demonstrating the effect of pulse narrowing. The pulse narrowing is a result of the reduction in the net chirp. The effect

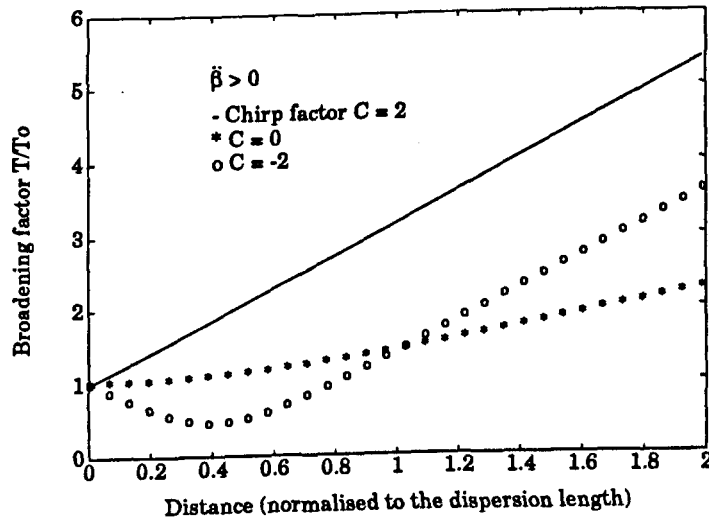


Figure 3.2: Broadening factor of a Gaussian pulse against distance for a range of chirp factors with $\beta > 0$. The dispersion length L_D is defined as the propagation length over which the dispersive effects become important $L_D = \frac{T_0^2}{|D|}$ [42]

of the fibre dispersion cancels the initial pulse chirp at a particular propagation length resulting in a compressed pulse shape[43]. As the fibre length is further increased the pulse starts to broaden again as the fibre dispersion becomes predominant. Iwashita et al. demonstrated this effect for a directly modulated DFB laser diode at $1.55\mu\text{m}$ over standard monomode fibre of 15ps/km.nm dispersion. Pulse compression was achieved by using a DFB LD for which increases in the injection current resulted in the shift towards the shorter wavelengths of the emission spectrum. In this manner the authors observed a pulse reduced to 21% of its original pulse width after 100km of transmission.

The extent to which the pulse broadens is given by the expression[42]

$$\frac{T}{T_0} = \left[1 + \frac{\Gamma(\frac{1}{2m}) C \beta L}{\Gamma(\frac{3}{2m}) T_0^2} + \frac{\Gamma(2 - \frac{1}{2m}) (1 + C^2) (m \beta L)^2}{\Gamma(\frac{3}{2m}) T_0^4} \right]^{\frac{1}{2}} \quad (3.2)$$

where Γ is the gamma function, $\beta = -20\text{ps}^2/\text{km}$ and L is the fibre length.

The mechanism of balancing the chirp with the fibre dispersion has been exploited to attain multigigabit transmission in excess of the dispersion limit using pre-chirping

methods by many authors[44, 45, 46, 47].

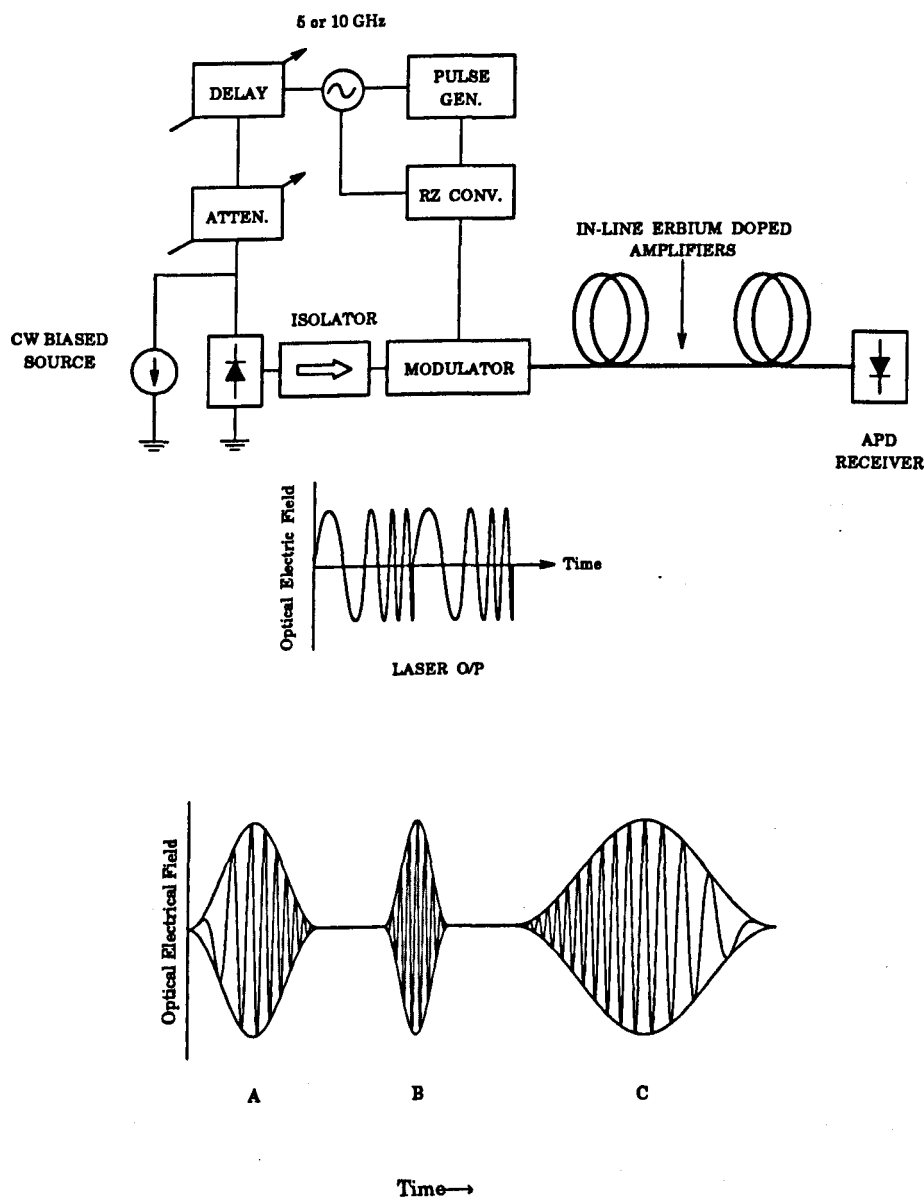


Figure 3.3: Optical pre-chirping transmission system illustrating propagation of pre-chirped pulse; A) before transmission, B) in transmission and C) received optical pulse [44]

The pre-chirp techniques are based on the pre-distortion methods outlined by Koch et al. With this method a frequency modulated light signal is obtained from the output of the DFB LD, achieved by modulating the injection drive current to the laser diode. The output of the laser diode is then intensity modulated. The frequency modulation of the LD signal results in producing a signal consisting of the low frequency components at

the front end of the pulse and the higher frequency components at the rear end of the pulse. As illustrated in figure 2.7 the high frequency (smaller wavelength) components travel faster than the low frequency (longer wavelength) components. Therefore on transmission the pulse becomes narrower when the fibre chromatic dispersion counter balances the chirp effect. The net pulse width is at a minimum but then starts to increase in sympathy with the distance such that a broadened pulse is detected at the receiver as illustrated in figure 3.3. With this method, combining pre-chirping and external modulation, 10Gbit/s transmission over 100km of standard single mode fibre has been reported. This fibre span is twice the dispersion limited distance.

In the previous chapter nonlinear effects such as four wave mixing FWM, stimulated Brillouin scattering SBS, and stimulated Raman scattering SRS were introduced addressing the implication of these effects on FDM coherent systems. The effects of these fibre nonlinearities can be minimised in a number of ways, but there are circumstances in which their presence is favoured for the realisation of optical equalisation.

Intensity dependent variations in the refractive index are referred to as Kerr nonlinearities. The high optical field perturbs the atomic structure of the medium to induce an oscillating polarisation which upon radiation produces a distorted field. The variations in the refractive index cause phase shifts resulting in the peak of a pulse having a different transmission phase as compared to the leading or trailing pulse edges. The time varying phase changes give rise to a time varying frequency spectrum of the pulse. This is referred to as self phase modulation (SPM).

Self phase modulation is a favoured nonlinear effect as it allows for pulse compression[42] in addition to pulse broadening when combined with fibre chromatic dispersion. Furthermore, pulse compression can be obtained in the fibre itself when critical pulse shapes of high optical powers are used. Such pulses are known as solitons. Solitons are the only stable solution (hyperbolic secant pulse) to the nonlinear differential equation that governs the transmission of pulses in a fibre [48]. The interplay of the nonlinear self phase modulation (SPM) and fibre dispersion effects allow pulse compression and pulse spreading to balance each other giving rise to the solitons. If on transmission the

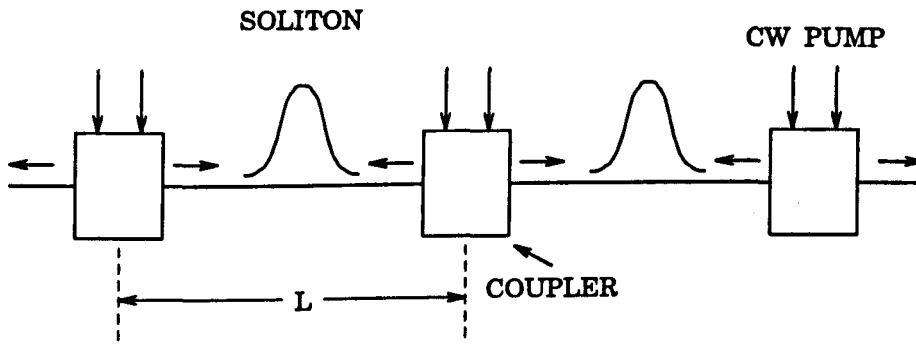


Figure 3.4: Soliton transmission system comprising of many repeaters of L separation. The pump lasers inject cw light in both directions through wavelength-dependent directional couplers [42]

pulse shape is not quite right, but is of sufficient power to sustain soliton propagation, then the pulse will reshape itself until it becomes a soliton and propagate undistorted inside an ideal lossless fibre for arbitrarily long distances. However, in practical systems fibre losses limit the transmission of solitons and therefore in-line optical regenerators (Erbium doped fibre amplifiers EDFAs) are generally employed to pump-up the optical powers at intermediate stages as illustrated in figure 3.4. A draw back of the in-line intermediate amplifying stages is that spontaneous emission noise is introduced to the soliton pulses. The noise, in addition to degrading the signal to noise ratio causes a subtle frequency shift of the carrier. The change in the average pulse frequency due to the interaction between the soliton and the amplifier spontaneous emission noise is referred to as the Gordon-Haus effect [49]. The change in the average pulse frequency translates to a change in the group velocity introducing an uncertainty in the pulse arrival time (timing jitter). As a consequence of the uncertainty in the arrival time, the pulses have to be separated by a spacing of approximately ten pulse widths. This separation also serves to avoid any soliton - soliton interaction. The B^2L product for soliton propagation is limited by the noise induced timing jitter and is given by [42]:

$$B^2L \leq 10000 \text{ (Gbit/s)}^2 \text{ km} \quad (3.3)$$

Even with the noise limitations associated with in-line amplification stages soliton propagation over 10,000km at bit-rates in excess of 5Gbit/s have been demonstrated [50, 51]. The manifestation of the soliton illustrates the natural solution to optical equalisation through the interplay of the fibre nonlinear effects.

3.2.2 In-line equalisation

Dispersion shifted and dispersion flattened (DF) fibres offer the simplest solution to in-line optical equalisation. By reducing the fibre core size and increasing the core-cladding refractive index difference shifts the fibre dispersion profile towards the longer wavelengths. The dispersion flattened fibre possesses two zero dispersion points and has a flat dispersion profile over the entire wavelength range $1.3\mu\text{m} - 1.6\mu\text{m}$. The flat dispersion characteristic is obtained with multilayer index profiles providing an overall dispersion of less than 2ps/nm.km , as illustrated in figure 3.5. A type of DF fibre based on the segmented core design has been demonstrated for optical equalisation purposes[52] with a near flat dispersion characteristic over a range $1.1\mu\text{m} - 1.7\mu\text{m}$.

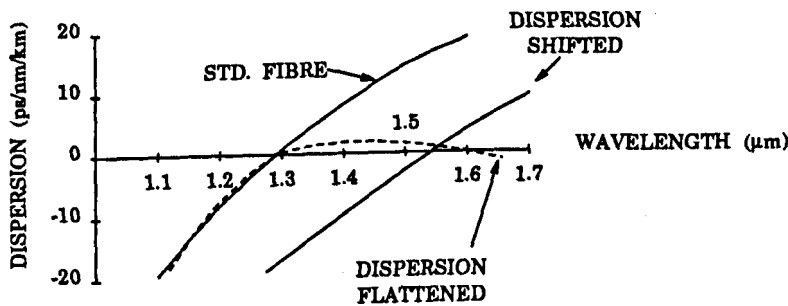


Figure 3.5: Dispersion characteristics for various fibres

Employing in-line amplifiers (EDFAs), Dugan and co-workers have reported 10Gbit/s transmission over 150km using the $1.31\mu\text{m}$ optimised dispersion compensating fibre.

Another fibre based technique exploits the negative dispersion characteristic of the linearly polarised (LP) spatial modes propagating in the fibre[53]. With this method the fundamental LP_{01} mode in the single mode fibre is converted into the LP_{11} mode, by means of a spatial mode converter[54]. The spatial mode converter is simply a fibre subject to helical microbending that allows coupling from the LP_{01} mode to the LP_{11} mode. A specially drawn two mode fibre of a specific length and a specific LP_{11} mode cut-off frequency is excited with the two mode pulses, such that restored pulses are obtained at the end of the two mode fibre. By appropriately choosing the cut-off wavelength of the LP_{11} mode a dispersion characteristic of opposite sign to that of the standard monomode fibre can be obtained[55]. In this way Poole and co-workers

corrected for the dispersion produced by 5km of standard monomode fibre with 400m of two mode fibre.

The lengths of dispersion flattened (DF) and two mode fibre required for optical equalisation using the techniques mentioned suggest that for long haul communication systems excessive lengths of correction fibre will be required.

A cheaper and practical solution to optical equalisation is one that employs in-line semiconductor laser amplifiers (SLAs). Semiconductor laser amplifiers (SLA) have been used in many system experiments as primary in-line optical regenerators to achieve long haul transmission. The SLA is generally operated in the linear gain region where the signal is optically amplified. While operating in the linear gain region the output of the SLA is a magnified replica of the input signal. However, increasing the gain of the SLA causes the amplifier to saturate. This leads to intensity dependent variations of the cavity refractive index thereby causing pre-chirping of the optical pulse through self phase modulation. Hence both fibre loss and pulse dispersion can be corrected by the SLA[56]. In this manner a transmission distance of four times the dispersion limit has been achieved, by transmitting a signal at 16Gbit/s over a 70km fibre length.

The advantage of this dispersion equalisation technique is that it is independent of the fibre nonlinearities and loss. The extent of SPM can be controlled by the amplifier gain to compensate for the dispersion produced by various fibre lengths.

The major disadvantage of this scheme is that rare earth doped fibre amplifiers, such as the erbium doped fibre amplifier (EDFA) are favoured over the SLAs mainly because of the high gains attainable[16], lower noise[57] and fewer compatibility problems associated with EDFAs.

A novel in-line dispersion equalisation method not relying on any dispersion shifted fibres or dispersion correcting devices, is that reported by Wedding [58], achieving transmission well beyond the dispersion limit.

This method is illustrated in figure 3.6, exploiting the dispersive nature of the fibre

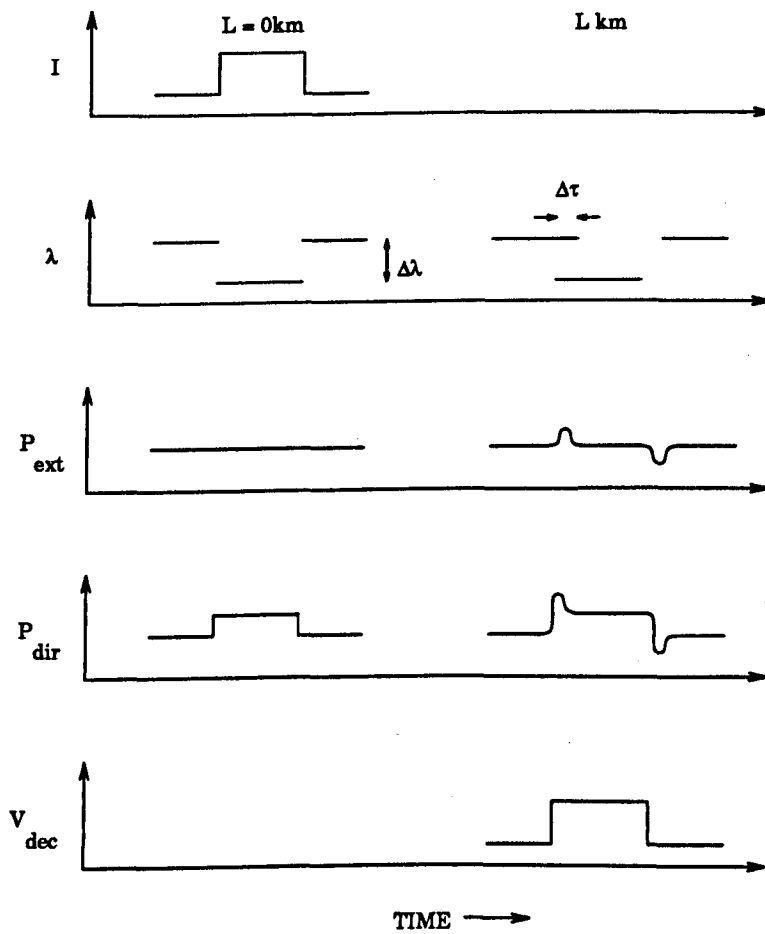


Figure 3.6: Dispersion-supported transmission [58]; I - laser drive current, λ - transmitter wavelength, P_{dir} and P_{ext} - optical power with direct and external modulation and V_{dec} - voltage after decision circuit

to emulate a frequency discriminator. The initial frequency modulated signal is transformed while in transmission in the fibre, into an amplitude modulated signal that can be detected by the receiver. The frequency discriminator behaviour of the fibre is a result of the frequency transitions in the transmitted signal giving rise to pulses in intensity. The polarity of the intensity variation is dictated by the direction of the frequency transitions. Any overlapping of the signal components results in power addition such that a positive pulse is observed. If however there is no signal component present then a negative going pulse, relative to the mean level, is observed.

Using an integrator or a low-pass filter in conjunction with a decision circuit allows the receiver to recover the non-return-to-zero (NRZ) signal.

For 10Gbit/s transmission the dispersion limited transmission length from equation 2.11 is $\approx 40\text{km}$. Wedding has reported transmission beyond the dispersion limit by four fold by transmitting at 10Gbit/s over 128km of standard fibre using a directly modulated laser diode at $1.55\mu\text{m}$. As this method relies on the fibre emulating a frequency discriminator, then amplitude modulated formats cannot profit from this equalisation technique.

3.2.3 Pre-detection equalisation

An effective optical domain equalisation method designed to counter the effect of the fibre's quadratic phase response is based on the Fabry-Perot etalon [59, 60, 61]. The equaliser has the characteristics of an all pass network; flat amplitude response with variable phase characteristics. The equaliser is positioned immediately prior to the detector as illustrated in figure 3.7 where the all pass optical equaliser is illustrated in

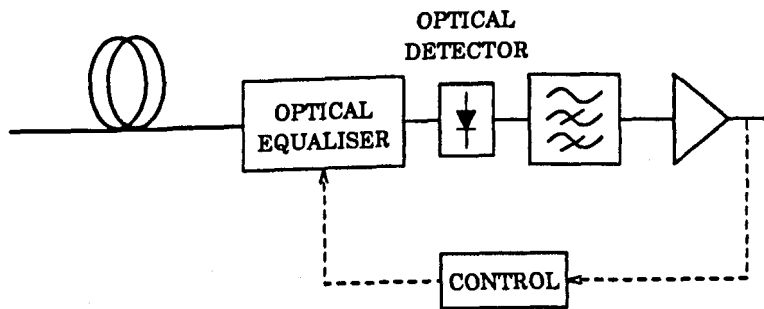


Figure 3.7: Transmission system with optical equalisation

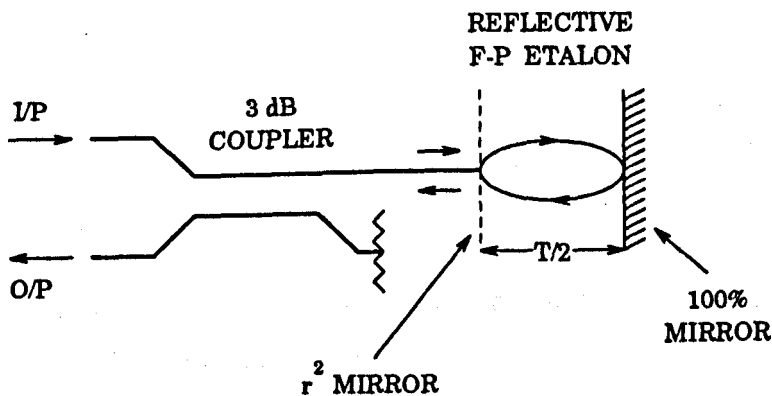


Figure 3.8: Transmissive equaliser

figure 3.8 utilising a 3dB coupler to transform the reflective structure into a transmissive

structure. The frequency response of the single-cavity reflective structure is

$$H_{eq}(\omega) = A \frac{1 + re^{j\omega T}}{1 + re^{-j\omega T}} = Ae^{j\psi(\omega)} \quad (3.4)$$

The phase ($\psi(\omega)$) in this case is given by

$$\psi(\omega) = 2\tan^{-1} \left[\frac{r \sin \omega T}{1 + r \cos \omega T} \right] \quad (3.5)$$

where r^2 is the power reflectivity of the front mirror, T is the round trip delay of the cavity and A is the amplitude constant. The delay can then be obtained from 3.5

$$\tau(\omega) = -\frac{d\psi(\omega)}{d\omega} = -2rT \frac{r + \cos \omega T}{1 + r^2 + 2r \cos \omega T} \quad (3.6)$$

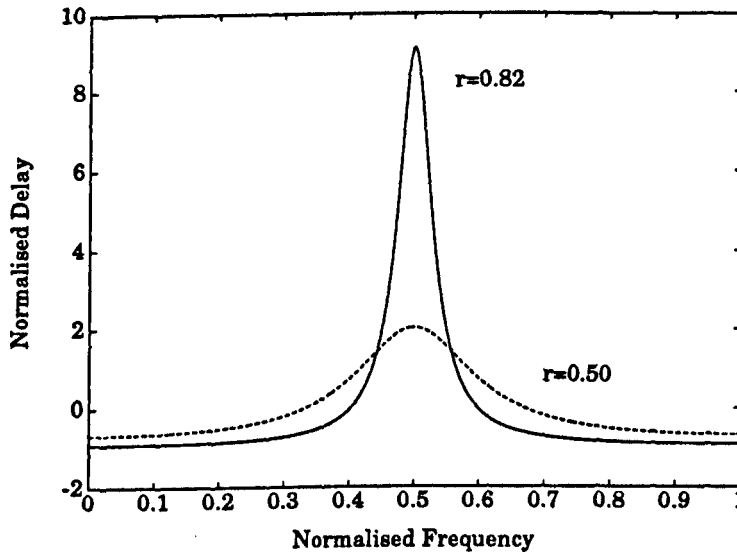


Figure 3.9: Delay characteristics of the optical equaliser

The delay characteristics of the optical equaliser for two front mirror reflectivity values is illustrated in figure 3.9. Any linear region of the delay characteristic can be used to correct for the fibre dispersion as the fibre delay about the $1.55\mu\text{m}$ window can be assumed to be linear. The feed back control loop shown in figure 3.7 allows the linear region of the equaliser delay response to be positioned relative to the signal centre frequency. This is done by piezoelectrically adjusting the length of the cavity which alters the round trip delay within the cavity. This method of optical equalisation has

been demonstrated for transmission of 8Gbit/s over 100km, extending the dispersion limit by two fold [62].

The correctable bandwidth may be extended by cascading two cavity structures, but this has the added problem of accurately controlling the cavity spacing.

3.3 Electrical Domain Equalisation

The linear mapping of the dispersion from the optical domain into the electrical domain associated with coherent systems can allow for the application of post detection microwave equalisation techniques, based on waveguide[63] or microstrip[41] structures. By varying the physical dimensions of the microwave structures the group delay characteristics can be altered to mirror those of the fibre delay. An equalised coherent heterodyne detection system is depicted in figure 3.10.

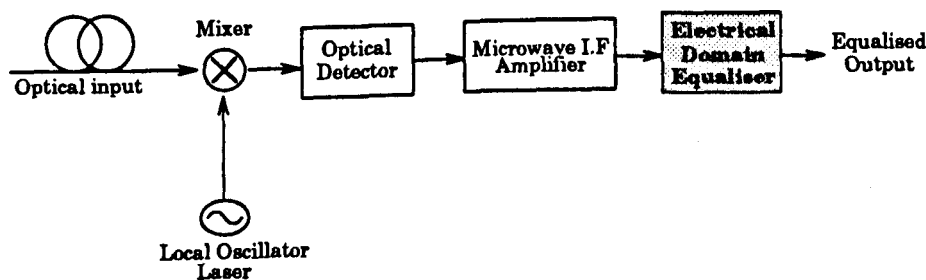


Figure 3.10: Heterodyne detection system with electrical equaliser

3.3.1 Waveguide Equalisers

Lumped element all-pass networks have been widely used at radio frequencies as phase equalisers while complex waveguide equalisers have been developed for narrow band millimeter-wave communication systems [64, 65], as illustrated in figure 3.11, while synchronous tapped delay line equalisers realised with short accurate lengths of transmission line have been proposed as adaptive equalisers [66].

At microwave frequencies, simple lengths of waveguide behave as all-pass structures, attenuating the signal very slightly while altering the phase. A waveguide equaliser

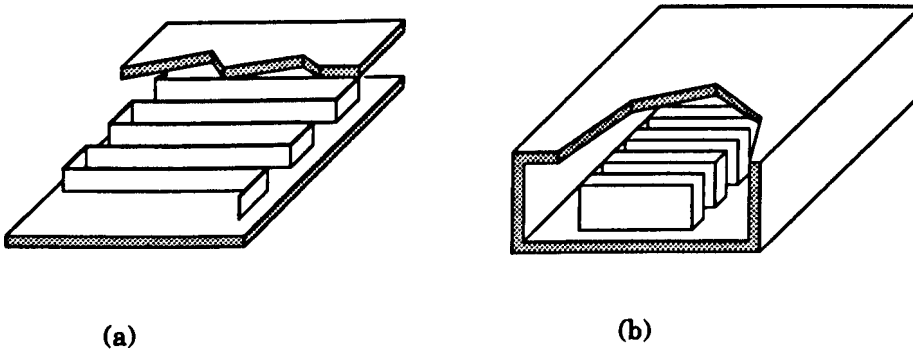


Figure 3.11: Waveguide delay equalisers. (a) Folded-tape meander-line type and (b) comb-type

reported by Winters works on this principle. By adjusting the different physical parameters of a waveguide, the phase and consequently the group delay characteristics are tailored to compensate for the delay produced by the fibre. As an equaliser with a delay slope opposite to that of the fibre delay is required, then by appropriately choosing the local oscillator frequency this condition can be satisfied. With the local oscillator set higher than the signal a waveguide equaliser can be used, as the inband delay slope is opposite in this case to that of the waveguide, as illustrated in figure 2.9.

An approximately linear delay is observed near twice the cut-off frequency when the the waveguide is utilised in the dominant mode, TE_{10} .

The cut-off frequency of a waveguide is given by:

$$f_c = \frac{c}{2a} \quad (3.7)$$

where c is the speed of light in free space (3×10^8 m/s), and a is the width of the waveguide of cross section $a \times b$ ($b = a/2$). The time delay across a fraction α of the bandwidth (B) is then given by [63]:

$$\Delta T(\alpha) = \frac{L_w}{c} \left\{ 1.186 - \frac{1}{\sqrt{1 - \left(\frac{1}{1.86 - \alpha B / f_c} \right)^2}} \right\} \quad (3.8)$$

As a safety margin the bandwidth B is restricted to $(1.86f_c - B < f < 1.86f_c)$. L_w is the length of the waveguide and the range of α is $0 \leq \alpha \leq 1$, such that at frequency f , $\alpha = (1.86f_c - f)/B$. The delays obtained with various values of B/f_c are illustrated

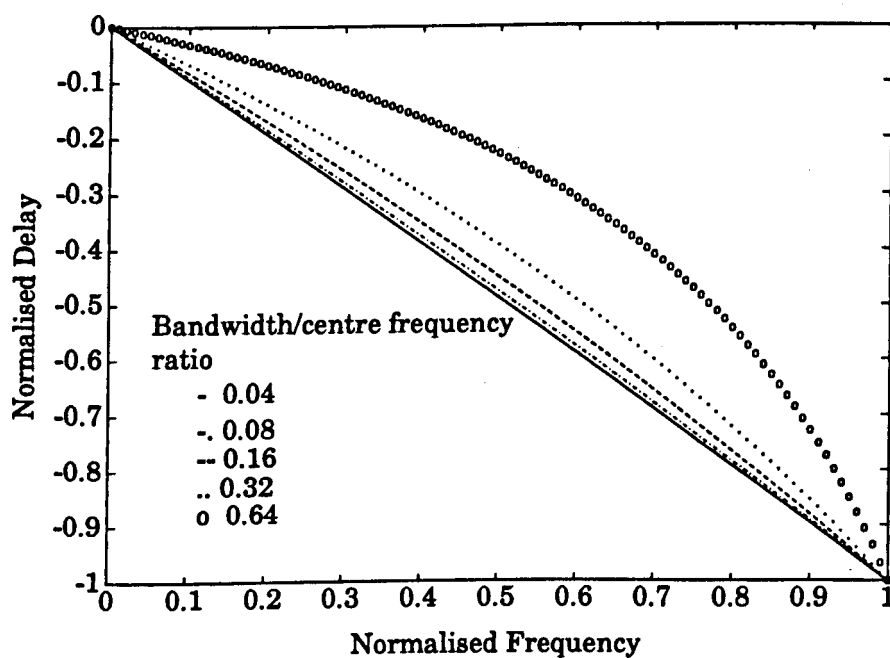


Figure 3.12: Normalised time delay versus frequency (α) for various values of B/f_c [63]

in figure 3.12 for 8Gbit/s transmission at $1.55\mu\text{m}$ over 68km of $1.33\mu\text{m}$ zero dispersion fibre. In order to obtain an approximately linear time delay, a low value of B/f_c is required, which results in a very long waveguide of a high cut-off frequency as shown in table 3.1.

Tight control on the deviation of the delay from the target not only increases the waveguide cut-off frequency but also increases the waveguide insertion loss. The waveguide

f_c (GHz)	B/f_c	a (mm)	L_w (m)	attn. (dB)
200	0.04	0.75	2.1	30
100	0.08	1.5	1.0	5.1
50	0.16	3.0	0.46	0.83
25	0.32	6.0	0.17	0.11
12.5	0.64	12.0	0.041	0.0093

Table 3.1: Characteristics of waveguide equalisers with $B=8\text{Gbit/s}$ and $L=68\text{km}$ [63]

loss is directly related to the cut-off frequency and is given by the expression (using a silver waveguide)[63]:

$$attn. = 5.14 \times 10^{-3} f_c^{3/2} L_w \quad (dB) \quad (3.9)$$

where f_c is in GHz. Both figure 3.12 and table 3.1 suggest that a trade-off needs to be effected between the maximum allowable deviation of the delay and the dimensions of the waveguide for the realisation of practical equalisers to compensate for long fibre lengths. Thus this method of equalisation is limited by the practicability of the physical dimensions of the waveguide.

3.3.2 Microstrip Equalisers

The second post detection equalisation method to be reviewed is microstrip based [41]. The microstrip equaliser is simply a dielectric substrate sandwiched between a single conducting strip and a conducting ground plane, as shown in figure 3.13. As with the waveguide case, the microstrip behaves as an all-pass network, thereby only affecting the phase of the signal. By choosing the length of the microstrip appropriately, the dispersion produced by a given length of fibre is corrected. The slope of the microstrip delay is opposite to that of the waveguide and thus the local oscillator frequency is set lower than that of the signal frequency as illustrated in figure 2.8. The application

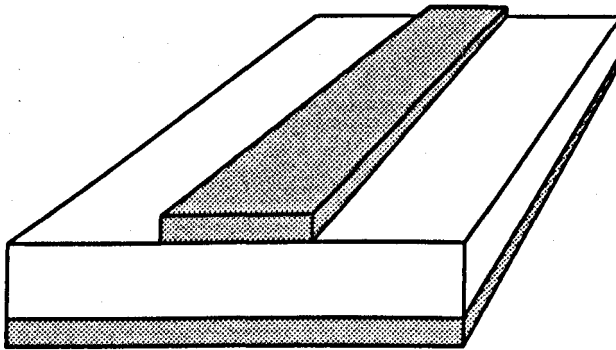


Figure 3.13: Microstrip line equaliser

of the microstrip equalisation technique for various fibre spans is illustrated in figure 3.14, based upon microstrip lines of varying lengths. The microstrip group delay τ_m is a function of the effective permittivity of the substrate dielectric and is given by the

Taylor expansion, taking into account the frequency dependent effective permittivity.

$$\tau_m = \frac{l}{c} \left\{ \sqrt{\epsilon_{\text{reff}}} + f \frac{d}{df} (\sqrt{\epsilon_{\text{reff}}}) \right\} \quad (3.10)$$

where l is the compensator length, c is the velocity of light in free space and ϵ_{reff} the frequency dependent effective permittivity.

The microstrip type equaliser has been demonstrated for 4-8Gbit/s over 200km of stan-

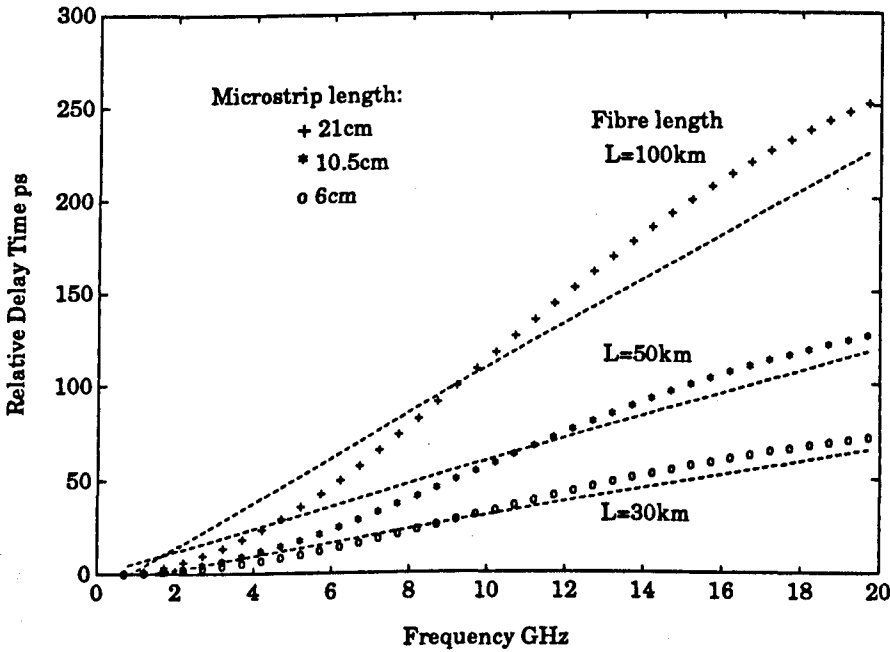


Figure 3.14: Delay characteristics for various microstrip equalisers. Dashed lines show the delay produced by a given fibre span

dard single mode fiber. The drawback of this method is that for large fibre spans, as with the waveguide case, large equalisers are needed; by way of example, compensation of 200km of fibre dispersion requires an equaliser 42cm long. A closer approximation to the fibre delay characteristics has been obtained by Nakagawa and Okoshi with the aid of a nonuniform optimised microstrip line [67]. Simulated system results employing the nonuniform equaliser suggest the possibility of equalisation of the fibre dispersion over a fibre length of 10,000km. However, correction of the dispersion for such a transmission distance requires a microstrip line 12m long! Although the uniform microstrip equalisers offer an effective approach to electrical domain equalisation, their physical size makes this approach impractical for long haul amplified systems.

Equalisation Technique	Pre-transmission		In-line		Pre-detection	Post-detection	
	Pre-distortion (TDM)	Pre-chirp	Dispersion Flattened (DF) Fibre	SLA	Wedding	Eta lon	Microstrip
Bit rate (Gbit/s)	10	5	10	16	10	8	8
Transmission distance (km)	100	450	150	70	128	130	200
Tx. distance normalised to dispersion limit	2.5	2.8	3.75	4.5	3.2	2	3.2
Modulation format	Amplitude	Amplitude	Amplitude	Amplitude	Frequency	Amplitude	CPFSK
Modulator type (Ext. or Dir.)	Both	External	—	Direct	Direct	External	External
Advantages	Exploits the fibre non-linear effects	Exploits the fibre non-linear effects	Independent of modulation type Can be tailor made	Independent of fibre non-linearity and fibre loss SPM can be controlled by SLA gain	No ext. modulator needed or any optical equalisation required	Reasonably adaptive	Can be integrated with other Rx. circuitry
Disadvantages	Need for current shaping ccts.	Need for current shaping ccts.	Large length of DF fibre needed	EDFAs preferred	Works with FM format only	Accurate tuning needed	Excessively large
References	[44]	[47]	[52]	[56]	[58]	[62]	[41]

Table 3.2 Comparison of various equalisation strategies

The study of microstrip equalisation techniques is extended further in the following chapter, exploring specifically the influence of variations in the substrate constituent material and geometry of the microstrip. Implications of equalisation for amplified systems will also be discussed.

A comparison of various equalised optical transmission systems is effected in table 3.2, highlighting some of the key features of the individual schemes. The in-line and post-detection equalisation strategies offer the best results for the B^2L product, with the SLA equalisation technique being superior. The SLA equaliser allows transmission well beyond the dispersion limit, but this has been superseded by the rare earth doped fibre amplifiers due to their better gain and compatibility with the transmission fibre.

3.4 Summary

This chapter has reviewed the various optical and electrical domain equalisation strategies that allow for the realisation of high bit-rate transmission beyond the dispersion limit. Of the many techniques discussed, the in-line optical domain techniques equalised for the fibre dispersion better than the other optical domain techniques. This feature is reflected in a higher B^2L product for the in-line methods.

Direct detection requires optical domain equalisation, and this can also be readily applied to coherent systems. However electrical domain equalisation is possible for heterodyne detection. This allows for full integration of the equaliser with the receiver in addition to offering an impressive transmission span beyond the dispersion limit.

The following chapter will address the implications of the electrical domain microstrip equaliser on transparent optically amplified systems exploring specifically the influence of the equaliser dimensional parameters on the delay characteristic

Chapter 4

Microstrip Equalisation Strategies

4.1 Introduction

The previous chapter reviewed various optical domain and electrical domain equalisation techniques drawing attention to the capabilities and practicalities of each. This chapter explores electrical domain equalisation, in particular microstrip based strategies, with a view to implementation in a coherent detection receiver.

The validity of the various available models for the frequency dependent substrate effective permittivity are evaluated and a comparison is effected with practical microstrip realisations.

The influence of the microstrip constituent material and physical geometry on the group delay characteristics is illustrated, and the implications for in-line transparent amplification are assessed.

4.2 Aspects of Microstrip Technology

Planar microwave integrated circuits (MICs) are now very widely used. The MIC structures comprise of a combination of a metal and the dielectric which is used to influence the wave propagation. A planar distributed circuit pattern is etched into a

metal layer supported on a low-loss dielectric - the substrate. There are various forms of MIC structure, each affording potential advantages for particular applications. Some transmission line MIC structures that can be utilised are illustrated in figure 4.1. The more common of these are the microstrip and coplanar waveguide types.

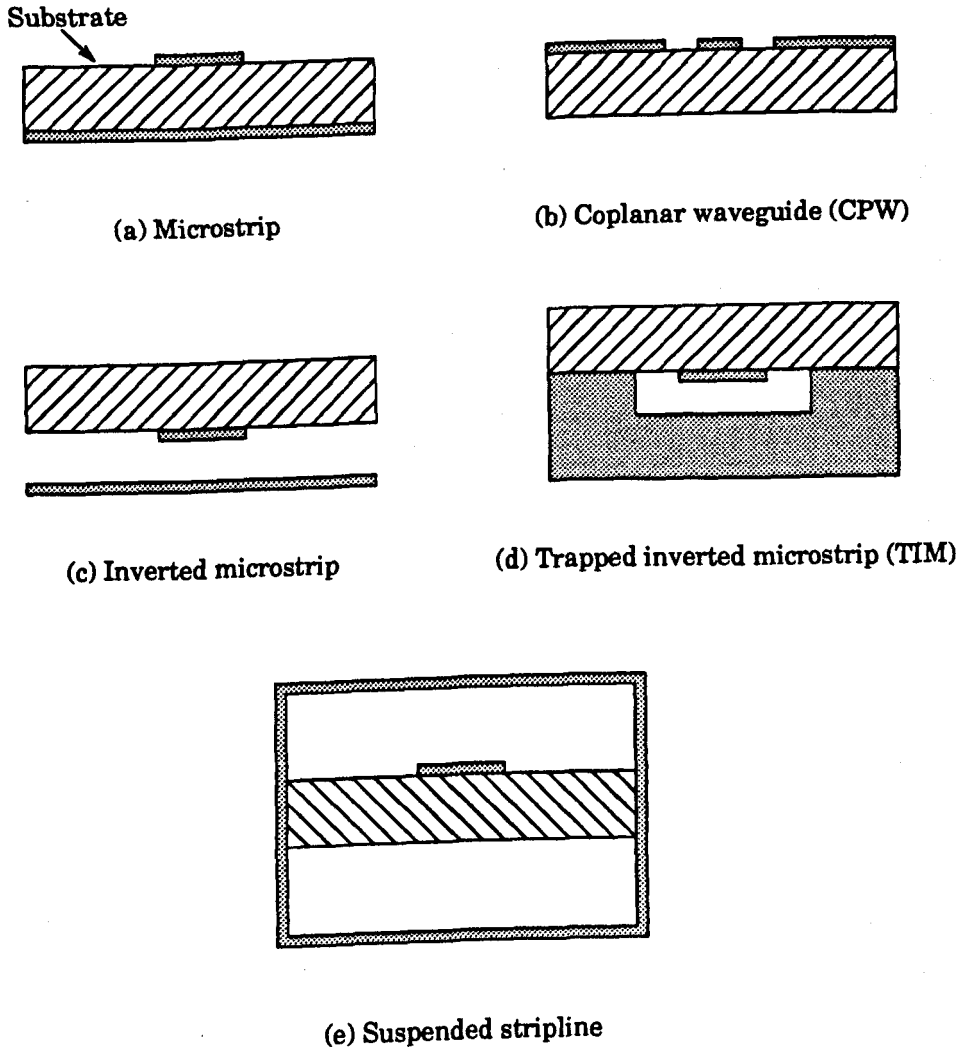


Figure 4.1: Some transmission line MIC structures [68]

The types of substrates available vary considerably and are chosen appropriately depending on the required tolerances and characteristic impedances of the circuits to be integrated onto the microstrip. The microstrip material is characterised by the permittivity of the substrate which can vary from 2 for a plastic (organic) substrate, to in excess of 80 for an inorganic substrate. Some of the key microstrip substrate materials are listed in table 4.1.

Substrate type	ϵ_r	Material type	Comments
Ceramic Al_2O_3 (99.5%, 96% pure)	9.8, 9.6	Inorganic	Commonly used. Low loss
Quartz glass	3.75	Inorganic	Low loss up at mm-wave operation
Titanium Oxide TiO_2	85	Inorganic	Highly temperature dependent.
PTFE glass fibre reinforced	2 - 2.5	Plastic	Slightly anisotropic due to inter-woven glass fibre.

Table 4.1: Some key microstrip substrates

Small size and accurately and reliably producible circuits achieved by means of photoetching techniques are some of the key factors that make microstrip technology attractive, whereas for some applications the low power handling capabilities and modest Q factor may favour waveguide technology over microstrip.

4.2.1 Microstrip Wave Propagation

A microstrip line as illustrated in figure 4.1 (a) comprises two conductors separated by a dielectric substrate. One of the conductors is used as the ground plane whereas the other is a thin strip transmission line of width w and thickness t . Both of the conductors are constructed of the same material of resistivity ρ and electrical conductivity κ . The dielectric substrate is defined by its height h , permittivity ϵ_r , dielectric loss factor $\tan\delta$ and effective surface roughness σ_{eff} .

Waveguide and coaxial transmission lines that contain a uniform dielectric can support a single well defined mode of propagation over a specified range of frequencies - TE for waveguides and TEM in the case of coaxial. At very low frequencies, mi-

crostrip wave propagation resembles closely the pure TEM mode. The presence of the inhomogeneous dielectric however causes perturbation in the field distribution along the transmission line. Increasing the operating frequency alters the field pattern from the static approximation. The wave propagating on the microstrip is then a hybrid mode, termed *quasi-TEM*, and there can exist other higher order modes in addition to the fundamental quasi-TEM mode. This is illustrated in figure 4.2 and the cut-off frequencies f_{HE_m} of the higher order HE_m modes are given by the expression [69]:

$$f_{HE_m} = \frac{c \cdot m}{2w_{eff}\sqrt{\epsilon_{r,eff}}} \quad (4.1)$$

where c is the velocity of light in free space, m is the m^{th} higher order mode, w_{eff} is frequency dependent effective strip width and similarly $\epsilon_{r,eff}$ is the frequency dependent effective substrate permittivity.

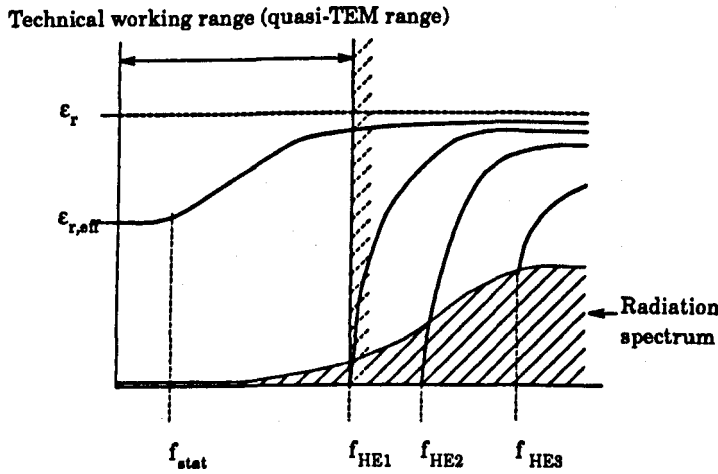


Figure 4.2: Hybrid modes in microstrip [69]

The width of the strip, the effective substrate permittivity and the characteristic line impedance are all frequency dependent parameters. Thus both the static and dynamic field distributions must be taken into account for an accurate definition of the longitudinally propagating wave. The electric and magnetic field distributions in microstrip for both static and dynamic cases have been well documented. The static approximation generally holds true for frequency ranges from $f = 0$ to $f \approx f_{stat} \approx 1-5\text{GHz}$, but a closed form approximation for any substrate of a given height and track thickness may

be obtained from:

$$f_{stat} = \frac{21.3}{(w + 2h)\sqrt{\epsilon_r + 1}} \quad (4.2)$$

At low frequencies the electric field between the conducting line and the ground plane corresponds to a parallel plate capacitor, a consequence of the presence of the transverse E - and H - fields. At low frequencies the magnetic field distribution is regular and unperturbed as in the case when there is no substrate present. The electric field on the other hand varies transversely along the face of the substrate. Immediately between the conductor and the ground plane the E_y component of the electric field dominates, giving rise to the effective parallel plate capacitance. The edges of the strip are pronounced with fringing fields resulting from the E_x and E_y components of the electric field as illustrated in figure 4.3.

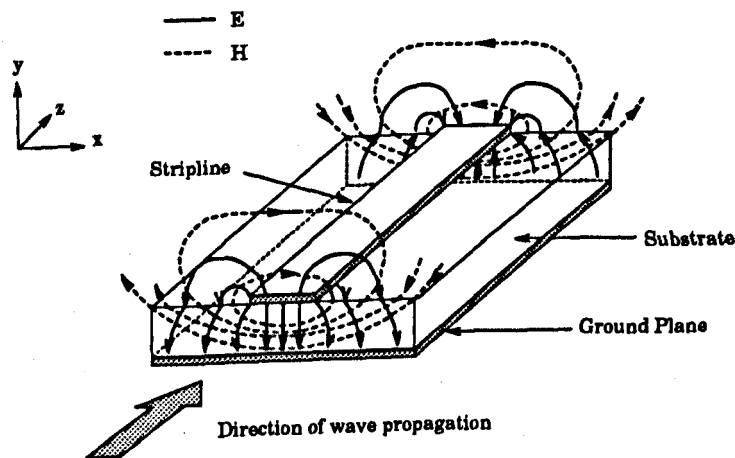


Figure 4.3: Static model of the electric and magnetic fields in the microstrip transmission line [69]

As the frequency increases then the longitudinal fields tend to dominate and the fringing is reduced. This results from the electric field concentrating greatly in the region immediately under the conductor, the coupling between the modes causing the field to be pulled into the substrate. Most of the wave propagation is then confined within the substrate and the effective permittivity of the substrate then approaches the asymptotic value ϵ_r . The dynamic field distribution for the fundamental hybrid mode (quasi-TEM) of a $\lambda/2$ microstrip line is illustrated in figures 4.4 and 4.5.

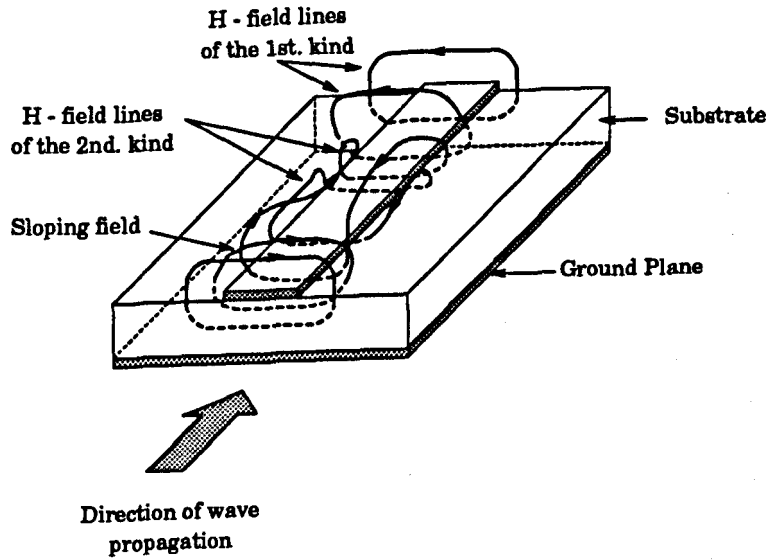


Figure 4.4: Dynamic model of the magnetic field in the microstrip transmission line of length $\lambda/2$ [69]

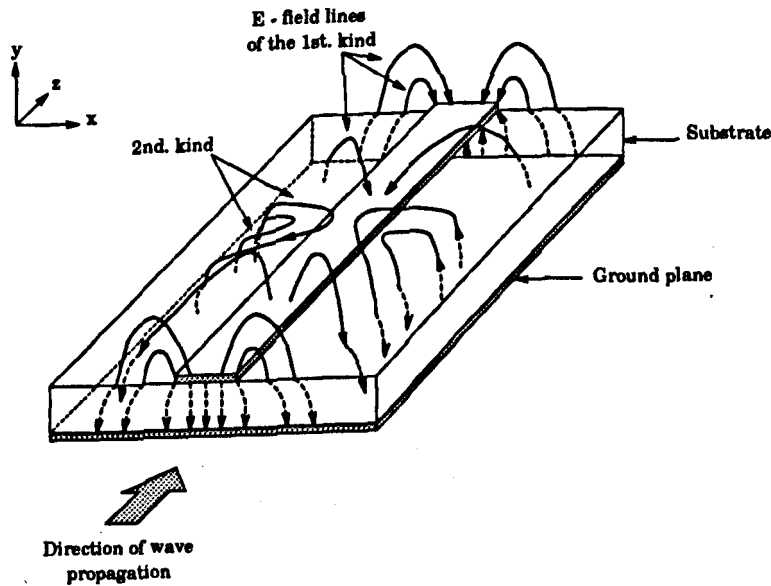


Figure 4.5: Dynamic model of the electrical field in the microstrip transmission line of length $\lambda/2$ [69]

Operation at high frequencies confines more of the wave to the area directly under the conductor implying an increase in $\epsilon_{r,eff}$ and thereby reducing the phase velocity (v_p) of the wave travelling along the line as given by the expression,

$$v_p = \frac{c}{\sqrt{\epsilon_{r,eff}}} \quad (4.3)$$

This suggests that the lower frequency components of a signal of finite bandwidth will propagate faster over microstrip than the higher frequency components. The microstrip structure thus has a delay characteristic opposite to that of the fibre, making it ideal for delay equalisation purposes if the local oscillator frequency at the receiver (heterodyne detection) is chosen appropriately.

4.3 Phase Equalisation Characteristics of Microstrip lines

In the previous chapter the utilisation of microstrip as a group delay equaliser was illustrated. In extension to this work, the implications of the group delay characteristics for variation in the choice of substrate, height of substrate and thickness of the conductor are now examined.

The group delay for a simple length of microstrip is given by (3.10)

$$\tau_m = \frac{l}{c} \left\{ \sqrt{\epsilon_{r,eff}} + f \frac{d}{df} (\sqrt{\epsilon_{r,eff}}) \right\}$$

where l is the compensator length, c is the velocity of light in free space and $\epsilon_{r,eff}$ the frequency dependent effective permittivity.

From 3.10 it is clear that the microstrip delay is a function of the effective substrate permittivity $\epsilon_{r,eff}$. As a first approximation to the microstrip dispersion $\epsilon_{r,eff}$ is approximated at the two frequency extremes as [68]

$$f \rightarrow \infty \quad \epsilon_{r,eff} \rightarrow \epsilon_r \quad (4.4)$$

$$f = 0 \quad \epsilon_{r,eff} \simeq \frac{1}{2}(\epsilon_r + 1) \quad (4.5)$$

An accurate frequency dependent effective permittivity model is required in order to examine the affects of varying the microstrip compositional and dimensional parameters on the group delay characteristics. There exist many reported models defining the dynamic dispersion characteristics of microstrip. A few robust models are examined now and a comparison is effected with practical microstrip delay line realisations. The best fit model is then used further for calculation of the microstrip group delay behaviour with respect to variation in the microstrip design parameters.

4.3.1 Microstrip Dispersion model

A number of "accurate" dispersion models have previously been reported, with one result varying substantially from the next. Therefore, to study the influence and implications of substrate composition and dimensions on the group delay characteristics, a model is required that is in good agreement with practical results for a large variety of substrates.

An accepted component in all the definitions of microstrip dispersion is the zero frequency substrate effective permittivity ($\epsilon_{r,eff,stat}$). A widely used model of $\epsilon_{r,eff,stat}$ is given by Wheeler [70], accounting for finite track thickness and the equivalent width arising as a consequence of the fringing fields.

Static value $\epsilon_{r,eff}$ model for finite strip thickness

At low frequencies the electric field distribution around the conductor is shared between the substrate and air dielectric. There exists a parallel plate capacitance effect between the conducting strip and the ground plane, while the electric field component at the edge of the strip fringes out.

A widely used model, taking into account strips of finite thickness, has been developed by Wheeler allowing for an accurate description of $\epsilon_{r,eff,stat}$. A conductor of thickness t and width w may be represented by a track of thickness $t = 0$, the same substrate

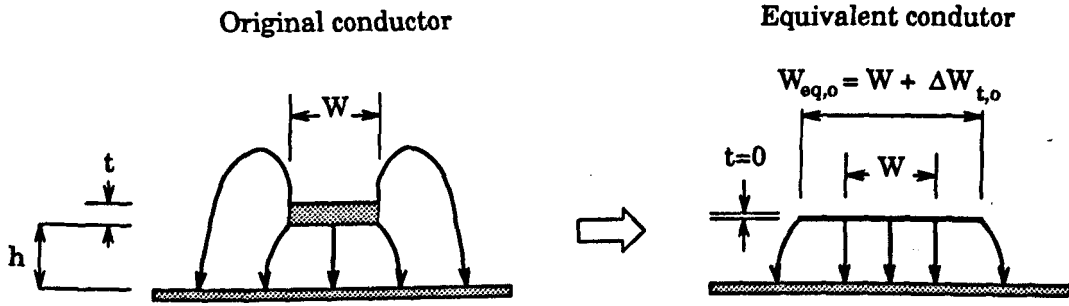


Figure 4.6: Equivalent model for strip of finite width

permittivity ϵ_r , but with a corrected width taking into account the effect of the fringing fields.

Wheeler's approach is to firstly define a transmission line of finite thickness in terms of the equivalent conductor width ($w_{eq,o} = w + \Delta w_{eq,o}$) without the presence of a substrate to compensate for the effects of the fringing fields in an homogeneous dielectric, as illustrated in figure 4.6. The electrical characteristics of the original circuit are maintained in the translation from the original to the equivalent representation. For narrow strip transmission lines the fringing effect is quite pronounced, more so than for wide lines where it may be absorbed by the physical width dimensions. An expression giving the equivalent width $w_{eq,o}$ for a track of thickness t without the presence of the substrate and taking into account the fringing field effect is of the form[69] :

$$w_{eq,o} = w + \Delta w_{t,o} \quad (4.6)$$

where the small change in the width without a substrate present $\Delta w_{t,o}$ is given by

$$\Delta w_{t,o} = \frac{t}{\pi} \ln \left[\frac{4 \cdot \exp(1)}{\sqrt{(t/h)^2 + \left\{ \frac{1/\pi}{(w/t) + 1.10} \right\}^2}} \right] \quad (4.7)$$

t is the track thickness, h is the substrate height and w is the physical conductor width.

This is extended further for mixed media structures considering the influence of the dielectric ($\epsilon_r > 1$) on the parallel plate capacitance effect and the fringing fields. The equivalent conductor width with the substrate present ($w_{eq,s} = w + \Delta w_{eq,s}$) is as illus-

trated in figure 4.7. The introduction of the substrate has the implication of concentrating the field more within the substrate. The net increase in the equivalent width is less than that for the homogeneous case. The introduction of the substrate not only results in an increase in the effective width but also in the capacitance of the line. The new effective width (with the substrate present) of the line taking into account the capacitance C is a function of the substrate permittivity ϵ_r and $\Delta w_{t,o}$, given by

$$\Delta w_{t,c} = \Delta w_{t,o} / \epsilon_r \quad (4.8)$$

where $\Delta w_{t,c}$ is equivalent to $\Delta w_{t,i}$ with respect to figure 4.7.

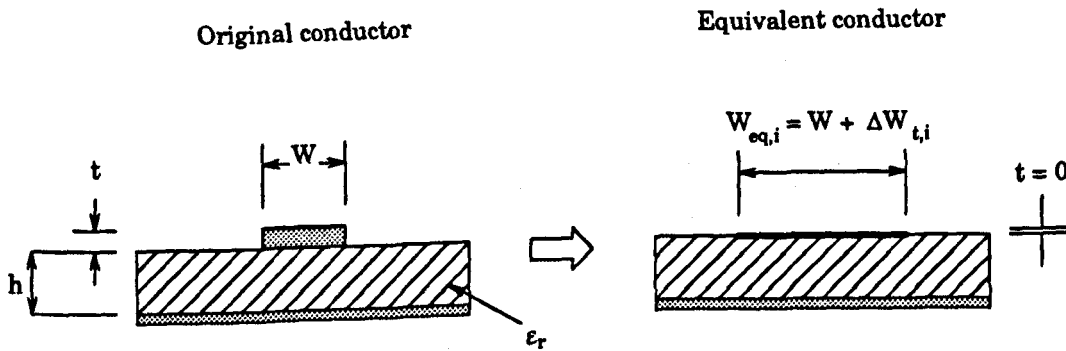


Figure 4.7: Equivalent model for strip of finite thickness

The corrected transmission line widths normalised to the substrate height are then given by

$$U_{t,o} = \frac{w + \Delta w_{t,o}}{h} \quad (4.9)$$

$$U_{t,c} = \frac{w + \Delta w_{t,c}}{h} \quad (4.10)$$

To obtain the static value of the substrate permittivity $\epsilon_{r,eff,stat}$, the corrected widths in equations 4.9 and 4.10 are then included in the following expressions defined by Hammerstad and Jensen [71] for the effective substrate permittivity.

$$A(U) = 1 + \frac{1}{49} \ln \left\{ \frac{U^4 + (U/52)^2}{U^4 + 0.432} \right\} + \frac{1}{18.7} \ln \left\{ 1 + \left(\frac{U}{18.1} \right)^3 \right\} \quad (4.11)$$

$$B(\epsilon_r) = 0.564 \cdot \left\{ \frac{\epsilon_r - 0.9}{\epsilon_r + 3} \right\}^{0.053} \quad (4.12)$$

where $A(U_{t,o})$ and $A(U_{t,c})$ are then substituted into

$$\epsilon_{r,eff}(\epsilon_r, U) = \frac{\epsilon_r + 1}{2} + \frac{\epsilon_r - 1}{2} \cdot \left\{ 1 + \frac{10}{U} \right\}^{(-A(U) \cdot B(\epsilon_r))} \quad (4.13)$$

The translation of the microstrip model from the homogeneous structure to the multi-dielectric equivalent needs to take into consideration the line impedance correction factors which are given for both cases, by the general expression

$$Z_o(U) = \frac{\eta}{2\pi} \cdot \ln \left\{ \frac{f(U)}{U} + \sqrt{1 + \left(\frac{2}{U} \right)^2} \right\} \quad (4.14)$$

where η is the wave impedance of the medium ($\eta = \sqrt{\frac{\mu_0}{\epsilon_0}} = 376.73\Omega$ in vacuum) and

$$f(U) = 6 + (2\pi - 6) \exp \left\{ - \left(\frac{30.666}{U} \right)^{0.7528} \right\} \quad (4.15)$$

With all the necessary correction factors accounted for, the static value for the effective permittivity $\epsilon_{r,eff,stat}$ is then defined as

$$\epsilon_{r,eff,stat}(w/h, t/h, \epsilon_r) = \frac{Z_o(U_{t,o})}{Z_o(U_{t,c})} \cdot \sqrt{\epsilon_{r,eff}(\epsilon_r, U_{t,o}) \cdot \epsilon_{r,eff}(\epsilon_r, U_{t,c})} \quad (4.16)$$

Similarly the static line impedance is then defined as a function of the substrate and track dimensions as

$$Z_{o,stat}(w/h, t/h, \epsilon_r) = \sqrt{\frac{Z_o(U_{t,o}) Z_o(U_{t,c})}{\epsilon_{r,eff}(\epsilon_r, U_{t,c})}} \quad (4.17)$$

The microstrip line impedance varies with frequency and therefore a frequency dependent expression for the line impedance in terms of the frequency dependent effective permittivity is as given by Hammerstad and Jensen [71]:

$$Z_o(f) = Z_{o,stat} \cdot \sqrt{\frac{\epsilon_{r,eff,stat}}{\epsilon_{r,eff}(f)}} \cdot \frac{\epsilon_{r,eff}(f) - 1}{\epsilon_{r,eff,stat} - 1} \quad (4.18)$$

where the frequency dependent $\epsilon_{r,eff}(f)$ can be obtained from any one of the models to be outlined next.

Dynamic microstrip dispersion models

Of the many microstrip dispersion models a few are reported here, illustrating the discrepancies from one model to the next. Some of the reported models are extremely effective for specific substrates or for transmission lines of thicknesses confined to within a given range. Here a comparison is effected between some of the more common models and practical microstrip transmission line realisations for both the PTFE and ceramic based substrates. The more accurate of the models is then used for further microstrip group delay analysis.

- Getsinger's model [72]

Getsingers' frequency dependent microstrip dispersion model is based around the ceramic substrate Al_2O_3 with a permittivity of $\epsilon_r \simeq 10$.

$$\epsilon_{r,eff}(f) = \epsilon_r - \frac{\epsilon_r - \epsilon_{r,eff,stat}}{1 + G_1 \cdot (f/f_{p1})^2} \quad (4.19)$$

$$f_{p1} = Z_{o,stat} / (2\mu_o h) \quad (4.20)$$

$$G_1 = 0.6 + 0.009.Z_{o,stat} \quad (4.21)$$

where $\mu_o = 4\pi \times 10^{-7}$ H/m. The following expression for G_1 has been modified by Hammerstad and Jensen [71] to account for a variety of substrates:

$$G_1 = \frac{\pi^2}{12} \cdot \frac{\epsilon_r - 1}{\epsilon_{r,eff,stat}} \cdot \sqrt{\frac{2\pi Z_{o,stat}}{\eta}} \quad (4.22)$$

• Carlin's model [72]

The microstrip dispersion model reported by Carlin is based on a TEM-TE coupled line model. The coupling between the TEM and TE modes produces the two lowest stripline hybrid modes [73] leading to an expression for the dispersion :

$$\epsilon_{r,eff}(f) = \epsilon_{r,eff,stat} \left[1 + \frac{2k^2}{(f_{p2}/f)^2 + \sqrt{(2k)^2 + (f_{p2}/f)^4}} \right] \quad (4.23)$$

$$f_{p2} = \frac{cZ_{o,stat}}{h\eta} \cdot \sqrt{k/(4.143G_2)} \quad (4.24)$$

$$k = (\epsilon_r - \epsilon_{r,eff,stat})/\epsilon_{r,eff,stat} \quad (4.25)$$

$$G_2 = 0.5 + 0.001.Z_{o,stat}^{3/2} \quad (4.26)$$

where k is the coupling coefficient between the TEM and the TE lines. f_{p2} is the turning point of the dispersion curve for the TE line. This model has been validated by Carlin for frequencies in the range of 0-12GHz.

- Schneider's model [69]

An approximate expression for the microstrip dispersion is that reported by Schneider.

The model developed by Schneider is based on the following assumptions:

1. $\epsilon_{r,eff}(f)$ increases with frequency.
2. At low frequencies $\epsilon_{r,eff}(f)_{(f \rightarrow 0)} \Rightarrow \epsilon_{r,eff,stat}$
3. At high frequencies $\epsilon_{r,eff}(f)_{(f \rightarrow \infty)} \Rightarrow \epsilon_r$
4. The phase velocity $v_p(f)$ has a turning point close to the cut-off frequency of the TE_1 surface wave.

From these assumptions Schneider has presented a model of $\epsilon_{r,eff}(f)$ given by:

$$\epsilon_{r,eff}(f) = \epsilon_{r,eff,stat} \left[1 + \left(\frac{f}{f_{p3}} \right)^2 \cdot \frac{1 - \sqrt{\epsilon_{r,eff,stat}/\epsilon_r}}{1 + \left(\frac{f}{f_{p3}} \right)^2 \cdot \sqrt{\epsilon_{r,eff,stat}/\epsilon_r}} \right]^2 \quad (4.27)$$

where

$$f_{p3} = c/(4h\sqrt{\epsilon_r - 1}) \quad (4.28)$$

- Yamashita, Atsuki and Veda's model [74]

This model is determined from functional approximations to the numerically calculated values of $\epsilon_{r,eff}(f)$ as

$$\epsilon_{r,eff}(f) = \left[\frac{\sqrt{\epsilon_r} - \sqrt{\epsilon_{r,eff,stat}}}{1 + 4 \cdot F_1^{-1.5}} + \sqrt{\epsilon_{r,eff,stat}} \right]^2 \quad (4.29)$$

where

$$F_1 = ((4hf\sqrt{\epsilon_r - 1})/c) \cdot [0.5 + \{1 + 2\log(1 + (w/h))\}^2] \quad (4.30)$$

This expression is valid over the ranges:

$$\begin{aligned} 2 &\leq \epsilon_r \leq 16 \\ 0.06 &\leq w/h \leq 16 \\ 0.1\text{GHz} &\leq f \leq 100\text{GHz} \end{aligned}$$

In the development of this model the authors used a substrate of height $h = 1\text{mm}$ for all values of ϵ_r as the base for normalisation.

- Kirschning and Jansen's model [75]

The microstrip dispersion model developed by Kirschning and Jansen is similar in structure to that of Getsinger (4.19) and is of the form:

$$\epsilon_{r,eff}(f) = \epsilon_r - \frac{\epsilon_r - \epsilon_{r,eff,stat}}{1 + P} \quad (4.31)$$

$$P = P_1 \cdot P_2 \cdot \{(0.1844 + P_3 \cdot P_4)10fh\}^{1.5763} \quad (4.32)$$

$$P_1 = 0.27488 + (w/h) \cdot [0.6315 + \{0.525/(1 + 0.157fh)^{20}\}] \quad (4.33)$$

$$- 0.065683 \cdot \exp(-8.7513(w/h)) \quad (4.34)$$

$$P_2 = 0.33622 \cdot \{1 - \exp(-0.03442\epsilon_r)\} \quad (4.35)$$

$$P_3 = 0.0363 \cdot \exp(-4.6(w/h)) \cdot [1 - \exp\{-(fh/3.87)^{4.97}\}] \quad (4.36)$$

$$P_4 = 1 + 1.2751 \cdot [1 - \exp\{-(\epsilon_r/15.916)^8\}] \quad (4.37)$$

In this case h is in cm and f is in GHz. The frequency dependent term P has been accurately determined by hybrid mode analysis. This model has been reported by the authors as having an accuracy better than 0.6% at frequencies up to about 60GHz for 25mil substrates. The accuracy holds true for the ranges:

$$\begin{aligned} 0.1 &\leq w/h \leq 100 \\ 1 &\leq \epsilon_r \leq 20 \\ 0 &\leq h/\lambda_0 \leq 0.13 \end{aligned}$$

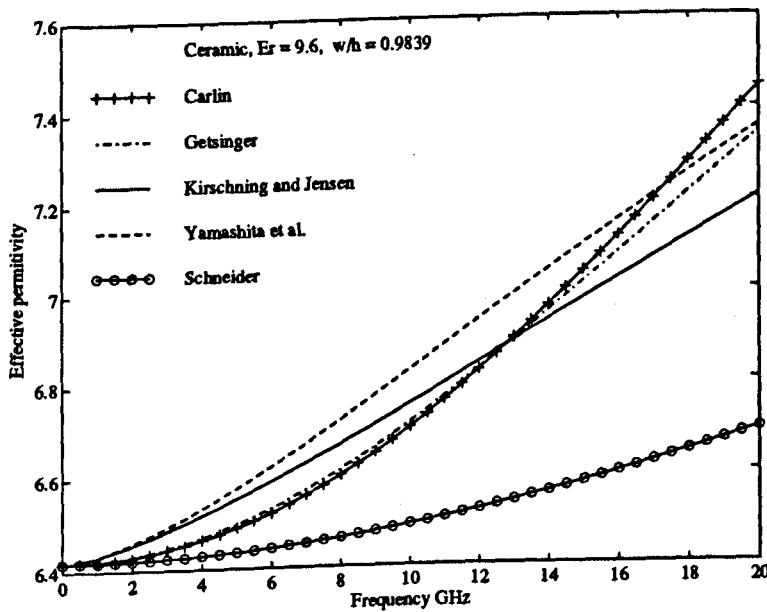


Figure 4.8: Various models for $\epsilon_{r,eff}(f)$

where λ_0 is the free space wavelength.

Figure 4.8 illustrates the various models of $\epsilon_{r,eff}(f)$ obtained for a ceramic substrate, demonstrating the discrepancies from one model to the next. The model offered by Schneider contrasts markedly with the others as this model is derived from approximations over the range $0 < f < \infty$.

A simple and effective measurement technique outlined by Hoffmann was employed to directly measure the substrate effective permittivity. By measuring the scattering parameters of a length of microstrip line, $\epsilon_{r,eff}(f)$ can be determined. The characteristic line impedance of the microstrip line (Z_0) is required to be matched to the measurement device reference characteristic impedance (Z_L). The value of the effective permittivity can then be obtained from:

$$\sqrt{\epsilon_{r,eff}(f)} = \frac{\arg(S_{21}) \cdot c}{2\pi f l} \quad (4.38)$$

where l is the length of the microstrip line used and $\arg(S_{21})$ defines the argument of the complex S_{21} parameter.

On comparison of the practical evaluation of $\epsilon_{r,eff}(f)$ to the models outlined previously, the model given by Yamashita et al. was found to most closely agree with the experimental data, as shown in figure 4.9. The microstrip practical realisation was a 10cm line fabricated on an alternative substrate of $\epsilon_r = 2.17$ the physical width of the line was calculated for a characteristic line impedance $Z_0 = 50\Omega$. By using a larger microstrip line, of a meandering form, the error in the $\arg(S_{21})$ can be reduced to obtain a better fit to the model.

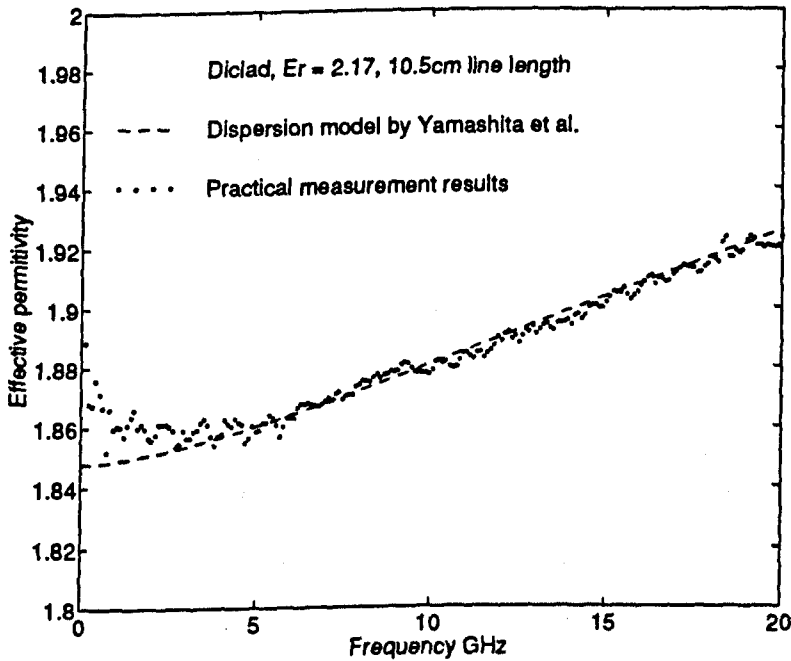


Figure 4.9: Comparison of $\epsilon_{r,eff}(f)$ obtained practically and the best matched model, that of Yamashita et al.

Other methods of measuring the frequency dependent effective dielectric constant $\epsilon_{r,eff}(f)$, based on the ring resonator and the straight gap-coupled resonator have been used by Medina et. al. [76]. The authors have performed a comparison between measured results and various reported models for $\epsilon_{r,eff}(f)$. The results presented by Medina et. al. show the model given by Yamashita to be one of the better ones for both the soft and alumina substrates.

Comparison of microstrip dispersion/group delay models with practical microstrip transmission line realisations

The validity and accuracy of the microstrip dispersion models is further verified in this section by means of effecting a comparison in terms of the group delay produced by the models and practical microstrip transmission line realisations. The substrate types used for this comparison are:

- DICLAD² 880 of permittivity $\epsilon_r = 2.17$. The substrate is of the PTFE type with interwoven glass fibre to enhance structural rigidity.
- RT/duroid³ 6010 of permittivity $\epsilon_r = 10.5$. This substrate is again PTFE based with ceramic uniformly dispersed within the dielectric.
- Ceramic Al_2O_3 of permittivity $\epsilon_r = 9.6$

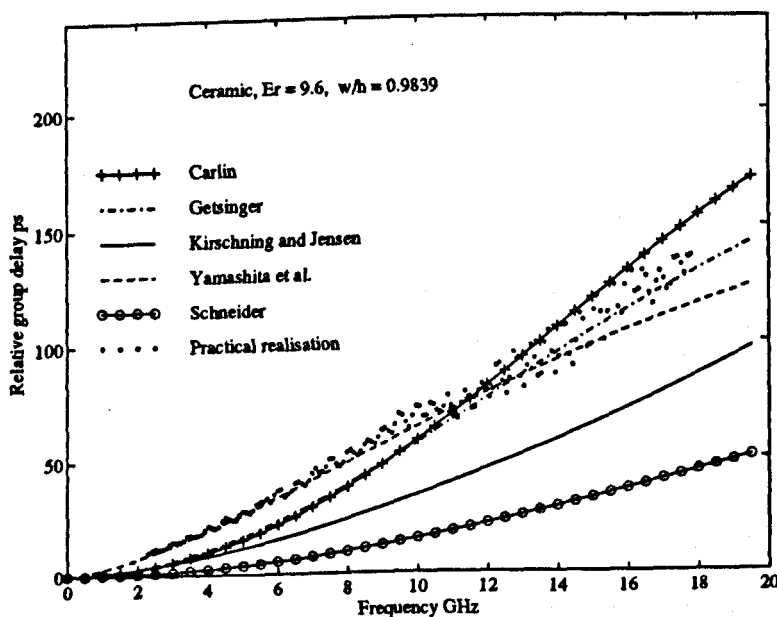


Figure 4.10: Relative delay obtained with various reported models and a practically realised microstrip transmission line on a ceramic Al_2O_3 substrate

²DICLAD is a registered trade mark of Arlon, Microwave Materials Division, Delaware 19701

³RT/duroid is a registered trade mark of the Rogers Corporation, USA.

As the emphasis here is on the equalisation properties of microstrip, the group delay characteristics of the transmission line are of importance. Thus the values of $\epsilon_{r,eff}(f)$ obtained from the previously mentioned models are substituted into the expression defining the microstrip group delay in equation 3.10 and compared to the group delay obtained with a practical microstrip transmission line realisation. The illustrated results are for a line with a characteristic impedance of 50Ω . From the results obtained in figures 4.10, 4.11 and 4.12 the accuracy of the model reported by Yamashita et al. is evident.

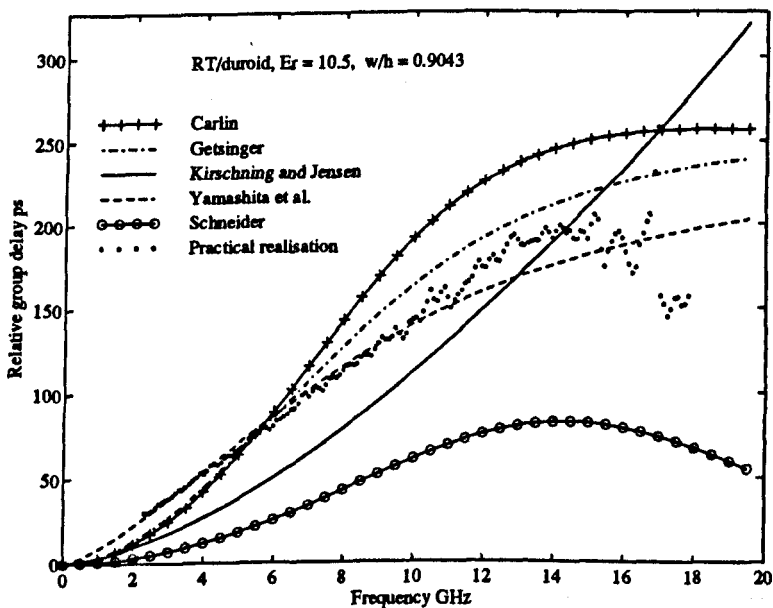


Figure 4.11: Relative delay obtained with various reported models and a practically realised microstrip transmission line on RT/duroid.

The model offers a more accurate description of $\epsilon_{r,eff}(f)$ and in turn of the group delay characteristics of a microstrip transmission line for the various substrate types used. The model reported by Getsinger but employing the Hammerstad and Jansen correction factor is found to provide the next best fit to the experimentally obtained results. Again the accuracy of this particular model is consistent for the range of substrates.

In the following discussion on the influence of material constituent and dimensional parameters, the model given by Yamashita et al. is used in any definition of the group

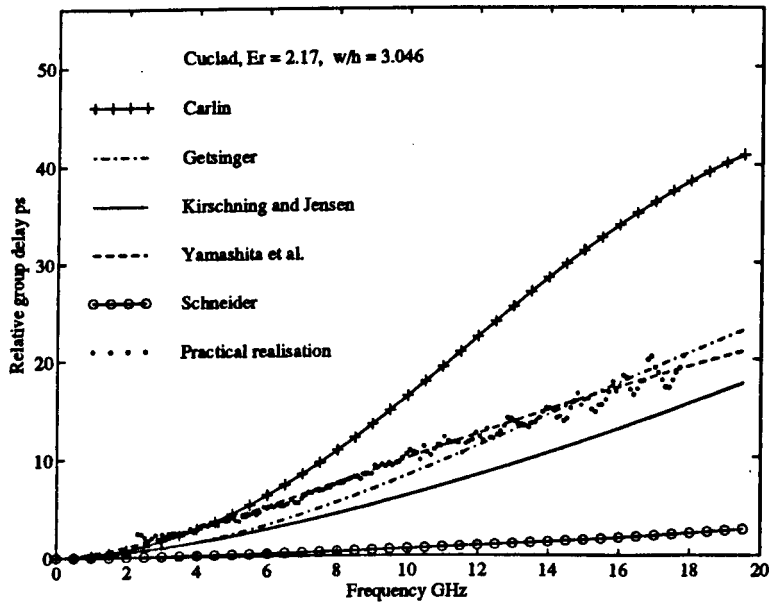


Figure 4.12: Relative delay obtained with various reported models and a practically realised microstrip transmission line on Cuclad

delay characteristics of the microstrip transmission line.

4.3.2 Influence of Substrate Material

The group delay characteristics of a microstrip transmission line are very much dependent on the substrate type used. When used as equalisers to correct for the group delay produced by a given length of fibre, the length of the compensator required can be altered by appropriate choice of substrate material [77]. The calculated $\epsilon_{r,eff}(f)$ characteristics for three types of substrate are illustrated in figure 4.13.

To standardise the substrates, a common substrate height of $625\mu\text{m}$ is used. The difference in the slope of the $\epsilon_{r,eff}(f)$ characteristics between RT/duroid and the ceramic substrate is not too pronounced, whereas with the Diclad a smaller gradient is evident. The group delay characteristics of each of the lines is illustrated in figure 4.14. Here again the fact that different substrates afford different group delay characteristics is highlighted. All aspects of the microstrip transmission line geometry have been kept constant in order to isolate the influence of the substrate type on the group delay char-

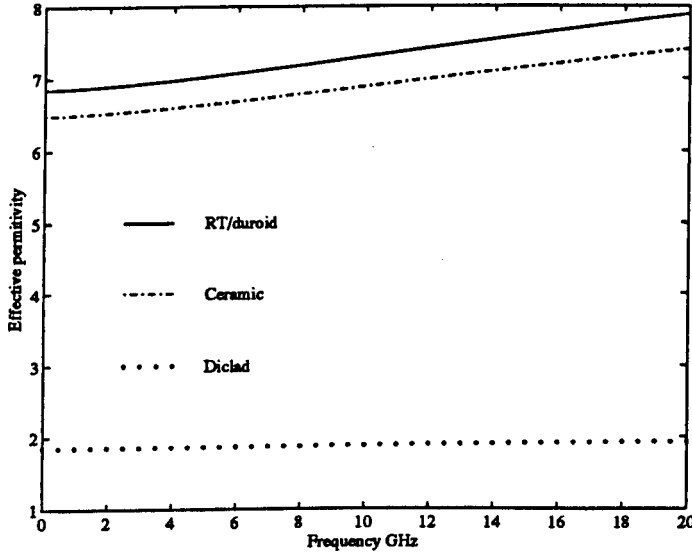


Figure 4.13: $\epsilon_{r,eff}(f)$ for a 10.5cm microstrip transmission line fabricated on various substrate types with a substrate height of $625\mu\text{m}$

acteristics. The higher substrate permittivities confine more of the field distribution to within the body of the substrate, therefore reducing the wave phase velocity as given in equation 4.3 and consequently increasing the absolute and relative group delay. This argument can be further supported in terms of the fringing fields resulting from an increase in substrate permittivity. From equation 4.8 any increase in ϵ_r results in a smaller increase in the effective width $\Delta w_{t,c}$ compared to the case with no substrate present $\Delta w_{t,o}$, implying tighter confinement of the field within the substrate.

4.3.3 Influence of Track Thickness and Substrate Height

Firstly, considering the variation of the track thickness (t), it must be noted that as t increases the field distribution changes such that it is scattered over a wider area. This results in the thick strip behaving as a thinner but wider line. The effective increase in the width implies an increase in capacitance and a decrease in the static effective permittivity $\epsilon_{r,eff,stat}$. At low frequencies the field distribution is generally shared between the air and substrate dielectric but at higher frequencies the field tends to concentrate largely in the substrate dielectric directly under the strip.

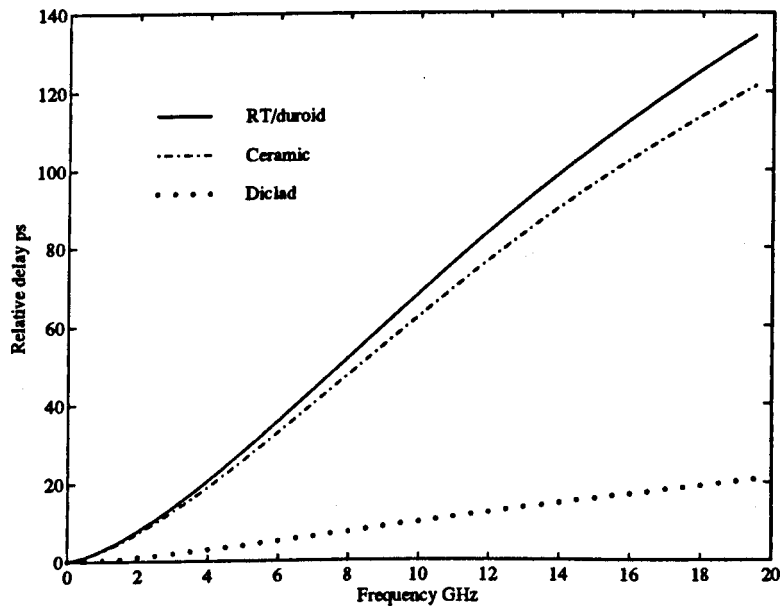


Figure 4.14: Group delay characteristics for a 10.5cm microstrip transmission line fabricated on various substrate types with a substrate height of 625µm

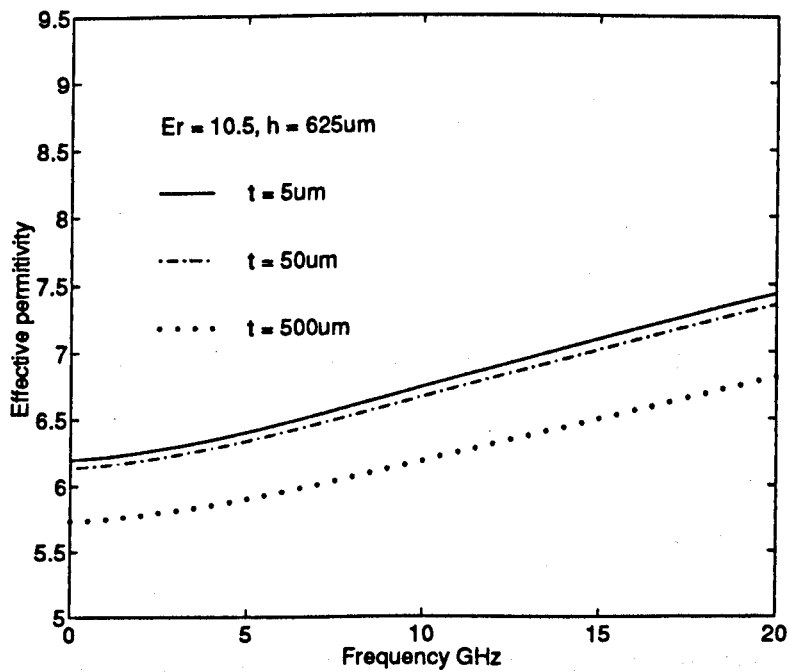


Figure 4.15: Influence of variations in the track thickness on the $\epsilon_{r,eff}(f)$ of a 10.5cm microstrip transmission line ($h = 625\mu\text{m}$ - constant). Note: The excessively large track thickness (500µm) is impractical and is used here to illustrate the effect only.

Equation 3.10 requires the derivative of $\epsilon_{r,eff}$. On examining the variation in the effective permittivity with frequency for a range of track thicknesses it is found that increasing the thickness reduces the static value of $\epsilon_{r,eff}$ as shown in figure 4.15. At higher frequencies the effective permittivities for all thicknesses converge to ϵ_r . The lower static value of $\epsilon_{r,eff,stat}$ for the thicker tracks results in a more linear group delay response over a 0 - 20GHz operating frequency range as shown in figure 4.16, thereby allowing for larger corrected bandwidths at the expense of a slightly shorter fibre length.

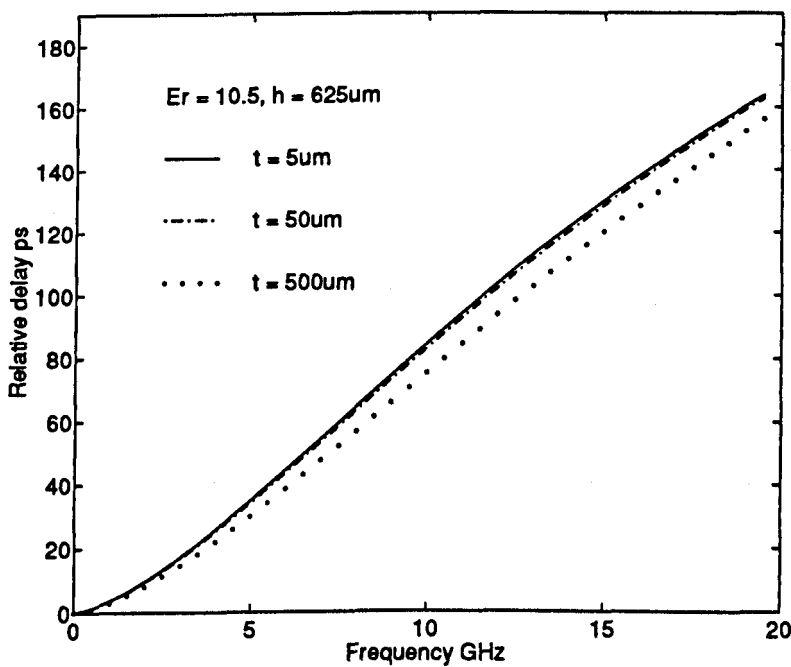


Figure 4.16: Influence of variations in the track thickness on the group delay characteristics of a 10.5cm microstrip transmission line ($h = 625 \mu\text{m}$ - constant)

Considering now the influence of substrate height (h) variations, the field distribution for larger substrate heights is found to be predominant within the substrate. Subsequently the static frequency value of $\epsilon_{r,eff}$ is slightly higher for the larger substrate heights. The convergence of $\epsilon_{r,eff}$ to ϵ_r occurs sharply and at lower frequencies for the larger values of h . This is shown in figure 4.17.

These steep transitions of the effective permittivity give rise to sharper delay charac-

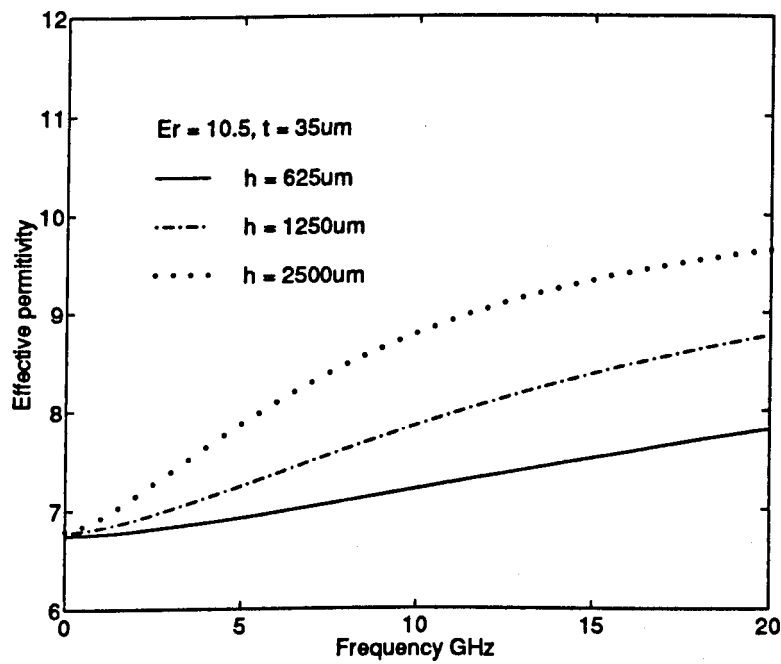


Figure 4.17: Influence of variations in the substrate height on the $\epsilon_{r,eff}(f)$ of a 10.5cm microstrip transmission line ($t = 35\mu m$ - constant)

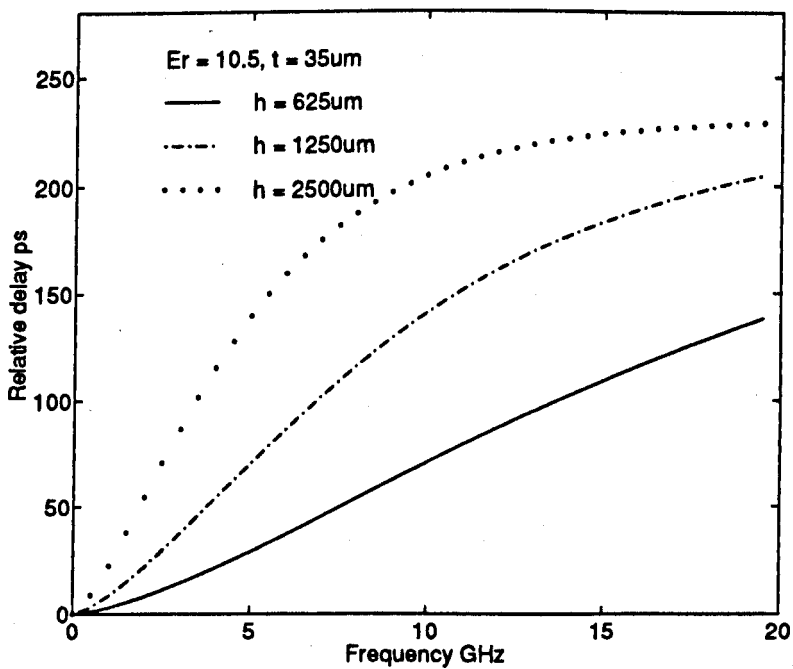


Figure 4.18: Influence of variations in the substrate height on the group delay characteristics of a 10.5cm microstrip transmission line ($t = 35\mu m$ - constant)

teristics but over a smaller frequency band. The effect of altering the substrate height on the relative group delay characteristics of the microstrip transmission line is highlighted in figure 4.18, where the group delay for large fibre spans may be corrected over a fixed bandwidth by increasing the height of the substrate. The maximum value of the substrate height is restricted however by the effect of the parasitic coupling from surface waves [68]. Parasitic surface waves propagate just beneath the surface of the substrate away from the microstrip discontinuities. On a single microstrip transmission line propagation of the surface wave will be away from the strip towards the edges of the substrate. The lower microstrip (electric) TM_o surface wave mode is easier to excite than the (magnetic) TE_o , as the TM_o mode resembles very closely the quasi-TEM microstrip mode. The surface wave interference becomes more influential with large substrate heights as coupling between the fundamental surface wave mode and microstrip transmission line modes occurs within the technical working frequency range. The coupling frequency, in terms of the substrate height is given by the expression [78]

$$f_s = \frac{c \cdot \tan^{-1}(\epsilon_r)}{\pi h \sqrt{2(\epsilon_r - 1)}} \quad (4.39)$$

Equation 4.39 implies that the influence of surface waves will be less severe for substrates of low permittivity. The surface wave parasitics result in a ripple on the magnitude response of the circuit, increasing with frequency.

The effect of surface waves may be suppressed by covering any bare substrate region away from the conducting structure with a lossy, resistive metallisation. Alternatively operation at frequencies below f_s will also avoid surface wave interference.

4.4 Illustrative Practical Equalisers

Having determined that the model by Yamashita et al. provides a good representation for the microstrip dispersion the group delay characteristics of a microstrip group delay equaliser can now be modelled accurately for a range of substrate types. This also

allows for an investigation of the impact of varying the substrate constituent and geometric parameters on the maximum achievable equalised transmission span and available bandwidth.

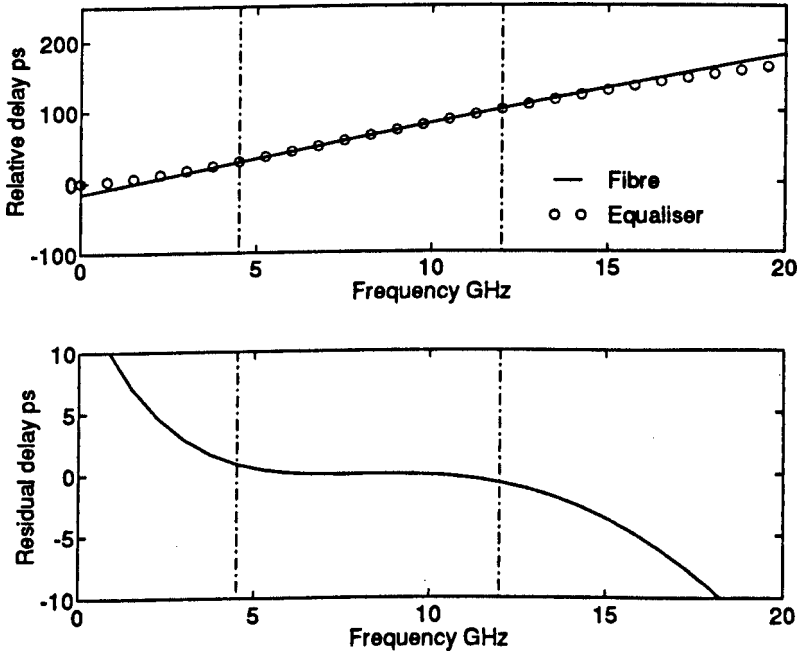


Figure 4.19: Group delay characteristics showing an equaliser fabricated on RT/duroid substrate to correct for given length of fibre (top) and the equalised bandwidth defined by ± 1 ps of residual delay (bottom)

4.4.1 Compensated Fibre Span and Bandwidth Available With Variations in Substrate Type

Different substrate types have been shown to afford different group delay characteristics, which are exploited here to correct for various lengths of fibre. A 10.5cm microstrip line of thickness $t = 35\mu m$ and $h = 625\mu m$ fabricated on different substrates is used as an equaliser. The effective maximum corrected bandwidth is taken as being ± 1 ps of residual error between the fibre and the microstrip delay characteristics, an arbitrarily chosen value. This is illustrated in figure 4.19 for a 10cm long 50Ω microstrip line fabricated on the soft PTFE composite substrate RT/duroid. For the various substrates the measure of corrected fibre length and bandwidth is shown in table 4.2.

Substrate type	Equalised Fibre length (km)	Equalised bandwidth (GHz)	Bandwidth distance product (GHz.km)
RT/duroid	83	8.5	705
Ceramic Al_2O_3	60	9	540
Diclad	10	20	200

Table 4.2: Influence of substrate type on the maximum attainable equalised fibre length and bandwidth for a 10cm microstrip line length of $Z_0 = 50\Omega$

The maximum corrected bandwidth is achieved with the substrate of the lowest permittivity (Diclad $\epsilon = 2.17$), but this substrate compensates for a limited fibre length. Larger fibre spans can be corrected for when substrates of higher permittivity are used. The group delay characteristics of the ceramic and RT/duroid substrate based microstrips are very similar and consequently result in approximately similar equalised fibre spans and bandwidths. However, a bandwidth distance product illustrates superior performance with the RT/duroid substrate.

4.4.2 Compensated Fibre Span and Bandwidth Available With Variations in Both Track Thickness and Substrate Height

The influence of varying the track thickness on the group delay characteristics is by no means pronounced. As illustrated in figure 4.16, only when the track thickness is increased by two orders of magnitude does the group delay characteristic show a substantial change. This is also reflected with the bandwidth distance product. The slope of the response shows a larger linear region for the thicker transmission strips. The gradient of the group delay characteristics are however very much the same for the range of thicknesses. These findings are presented in table 4.3, where the substrate RT/duroid of permittivity $\epsilon_r = 10.5$ and $h = 625\mu\text{m}$ was used for a 50Ω line.

Increases in the substrate height h for fixed t results in a rapid increase in the effective

Track thickness (μm)	Equalised Fibre length (km)	Equalised bandwidth (GHz)	Bandwidth distance product (GHz.km)
5	83	7	581
50	82	8	656
500	75	10	750

Table 4.3: Influence of the track thickness on the maximum attainable equalised fibre length and bandwidth for a 10cm microstrip line length of $Z_0 = 50\Omega$

permittivity from its static value to ϵ_r , thereby giving rise to steeper group delay characteristics. Consequently this implies that the dispersion produced by larger fiber spans can be corrected. However, the drawbacks of increasing the substrate height are that the equalised bandwidth as defined earlier is reduced but a constant bandwidth distance product is maintained. This is verified by the results shown in table 4.4.

Substrate height (μm)	Equalised Fibre length (km)	Equalised bandwidth (GHz)	Bandwidth distance product (GHz.km)
625	70	9	630
1250	140	4.5	630
2500	280	2.25	630

Table 4.4: Influence of the substrate height on the maximum attainable equalised fibre length and bandwidth for a 10cm length of microstrip line of $Z_0 = 50\Omega$

Of the substrate parameters examined, a pronounced affect is observed with variations in the substrate permittivity and height. Changes in the track thickness by an order of magnitude result in a more linear group delay response and consequently an increase in the equalised bandwidth. The two substrates of higher permittivity demonstrated the potential for equalising large lengths of fibre over modest bandwidths, but with the substrate Dicald the converse applied. From the results obtained, outlining the influence of the substrate constituent and dimensional parameters, it appears that for any given application the attainable bandwidth and corrected fibre span will be clearly

dependent on the tolerable residual delay dispersion.

4.4.3 Implication of In-Line Amplification on The Tolerable Residual Delay Dispersion

First generation long haul optical transmission of intensity modulated signals employed 3R (reshape-retch-regenerate) repeaters. New generation in-line optical amplifiers (EDFA's) omit the reshaping and retiming features to provide low complexity 1R repeaters, concentrating on regeneration of the optical signal, leaving any further signal processing required to be performed at the final receiver. The use of optical amplifiers in this way offers the prospect of flexible transparent systems avoiding irreversible dedication to a particular modulation scheme or signal format. Alterations to modulation schemes, laser operating wavelengths or multiplexing arrangement need only be performed at the terminals, avoiding excavation of the installed fibre network for system upgrades. With dispersion being a significant impairment limiting the attainable information capacity achievable with a single optical carrier, adoption of in-line optical amplifiers will inevitably exacerbate this problem, with chromatic dispersion then an accumulative property dependent on the number and length of sections between fully regenerative terminals. The multi-section transmission may then be corrected by using a cascade of single lengths of equalisers [41] designed to correct for the individual stages. Alternatively, a single length of compensator may be used to correct for the whole transmission span, but this requires an excessively large equaliser, typically 1.5m for 1000km fibre span. Realisation of such a length of equaliser is restricted by the attenuation characteristics and physical dimensions.

For multi-section long haul transmission employing in-line optical amplifiers the residual error then becomes an accumulative parameter as shown in figure 4.20 with the introduction of 2, 5 and 10 amplifiers.

The results of figure 4.20 have been generated using a 50Ω , 10.5cm microstrip single section compensator. The length of equaliser used was the same as that used by Iwashita and Takachio in demonstrating the principle of microstrip equalisation. The

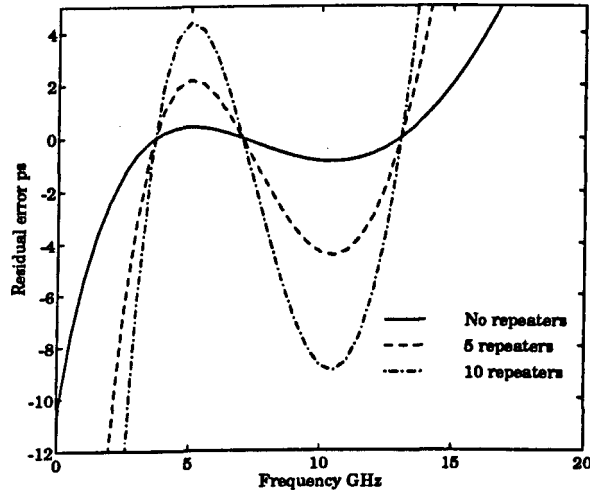


Figure 4.20: The residual group delay error, accumulative with the number of repeaters

authors found that a 10.5cm microstrip line fabricated on a ceramic substrate could correct for the dispersion produced by a 100km fibre length. However in this case rather than using a ceramic substrate, the softer RT/duroid substrate was preferred. The dimensions of the substrate were chosen appropriately such that a large equalised frequency bandwidth of approximately twice the bit-rate may be accommodated in correcting for a relatively modest fibre length (60-100km; constituting the distance between two repeater stages). A comparison is not affected here between the various substrate parameters as illustration of the residual error is of the essence.

By defining the $ABCD$ transmission matrix of the microstrip line, the implications of employing in-line optical amplifiers can be simulated by considering the effect of the accumulative residual error resulting from cascading the equalisers. The transmission system model used to simulate the following results shall be defined in chapter 6. The transmission matrix for a loss-less microstrip line is given as:

$$\begin{bmatrix} A & B \\ C & D \end{bmatrix} = \begin{bmatrix} \cos\theta & jZ_o \sin\theta \\ jY_o \sin\theta & \cos\theta \end{bmatrix} \quad (4.40)$$

where the admittance $Y_o = 1/Z_o$, Z_o is the frequency dependent characteristic line impedance as given in equation 4.18 and θ is the electrical length of the line given by

$$\theta = \frac{2\pi fl \sqrt{\epsilon_{r,eff}(f)}}{c} \quad (4.41)$$

l is the physical line length.

The measure of residual error resulting as a consequence of in-line amplification is illustrated in figure 4.21. The system performance using the microstrip group delay equalisers is shown by means of eye diagram simulations in figure 4.22. The eye diagrams illustrate the residual error after the relative number of cascaded sections. Simulation results demonstrate the influence of the residual error for 5, 10 and 60 repeated sections, where each section is 70km long. The simulation of long haul transmission system employing 60 repeaters is for illustrative purposes only neglecting the nonlinear effects which would be significant in practice. The attenuation per unit length of microstrip has not been accounted for which will have to be overcome in order to realise excessively long equaliser lengths correcting for the dispersion produced in long haul transmission.

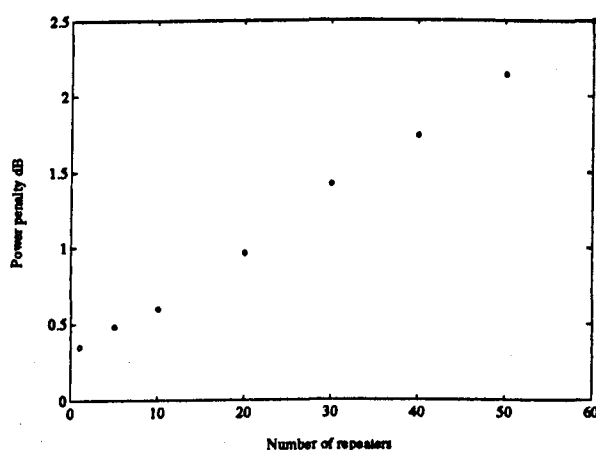


Figure 4.21: Dispersion power penalty resulting from the accumulation of the residual error from each of the cascaded equalisers

These results suggest that a cascade of microstrip group delay equalisers can allow high bit-rate transmission well over the dispersion limit. However, the residual error hinders the maximum equalised transmission distance and by optimisation of some of the intermediate equalisers within the cascade, the dispersion power penalty may be reduced. For the design of such equalisers, the correct choice of substrate parameters is imperative to realise an optimum approximation over a large bandwidth to the fibre dispersion characteristics.

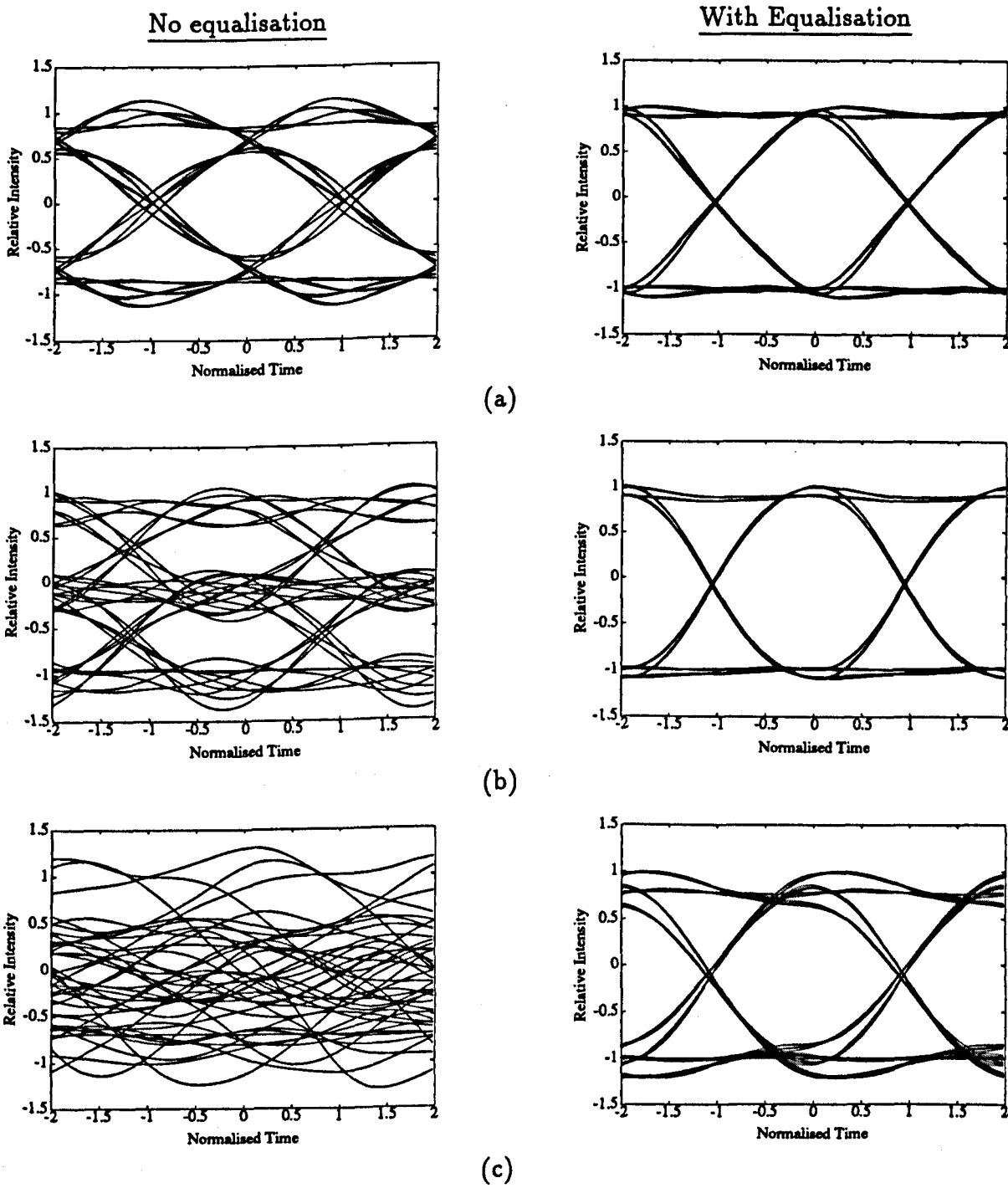


Figure 4.22: Impact of equalisation on long haul repeated transmission; a) with 5 repeaters, b) with 10 repeaters and c) 60 repeaters⁴

⁴A transmission system employing 60 repeaters is only for the purpose of illustrating what is possible in the absence of non-linearities.

4.5 Summary

This chapter has introduced various types of microwave integrated circuits (MIC) available, drawing specifically on the potential of microstrip for the realisation of fibre chromatic dispersion equalisers. In order to model correctly the group delay characteristics of the microstrip equaliser an accurate description of microstrip dispersion was required. The model presented by Yamashita et al. was found to be in good agreement with practical realisations.

The influence of various substrate parameters on the group delay characteristics was outlined and supported by practical results. The implications of in-line optical amplification on the residual error resulting from the discrepancies between the fibre and microstrip group delay characteristics have been addressed and illustrated by means of eye simulations.

The following chapter will address a novel approach to electrical domain equalisation, that of using Gallium Arsenide (GaAs) monolithic microwave integrated circuits (MMICs) to realise passive all-pass networks as group delay equalisers.

Chapter 5

GaAs Phase Equalisation

5.1 Introduction

The previous chapter highlighted the potential of microstrip technology for the realisation of fibre chromatic dispersion equalisers. The implications of utilising microstrip equalisers for an amplified transmission system were assessed and presented in terms of the eye patterns giving a measure of inter symbol interference (ISI). This method of equalisation is somewhat constrained in practice by the actual physical dimensions and insertion loss of the microstrip equaliser, as a lossy compensator of excessive length is required to correct for the dispersion resulting from a long haul link.

This has resulted in the investigation of gallium arsenide (GaAs) based pseudo-lumped element circuits for the realisation of monolithic microwave integrated circuit (MMIC) group delay equalisers. The MMIC structures offer the advantages of reduction in size and the potential of full scale integration with other receiver circuitry.

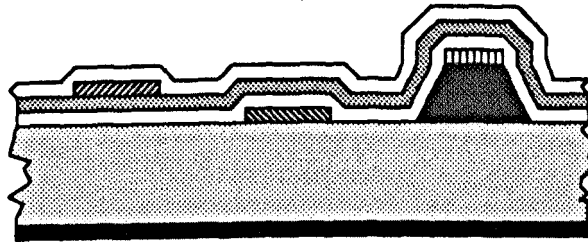
This chapter reviews some of the key features of the GaAs technology with emphasis on the realisation of group delay equalisers comprising pseudo-lumped passive components.

Second order single section networks employed as phase equalisers for low frequency operation are investigated and adapted for microwave operation as MMICs. These are further developed to realise wideband equalisation.

5.2 GaAs Technology

One of the most important and widely used compound semiconductor material is gallium arsenide (GaAs). This semiconductor material allows the fabrication of integrated circuits (ICs) with high frequency response and lower power demands. The advantages offered by GaAs MMICs over silicon based ICs are:

- Fewer process stages and less stringent requirements on mask alignment in designing MESFETs [79]
- Higher electron mobility (≈ 6 times that of Si)
- Lower parasitic capacitances and leakages due to semi-insulating (SI) GaAs substrate.



- | | |
|---|--|
| <input type="checkbox"/> Silicon nitride | <input checked="" type="checkbox"/> Ground plane |
| <input checked="" type="checkbox"/> Polymide | <input checked="" type="checkbox"/> Metallisation (M1) |
| <input checked="" type="checkbox"/> Mesa | <input checked="" type="checkbox"/> Metallisation (M2) |
| <input checked="" type="checkbox"/> SI GaAs substrate | <input checked="" type="checkbox"/> Metallisation (M3) |

Figure 5.1: GaAs MMIC cross section

The GaAs semi-insulating(SI) substrate has a resistivity of $\geq 10^8 \Omega\text{cm}$ and a cross section of the form shown in figure 5.1. The fabrication process for GaAs ICs, typical of those offered by commercial GaAs foundries involves direct implantation into the SI substrate. The functions of each of the mask layers are listed below:

Mesa	This layer provides the isolation of the active regions for FETs and resistors.
Metallisation (M1)	A metal alloy chosen for the sole purpose of making an ohmic contact to the mesa structure.
Metallisation (M2)	This metallisation layer forms a Schottky contact with the mesa and additionally the FET gates for active circuits. First level interconnections are made with M2 as are the low level metal-insulator-metal (MIM) capacitor contacts, interdigital capacitors, stacked spiral inductors and the bond pad base layer.
Nitride 1	A silicon nitride (Si_3N_4) passive layer acts as the insulating dielectric ($\epsilon_r = 7.2$) in the capacitor and passivates the active areas of the FETs.
Polymide	A second passive insulating layer used as an interlay dielectric in metal crossovers and as a dielectric ($\epsilon_r = 3.4$) in MIM capacitors.
Metallisation (M3)	The second metallisation layer is also used in the formation of interconnects, multi-turn spiral and stacked inductors, top electrode of the MIM capacitor and bond pads. <u>NOTE:</u> Both M2 and M3 layers can be used for the realisation of transmission lines but the M2 lines are more lossy.

Nitride 2

This final silicon nitride layer encapsulates the entire circuit leaving exposed only the bonding areas.

Before the wafer can be visually and electronically tested the rear of the wafer is lapped to reduce it to a thickness of $200\mu\text{m} \pm 10\mu\text{m}$ and via holes are etched to allow for grounding of the M2 layer. The fabrication process involves tight control of the dimensional tolerances, as summarised in table 5.1.

Layer	Tolerance (μm)
M1	+4, -0.0
M2	± 0.1
M3	± 0.5
Silicon Nitride	+0.4, -0.1
Polymide	± 0.6

Table 5.1: GaAs layer dimensional tolerances

5.2.1 GaAs Lumped Element Models

The foundry process allows the realisation of both passive and active elements for operation up to 20GHz. Here passive components are illustrated together with their parasitics.

Resistor

A typical GaAs resistor structure is illustrated in figure 5.2. Resistor values in the range of 10Ω - $10\text{K}\Omega$ can be directly fabricated with the mesa layer actually defining the resistance value. The resistor value is determined by three dimensions, the unetched length of the mesa (L_u), the etched length of the mesa (L_e) and the width of the mesa (W). In addition to this the resistor is orientation sensitive due to crystallographic variation. Ohmic contact is established with the mesa with M1 and further

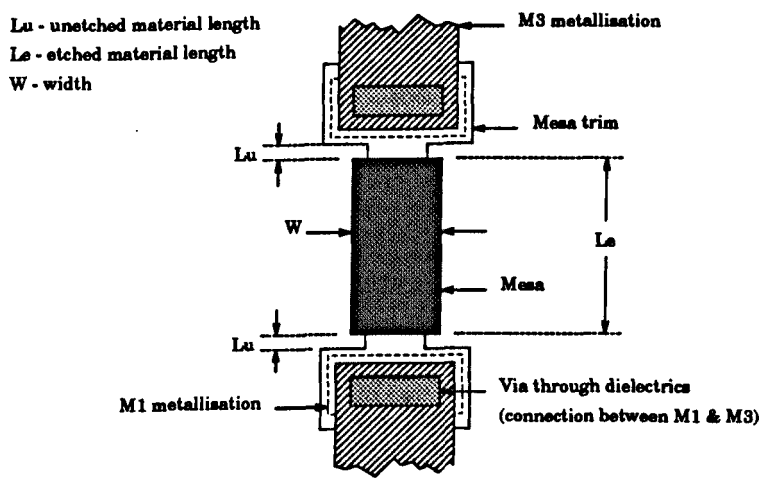


Figure 5.2: GaAs resistor structure

connections with M3 are made by means of vias in the polyimide and silicon nitride layers.

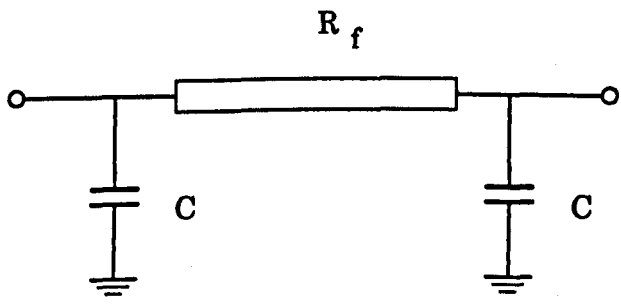


Figure 5.3: GaAs resistor equivalent circuit

The behaviour of the resistor is linear at only low voltages. The wideband frequency dependent model for the resistor is illustrated in figure 5.3 taking into account the parasitics. The expressions relating to R_f and C are provided by the foundry.

Inductor

The GaAs foundry process allows inductors to be realised in any one of three ways, depending on the inductance value and dimensional constraints. Inductors of values ranging typically from $\ll 1\text{nH}$ to 18nH can be fabricated by the GaAs foundry process.

The first of the methods is for realising inductances of very low values. Short lengths of transmission line, using either the M2 or M3 metallisation layers, may be treated as either a lumped inductance or as a distributed transmission line. The inductance produced by a given length of transmission line either on M2 or M3 can be evaluated from the expression :

$$L = \frac{Z_o l \sqrt{\epsilon_{eff}}}{300} \quad (5.1)$$

where L is the inductance in nH, l is the length of the transmission line in mm, Z_o is the characteristic line impedance and ϵ_{eff} is the effective dielectric constant. The characteristic line impedance is described with relation to the strip width by a fourth order polynomial, while the ϵ_{eff} , also related to the strip width, is described by a complex expression provided by the foundry.

The second of the inductors is the planar spiral structure. This is by far the most common method of realising inductors and the structure of such an inductor is illustrated in figure 5.4.

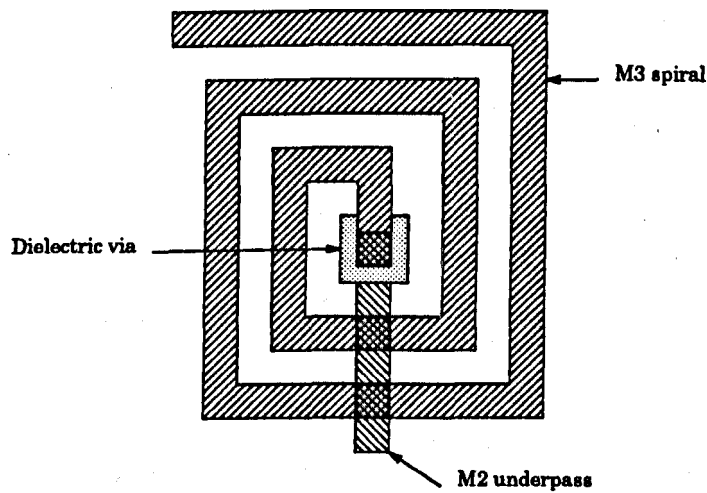


Figure 5.4: GaAs spiral inductor

The spiral inductor is formed by arranging a number of turns of the top level M3 track.

Connection to the centre of the inductor is made using a M2 underpass, while a via through the dielectric establishes contact between the M3 and M2 metallisation layers at the centre. The inductance value is calculated from an eighth order closed form expression valid for spiral inductors of an integer or quarter integer number of turns. An equivalent circuit for the spiral inductor is given in figure 5.5. The parasitics associated with the metallisation planes (C_{M2} and C_{M3}) and the track resistance R are all evaluated from a fourth order polynomial while the shunt feedback capacitance C_{FB} is expressed by a more complex eighth order polynomial provided by the foundry.

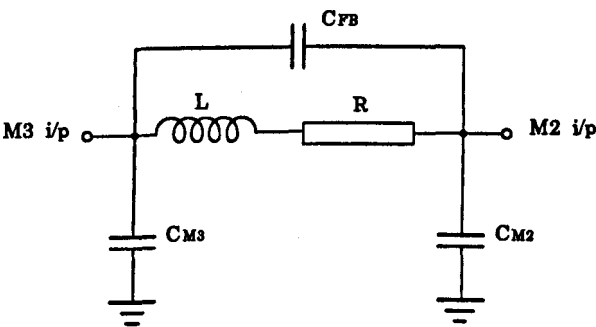


Figure 5.5: GaAs spiral inductor equivalent circuit

The third type is the stacked spiral inductor. This is essentially a stack of two spiral inductors isolated from each other by the dielectrics. Inductors realised in this manner suffer from slightly higher losses and lower Q than the standard spiral inductors. The stacked spiral inductor is mainly used for realising large inductances and when there is a constraint on the dimensions.

Table 5.2 illustrates the range of values afforded by the various inductor types.

Inductor type	Inductance range (nH)
Transmission line	$\ll 1$
Spiral	0.35 - 13
Stacked spiral	0.5 - 18

Table 5.2: GaAs inductor types

Polymide capacitors

The polymide parallel plate capacitor is formed using a composite polymide and silicon nitride dielectric filling giving capacitances in the range 0.06 - 2.5pF. The value of the capacitance is defined by a geometrically square M2 metallisation region which acts as one of the plates. The second plate is formed by a slightly larger area of M3. No vias are needed for polymide capacitors. A typical GaAs polymide capacitor is illustrated in figure 5.6.

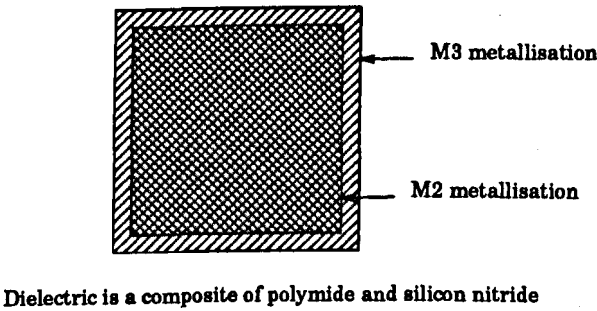


Figure 5.6: GaAs polymide parallel plate capacitor

The lumped element equivalent circuit model for the polymide capacitor is shown in figure 5.7.

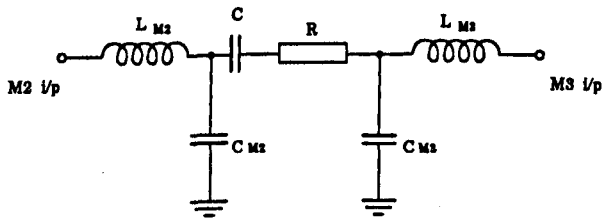


Figure 5.7: GaAs polymide capacitor equivalent circuit

L_{M2} , C_{M2} and L_{M3} , C_{M3} are the parasitics associated with the M2 and M3 plates respectively. C denotes the prime capacitance while R models the resistive and dielectric losses in the capacitor. The capacitances are expressed in terms of nonlinear expressions while a fifth order polynomial relates the inductances to the geometry of the parallel plate capacitor.

Nitride capacitors

The silicon nitride is an overlay capacitor similar to the polyimide, distinguishable only by its single silicon nitride dielectric, giving capacitances in the range 1.3 - 59pF. Again the capacitance is formed using a square base M2 plate and M3 top plate. In the fabrication stages a polyimide dielectric via is used to remove the polyimide layer from the capacitor and the capacitor is constructed around this via. The capacitance C is defined in this case by the area of the via and is illustrated in figure 5.8. Both the polyimide and nitride overlay capacitors are modelled as two port devices centrally fed at opposite edges such as to distort the field pattern as little as possible.

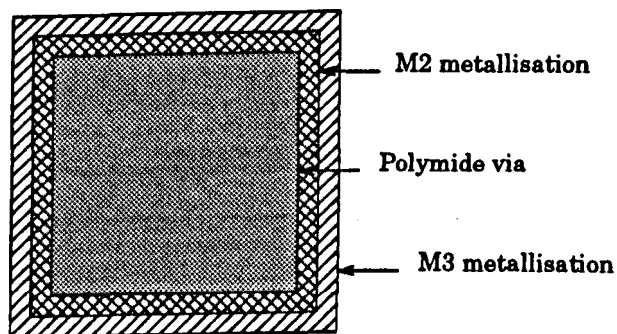


Figure 5.8: GaAs silicon nitride parallel plate capacitor

The lumped element equivalent model is the same as that in figure 5.7. The silicon nitride capacitor is different to the polyimide in that it exhibits symmetric rf behavior such that the input and output parasitic terms are equal. The series resistance has a negligible contribution due to the lower dielectric losses associated with the silicon nitride and is consequently omitted. The prime capacitance is defined by nonlinear expressions while the parasitic inductances are evaluated using the fifth order polynomials provided by the foundry.

Interdigital capacitors

This type of capacitor is used for obtaining very low values of capacitance, typically $<0.5\text{pF}$, and for high frequency operation. The interdigital capacitors are formed by interleaving track "fingers" deposited on the first metallisation layer (M2). The GaAs

structure of such a capacitor is shown in figure 5.9.

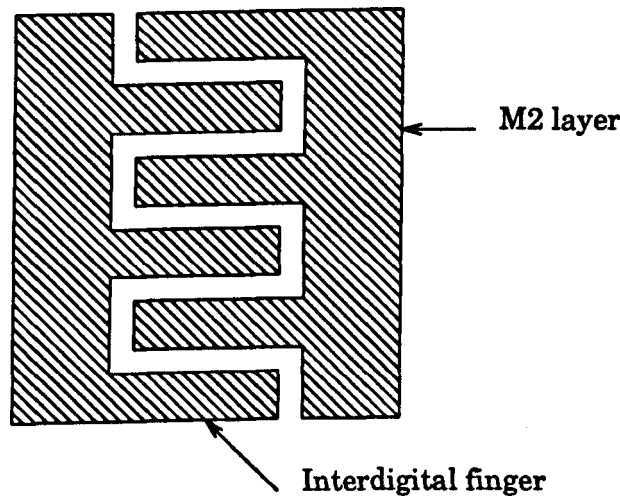


Figure 5.9: GaAs interdigital capacitor

The capacitance of an interdigital capacitor arises from the coupling between the fingers and is consequently a function of the number of fingers (maximum 20 for the process used). The equivalent model for the interdigital capacitor is shown in figure 5.10.

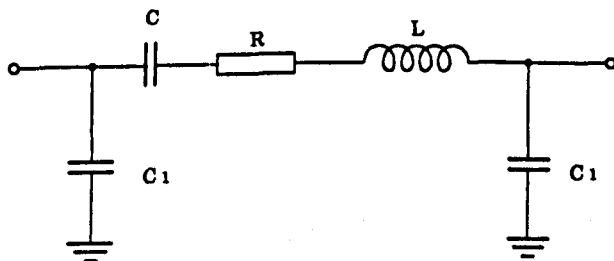


Figure 5.10: GaAs interdigital capacitor equivalent circuit

The associated parasitics C_1 , L and R are expressed by second, third and fifth order polynomials respectively, which are provided by the foundry. As the interdigital capacitor is fabricated with the M2 metallisation layer, the pattern definition and hence the tolerance of such capacitors is excellent, resulting from well defined gap spacings.

In general the tolerance and capacitance range of the various GaAs capacitor types are as summarised in table 5.3.

Capacitor realisation	Capacitance range (pF)	Tolerance
Polymide	0.06 - 2.5	± 12 %
Silicon nitride	1.3 - 59	± 13 %
Interdigital	<0.5	Negligible

Table 5.3: Tolerance and range of various GaAs capacitors

The tolerance of the whole fabrication process is approximately 12%, implying that all the capacitor values drift in unison.

Transmission lines

The conventional microstrip line is the most commonly used MMIC transmission line. This may be fabricated on either M2 or M3 level metallisation but the top (M3) level is preferred due to the lower loss characteristics. Figure 5.11 shows a cross section of a multi-dielectric microstrip line fabricated on GaAs that can allow for characteristic line impedances in the range of $40\Omega - 110\Omega$.

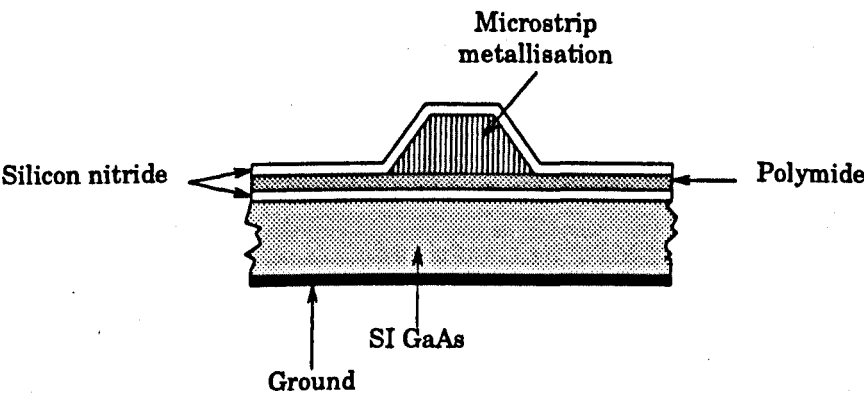


Figure 5.11: GaAs MMIC multi-dielectric microstrip line

Conventional microstrip line model simulators cannot be used due to the multi-dielectric nature of the GaAs MMIC transmission line. The dynamic behavior of the line is accurately described by closed form expressions provided by the foundry which relate the characteristic line impedance and effective dielectric constant to the width for both metallisation levels.

The interconnections on a GaAs MMIC layout need to be realised without any discontinuities. Discontinuities arising as a consequence of the T-junctions, bends and steps in track widths need to be accommodated. Correction factors for 50% chamfered bends, unchamfered bends and T-junctions are given by the foundry.

Interface components

Operation of the GaAs MMICs requires the connection between the chip and the outside environment. The chip input and output ports are represented by bond pads. The bond pads, located normally near the edges of the circuit, are built up from the M2 level, overlayed by the top M3 level. Contact is established between the two metallisations through vias in the silicon nitride and polyimide layers. A window in the nitride 2 level over the M3 layer is left open when the whole MMIC is encapsulated with the second blanketing silicon nitride passivation layer for bonding. Typically, the bond pad is $120\mu\text{m}$ square modelled as a 0.0004pF capacitor to ground.

The actual physical transition from the chip to a 50Ω microstrip line on an alumina substrate is by means of a $25\mu\text{m}$ gold bond wire. The bond wire contributes a series inductance of about $0.7\text{nH}/\text{mm}$. The equivalent model of the physical transition is illustrated in figure 5.12.

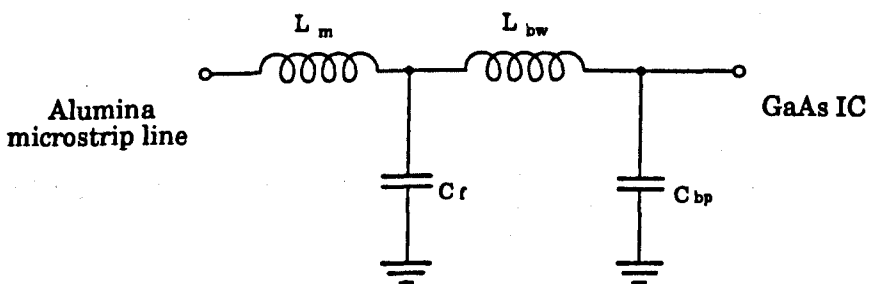


Figure 5.12: *Equivalent circuit of the physical GaAs/alumina transition*

L_{bw} represents the series inductance of the bond wire while C_{bp} represents the shunt capacitor to ground associated with the bond pad. The fringing field produced at the end of the microstrip line is modelled as the shunt capacitor to ground C_f and a series

inductance L_m to account for the change in current density at the transition between the wire and microstrip. Accurate models of the parasitics are given by the foundry for wideband operation.

Via holes

Ground vias are used for grounding purposes as vias cannot be made directly under the component low level metallisation. The vias are of $50\mu\text{m}$ diameter located in the middle beneath a square bond pad of $120\mu\text{m}$ width. The vias are modelled as a series inductance and resistance to ground with a -3dB cut-off at about 40GHz.

5.3 Lumped Element Phase Equaliser Networks

Lumped element phase equalising circuits are readily used at low and radio frequencies. However at microwave frequencies their operation is limited by the parasitics associated with the lumped elements. Surface mount components extend the usable operating range to the low microwave bands but for very high frequency operation GaAs pseudo lumped components as described earlier can be used. In this section phase equalising networks are designed and realised on GaAs for wideband microwave frequency applications.

Phase equalising circuits usually known as delay equalisers are essentially all-pass filters. These filters exhibit a flat frequency (magnitude) response and a variable phase shift. All-pass networks are characterised by the transfer function in which the absolute magnitude of the denominator and numerator equal a fixed constant. This implies that the zeros are mirror images of the poles. In order to satisfy the stability criterion the poles have to be in the left half of the complex-frequency plane and hence the zeros are in the right hand plane mirrored about the $j\omega$ axis. Illustrative pole-zero locations for first and second order all-pass transfer functions are shown in figure 5.13

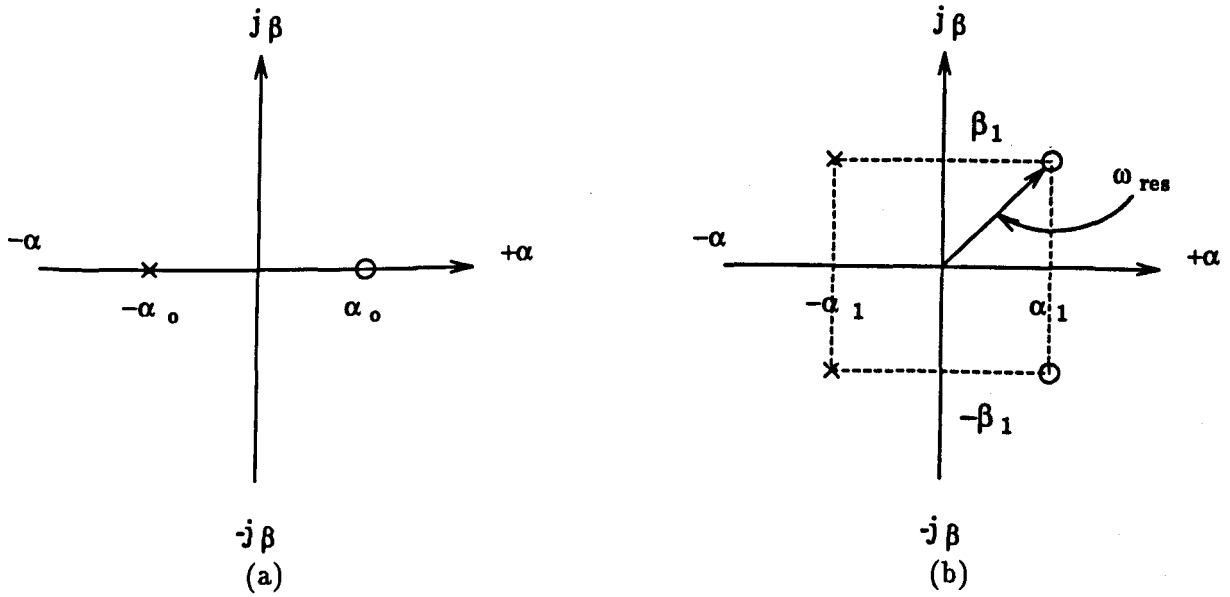


Figure 5.13: All-Pass pole-zero locations for (a) first order and (b) second order transfer functions

5.3.1 First order all-pass transfer function

The first order all-pass transfer function is a single pole/zero function given by the expression

$$T(s) = \frac{s - \alpha_0}{s + \alpha_0} \quad (5.2)$$

On making the substitution $s = j\omega$ and taking the absolute value of $T(s)$, the all-pass characteristics of equation 5.2 can be verified

$$|T(s)| = \frac{|s - \alpha_0|}{|s + \alpha_0|} = \frac{\sqrt{\alpha_0^2 + \omega^2}}{\sqrt{\alpha_0^2 + \omega^2}} = 1 \quad (5.3)$$

The phase of a first order network starts at 0° with $\omega = 0$ and approaches 180° as $\omega \rightarrow \infty$ and is described by:

$$\beta(\omega) = -2\tan^{-1}\left(\frac{\omega}{\alpha_0}\right) \quad (5.4)$$

The group delay is given by the derivative of the phase shift

$$T_{gd} = -\frac{d\beta(\omega)}{d\omega} = \frac{2\alpha_o}{\alpha_o^2 - \omega^2} \quad (5.5)$$

giving a maximum group delay when $\omega = 0$.

5.3.2 Second order all-pass transfer function

A second order transfer function gives rise to the pole/zero pattern as illustrated in figure 5.13b and is expressed as [80]:

$$T(s) = \frac{s^2 - \frac{\omega_{res}}{Q}s + \omega_{res}^2}{s^2 + \frac{\omega_{res}}{Q}s + \omega_{res}^2} \quad (5.6)$$

where ω_{res} is the pole resonant frequency in radians and Q is the pole Q given by

$$Q = \frac{\omega_{res}}{2\alpha_1} \quad (5.7)$$

The resonant pole frequency in terms of the pole/zero coordinates is given by

$$\omega_{res}^2 = \alpha_1^2 + \beta_1^2 \quad (5.8)$$

The absolute magnitude of the second order transfer function is found from

$$|T(s)| = \frac{\sqrt{(Z_e^2(s) - Z_o^2(s))}}{\sqrt{(P_e^2(s) - P_o^2(s))}} \quad (5.9)$$

where P_e, P_o, Z_e, Z_o are the even and odd components of the pole/zero describing polynomials respectively. Substitution of the coefficients of the polynomial results in

$$|T(s)| = \frac{\sqrt{(\omega_{res}^2 - \omega^2)^2 + \frac{\omega^2 \omega_{res}^2}{Q^2}}}{\sqrt{(\omega_{res}^2 - \omega^2)^2 + \frac{\omega^2 \omega_{res}^2}{Q^2}}} = 1 \quad (5.10)$$

By letting $a = \frac{\omega_{res}}{Q}$ and $b = \omega_{res}^2$, the phase shift in radians is given by the expression

$$\beta(\omega) = -2 \tan^{-1} \left(\frac{a\omega}{b - \omega^2} \right) \quad (5.11)$$

The group delay of the second order transfer function is then given by

$$T_{gd} = -\frac{d\beta(\omega)}{d\omega} = 2 \left\{ \frac{2a\omega^2 + a(b - \omega^2)}{(b - \omega^2)^2 + a^2\omega^2} \right\} \quad (5.12)$$

In the case of the second order transfer function variations in the phase are governed by two parameters (ω_{res}, Q) which, as shall be seen later, need to be traded off against one another when designing a second order network. The phase shift associated with a second order network is maximum (360°) at $\omega = \infty$ and 180° at $\omega = \omega_{res}$.

The peak of the group delay profile is subject to the value of $Q (= \omega_{res}/2\alpha_1)$ as illustrated in figure 5.14 and occurs when $\omega \approx \omega_{res}$.

5.3.3 All-pass networks

The synthesis of an all-pass function yields a lattice network. The lattice networks derived for first and second order transfer functions are depicted in figure 5.15. The output and input ports of the lattice network do not possess a common terminal and the lattice forms a balanced structure[81]. The constant resistance property of the lattice arises due to the fact that the impedance looking in at either port is of a constant resistance R when the other port is also terminated by the same resistance R . In this way many such structures may be cascaded without any of the networks loading the other, as indicated in figure 5.16.

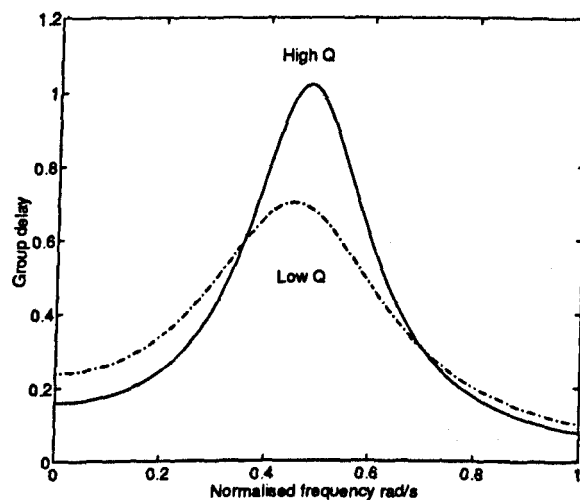


Figure 5.14: Effect of varying Q on the group delay profile of a second order transfer function

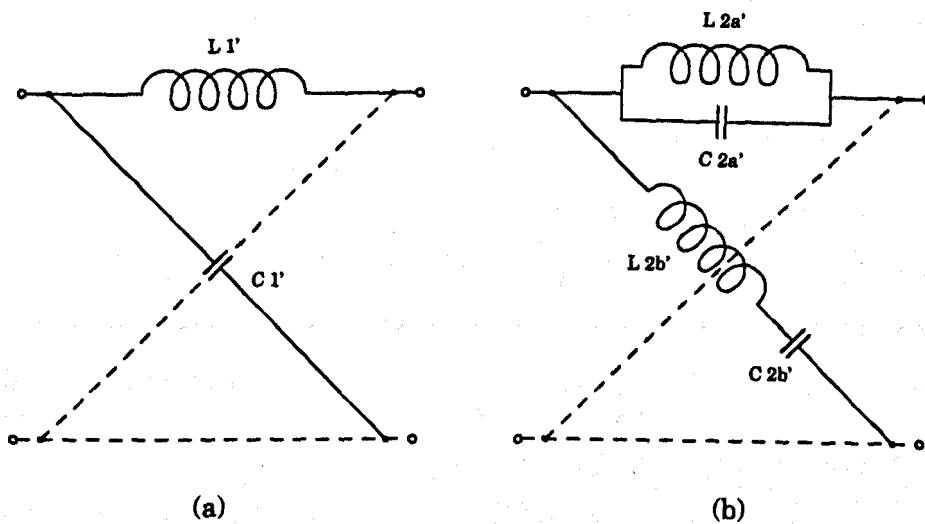


Figure 5.15: Lattice networks for (a) first order and (b) second order transfer functions

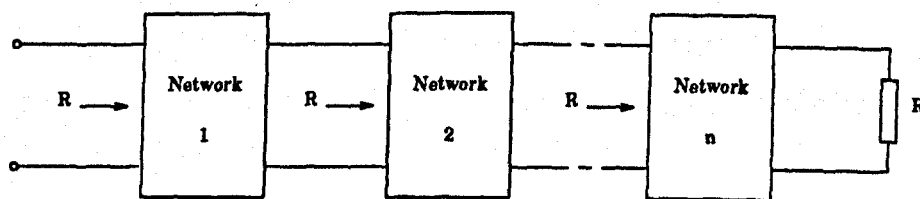


Figure 5.16: Cascade of constant resistance networks

In practical circuits it is often necessary to have an unbalanced network in which one port is grounded. Transformations allow the lattice networks to be realised as unbalanced bridged-T networks [82, 83]. For the case of a first order lattice an equivalent bridged-T using a centre-tapped inductor is required whereas second order lattices may be transformed into bridged-T networks with or without centre-tapped inductors. Centre-tapped inductor based bridged-T networks are not considered here. The bridged-T equivalents for the first and second order lattices are shown in figure 5.17.

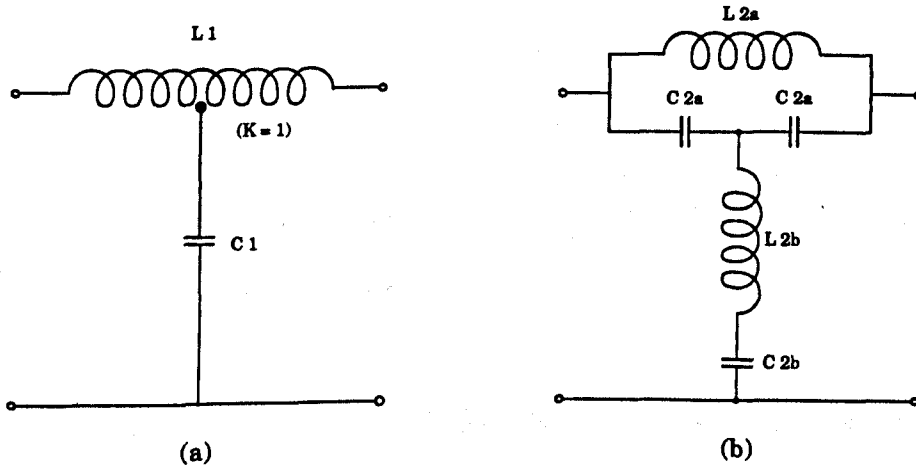


Figure 5.17: Bridged-T equivalents for the (a) first order and (b) second order lattice networks

The elements of the bridged-T networks are given in table 5.4 in terms of both the pole zero coordinates and the resonant frequency. All expressions are related to the circuit characteristic impedance R .

5.4 Single Section GaAs Phase Equaliser

We have seen that with coherent heterodyne detection mixing down to the IF achieves translation of the optical dispersion directly into the electrical domain and that with the IF signal in the microwave region the chromatic dispersion may be corrected with the aid of appropriately dispersive waveguide[63] or microstrip[41] structures. Which type of structure should be used is dependent on the choice of the local oscillator frequency f_{lo} . The local oscillator frequency must be set relative to the optical signal carrier frequency such that the fibre dispersion characteristic is of opposite sign, when

Order	Lattice elements	Bridged-T elements
1 st order	$L1' = \frac{R}{\alpha_o}$ $C1' = \frac{1}{\alpha_o R}$	$L1 = \frac{2R}{\alpha_o}$ $C1 = \frac{2}{\alpha_o R}$
2 nd order	$L2a' = \frac{R}{\omega_{res} Q} = \frac{Ra}{b}$ $L2b' = \frac{RQ}{\omega_{res}} = \frac{R}{a}$ $C2a' = \frac{Q}{\omega_{res} R} = \frac{1}{aR}$ $C2b' = \frac{1}{\omega_{res} QR} = \frac{1}{Rab}$ where $a = \frac{\omega_{res}}{Q}$ and $b = \omega_{res}^2$	$L2a = \frac{2R}{\omega_{res} Q} = \frac{2Ra}{b}$ $L2a = \frac{RQ}{2\omega_{res}} = \frac{R}{2a}$ $C2a = \frac{Q}{\omega_{res} R} = \frac{1}{aR}$ $C2b = \frac{2Q}{\omega_{res}(Q^2-1)R} = \frac{2a}{R(b-a^2)}$

Table 5.4: Expressions for the element values of the lattice and the equivalent bridged-T networks

mapped into the IF, to that of the compensator.

The group delay characteristic of a second order all-pass network is as illustrated in figure 5.14. With such circuits the linear portion of the group delay response is used to counter the fibre group delay characteristics. The approximate symmetry about the resonant frequency of the group delay characteristics offers two approximately linear regions of the curve that may be used to correct for the fibre dispersion. In this way such equalisers need not restrict the choice of local oscillator frequency, that is to say that the local oscillator frequency may be set above or below that of the incoming signal, unlike the microstrip and waveguide alternatives. However as only the linear region of the group delay response is being used to compensate for the fibre dispersion the maximum equalisable bandwidth is somewhat restricted.

5.4.1 Modelling the bridged-T

The model of the bridged-T is built up in terms of the ABCD matrix of the individual elements. The individual elements are regarded as two port networks such that any two individual elements may be considered to be cascaded by simply multiplying their individual ABCD matrices together. The ABCD matrix for a series impedance two port network is then given by

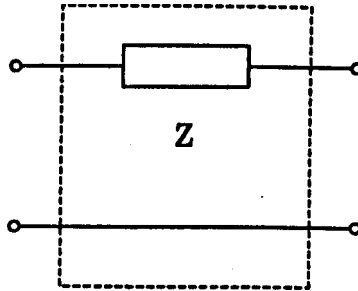
$$\begin{bmatrix} A & B \\ C & D \end{bmatrix}_{\text{series}} = \begin{bmatrix} 1 & Z \\ 0 & 1 \end{bmatrix}$$


Figure 5.18: ABCD matrix for a series impedance two port network

where Z is the element impedance (Ls or $1/Cs$). The ABCD matrix for a shunt impedance two port network is defined in terms of the element admittance as

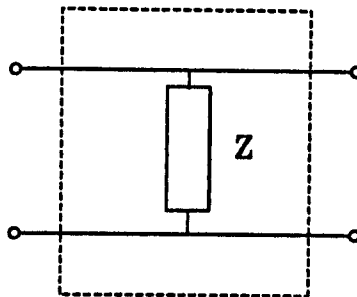
$$\begin{bmatrix} A & B \\ C & D \end{bmatrix}_{\text{shunt}} = \begin{bmatrix} 1 & 0 \\ Y & 1 \end{bmatrix}$$


Figure 5.19: ABCD matrix for a shunt impedance two port network

where $Y = 1/Z$ (ie. $Y = Cs$ or $1/Ls$).

The ABCD matrix of a parallel arm network requires firstly, the y -matrix of each arm to be calculated. All the y -matrices (equal to the number of parallel arms) are then summed and the result converted to an ABCD matrix[84].

Assuming that all the passive elements are defined as series impedance 2-port ABCD matrices (figure 5.18), the bridged-T structure of figure 5.17b can then be represented

in terms of an ABCD matrix using the pre-mentioned rules for cascaded and parallel element configurations. The steps leading to the bridged-T topology are then as follows:

- form the shunt arm first by cascading L_{2b} and C_{2b} . This is realised by multiplying the series impedance ABCD_{series} matrix representation of L_{2b} and C_{2b} . The resulting ABCD_{series} matrix is then translated into the ABCD_{shunt} matrix thereby forming the shunt arm - shunt 1.

$$[L_{2b}]_{C_{sr.s}} \times [C_{2b}]_{C_{sr.s}} = [arm1]_{C_{sr.s}}$$

$$[arm1]_{C_{sr.s}} \xrightarrow{\text{shunt}} [arm1]_{C_{shunt}} = shunt1$$

where $C_{sr.s}$ and C_{shunt} represents the ABCD matrix for the series and shunt impedance two-port network as depicted in figures 5.18 and 5.19 respectively.

- cascade shunt 1 with one of the C_{2a} 's and then cascade the result with the other C_{2a} giving a series impedance ABCD matrix for a T-network. The multiplication process of the ABCD matrices is given as

$$[C_{2a}]_{C_{sr.s}} \times [arm1]_{C_{shunt}} \times [C_{2a}]_{C_{sr.s}} = [T]_C$$

- convert the ABCD matrix of the T-network into a y-matrix and add to the y-matrix of L_{2a}

$$[T]_C \xrightarrow{y} [T]_y$$

$$[T]_y + [L_{2a}]_y = [network]_y$$

- finally convert the resulting y-matrix into an ABCD matrix defining the whole network.

$$[network]_y \xrightarrow{ABCD} [network]_C$$

The model of the bridged-T structure interms of its ABCD matrix is converted to the scattering S-matrix. From the forward transmission coefficient S_{21} of the scattering matrix the magnitude and group delay response of the equaliser can be calculated. The S_{21} parameter is used in the design of the group delay equaliser to be outlined next.

5.4.2 Design method of a single section equaliser

As a starting point, the linear region of the group delay of an ideal single section bridged-T network is roughly matched to the group delay produced by a given length of a standard single mode fibre of 17ps/km/nm dispersion when used in the 1550nm wavelength window. For a transformer-free lattice to bridged-T transformation, the element values are required to conform to the condition [85]

$$\frac{\alpha_1}{\beta_1} < 0.557 \quad (5.13)$$

where α_1 and β_1 are the real and imaginary pole coordinates respectively. The element values are chosen by firstly varying the parameters of equation 5.12 such that the fibre and equaliser group delay responses are approximately matched. The element values of the ideal network obtained from table 5.4 are used in the ABCD description of the bridged-T equaliser to evaluate the group delay and magnitude response of the network.

The ideal components are replaced by the more complex GaAs equivalent circuit together with the relevant interconnections and bond pads. The delay equaliser is then optimised, allowing for the parasitics. The optimisation routine constrains the GaAs element values to within pre-defined ranges. The group delay and magnitude characteristics of the ideal and optimised networks are illustrated in figure 5.20.

The length of fibre was chosen in accordance with the literature reported by Elrefaie et al. [40] where the authors observed a signal eye closure of 2dB for CPFSK (continuous phase frequency shift keying) transmission at 5Gbit/s over 100km of standard monomode fibre.

The magnitude response of the network is evaluated using the expression

$$\text{Attenuation (dB)} = 20.\log_{10}(S_{21}) \quad (5.14)$$

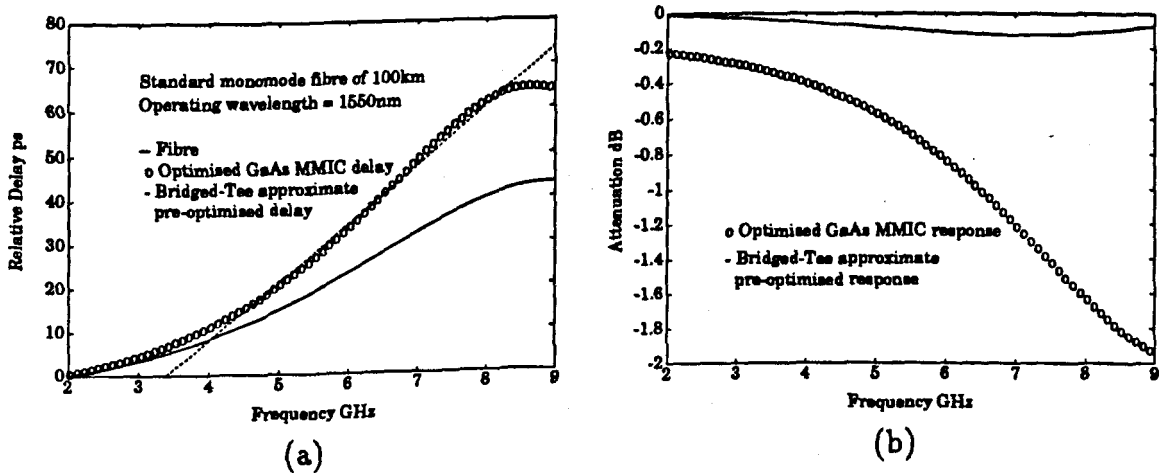


Figure 5.20: Analytically predicted (a) group delay and (b) magnitude responses of the equaliser

while the group delay is the derivative of the phase with frequency. The gradient of the fibre delay response is of opposite polarity to that shown. This form of presentation being selected to facilitate comparison between the equaliser and fibre delay responses.

The parasitics associated with the GaAs elements considerably influence the network response as shown in figure 5.20. The group delay equaliser is designed to correct for the dispersion produced by 100km of standard monomode fibre with an operation optical wavelength of 1550nm. The optimised equaliser compensates for the dispersion over a 4-5GHz bandwidth centred at 6GHz but suffers a modest degradation in the magnitude response of $\pm 0.75\text{dB}$ over the equalised bandwidth.

Using the optimised element values the GaAs network is laid out in-house using the CADENCE CAD suite, observing the foundry process design rules and constraints. The CAD output is shown in figure 5.21 while a photomicrograph, figure 5.22, depicts the GaAs MMIC realisation of the single section equaliser.

The degree to which the ideal network components are altered by the optimisation routine is illustrated in table 5.5.

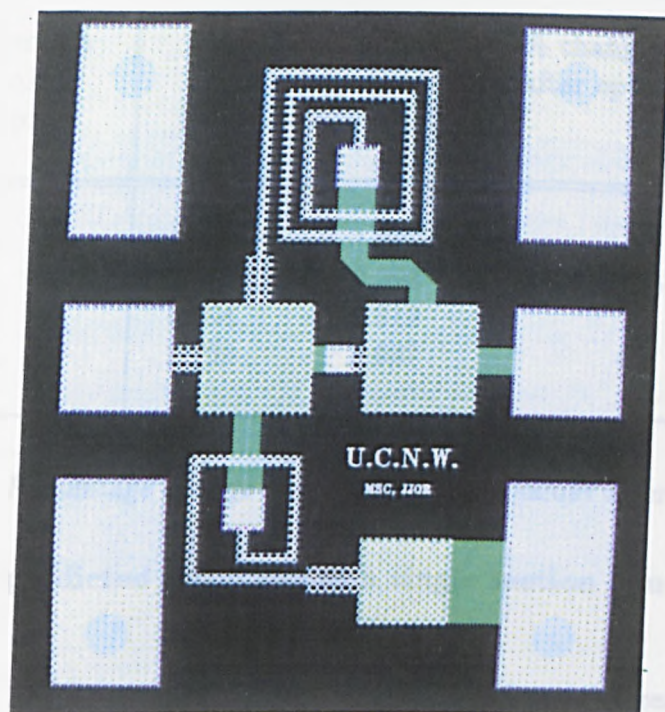


Figure 5.21: CAD layout of single section bridged-T equaliser

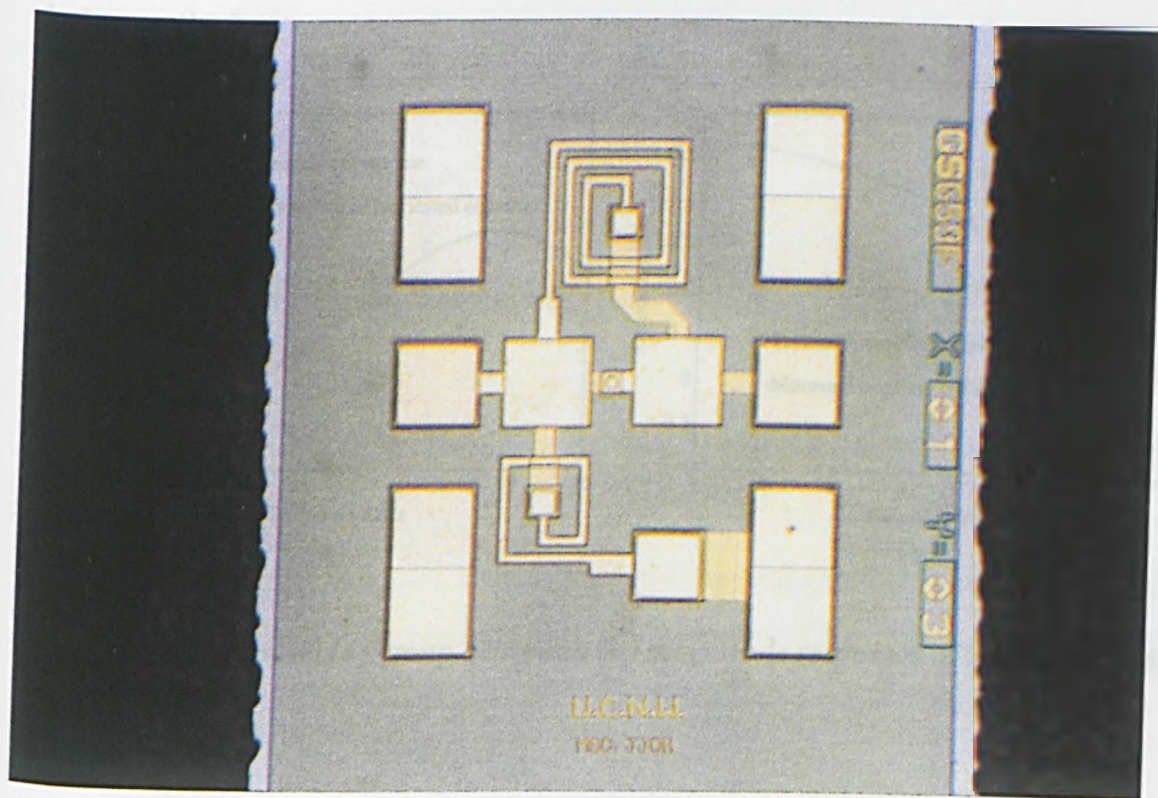


Figure 5.22: Photomicrograph of single section bridged-T equaliser

Element L(nH) C(pF)	Ideal	GaAs	% change in value after optimisation
L ₁	1.224	1.309	7
L ₂	0.394	0.393	0.25
C ₁	0.394	0.319	19
C ₂	3.758	3.937	4.8

Table 5.5: Percentage change in the component values after optimisation

Measured and predicted responses of a single section equaliser

The group delay and magnitude responses obtained from the realised GaAs MMIC equaliser [86] are shown in figure 5.23. The measured and predicted responses show very good agreement over the range of interest thereby verifying the GaAs models and design methods.

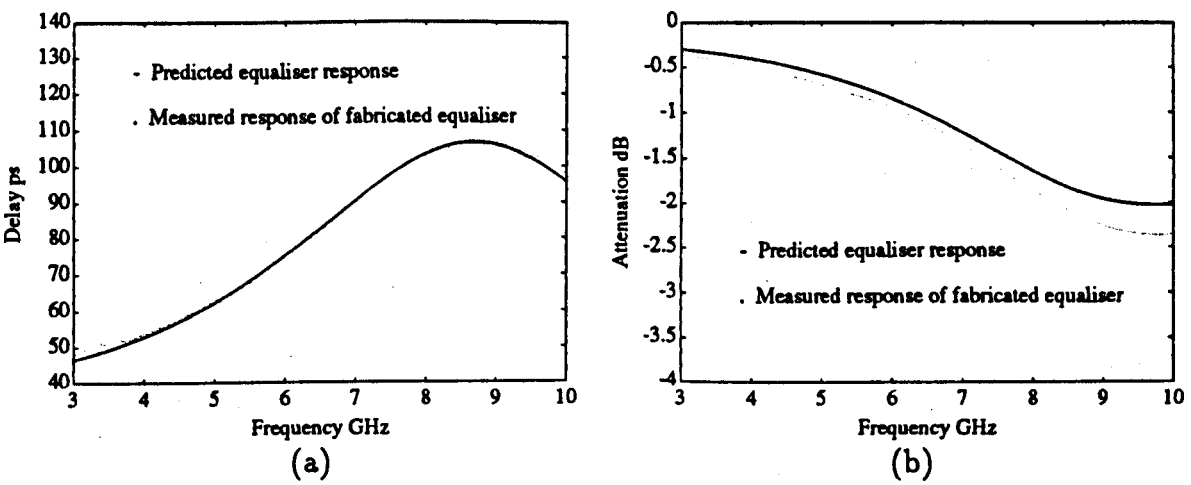


Figure 5.23: Measured (a) group delay and (b) magnitude responses of the GaAs MMIC equaliser

5.5 Cascaded Staggered Section Equaliser

A major disadvantage of single section equalisers is the limited maximum correctable bandwidth available, as only the linear region of the group delay characteristics of the single section bridged-T is utilised. In order to overcome this limitation a number of the single section networks with staggered group delay characteristics may be cascaded. The group delay is cumulative as illustrated in figure 5.24. The group delay responses of the individual sections are staggered from one another to achieve equalisation over larger bandwidths [87].

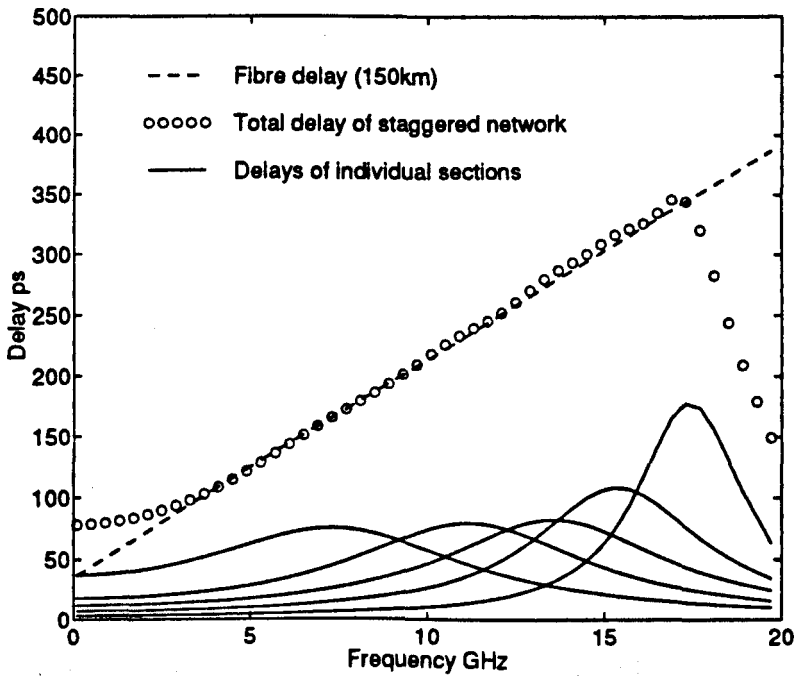


Figure 5.24: Realisation of wideband equalisers by cascading single sections with staggered delay responses

In realising the delay responses of each section a tradeoff needs to be effected between the network Q and ω_{res} , the resonant angular frequency. These parameters are traded against each other such that an optimum delay response is obtained for a transformer free network.

The design method for cascaded single section equalisers is similar to that outlined previously except in this case, rather than converting the ABCD matrix of the single

bridged-T network into the equivalent S -matrix, the ABCD matrices of the individual single sections are multiplied together to emulate the cascading process. The final product of the ABCD matrices is then converted to S -parameters for evaluating the group delay and magnitude responses.

The transfer function of the whole network is the product of the individual transfer functions given as

$$T(s) = \prod_{n=1}^M \frac{s^2 - a_n s + b_n}{s^2 + a_n s + b_n} \quad (5.15)$$

where n is the section number. The group delay of the whole network is the sum of the single sections given by

$$T_{gd} = \sum_{n=1}^M \left[2 \left\{ \frac{2a_n \omega^2 + a_n(b_n - \omega^2)}{(b_n - \omega^2)^2 + a_n^2 \omega^2} \right\} \right] \quad (5.16)$$

where again n is the section number.

5.5.1 Realisation of a staggered GaAs MMIC equaliser

The group delay and magnitude characteristics of an equaliser comprising a cascade of two second order networks is shown in figure 5.25. The staggered delays of the individual sections are summed to match the fibre target.

The ideal-component-based equaliser offers negligible attenuation while matching the fibre delay characteristics over a very large bandwidth. Replacing the ideal components with the GaAs counterparts results in the “pre-optimised GaAs MMIC” response. The parasitics attenuate considerably the network response. For an optimised single section bridged-T network around 2dB attenuation can be expected at ω_{res} , the frequency of the group delay peak. Therefore, for a network comprising a cascade of many sections a marked attenuation characteristic can be expected.

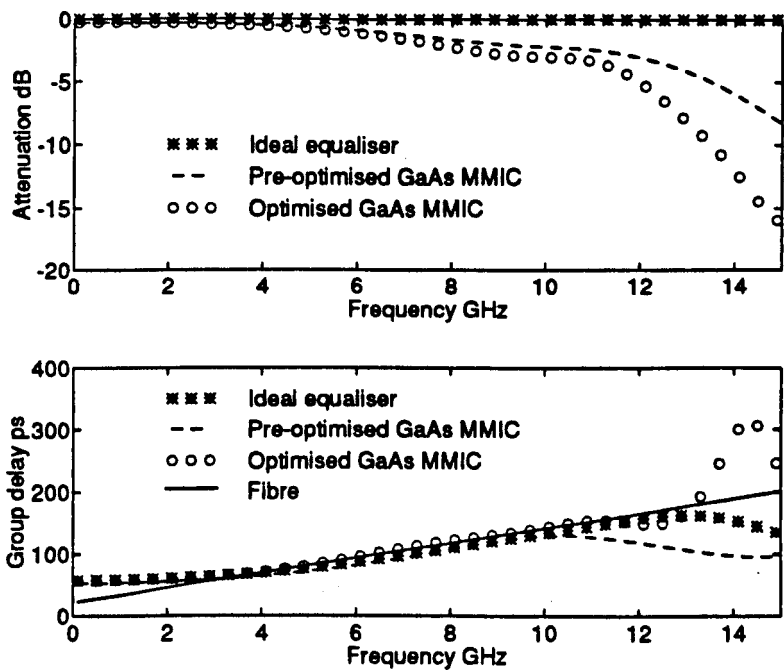


Figure 5.25: Realisation of GaAs MMIC wideband equaliser by cascading single sections with staggered delay responses; (top) magnitude (bottom) group delay

Allowing for the interconnecting tracks and bond pads the network is then optimised. The optimisation process yields a group delay response that matches the fibre target over a large bandwidth ($\approx 10\text{GHz}$). The magnitude response however is degraded slightly, fluctuating by $\pm 1.5\text{dB}$ over the equalised range. Equalisers designed to correct for the dispersion produced by large lengths of fibre will inevitably be hindered by the attenuation characteristics of the network due to the parasitics associated with the GaAs elements. It should be noted, thereby, that given the relatively unsophisticated criterion adopted for equalisation - pre-defined group delay flatness independent of modulation format and rate - a network designed for a given fibre span may in practice provide good performance for greater fibre lengths. We shall see that, depending on the bit-rate and modulation format an equaliser may be able to correct for a fibre span of twice the length for which it was originally designed.

The wideband twin bridged-T equaliser is realised on GaAs using spiral and transmission line inductors together with silicon nitride, polyimide and interdigital capacitors. A photomicrograph is shown in figure 5.26.

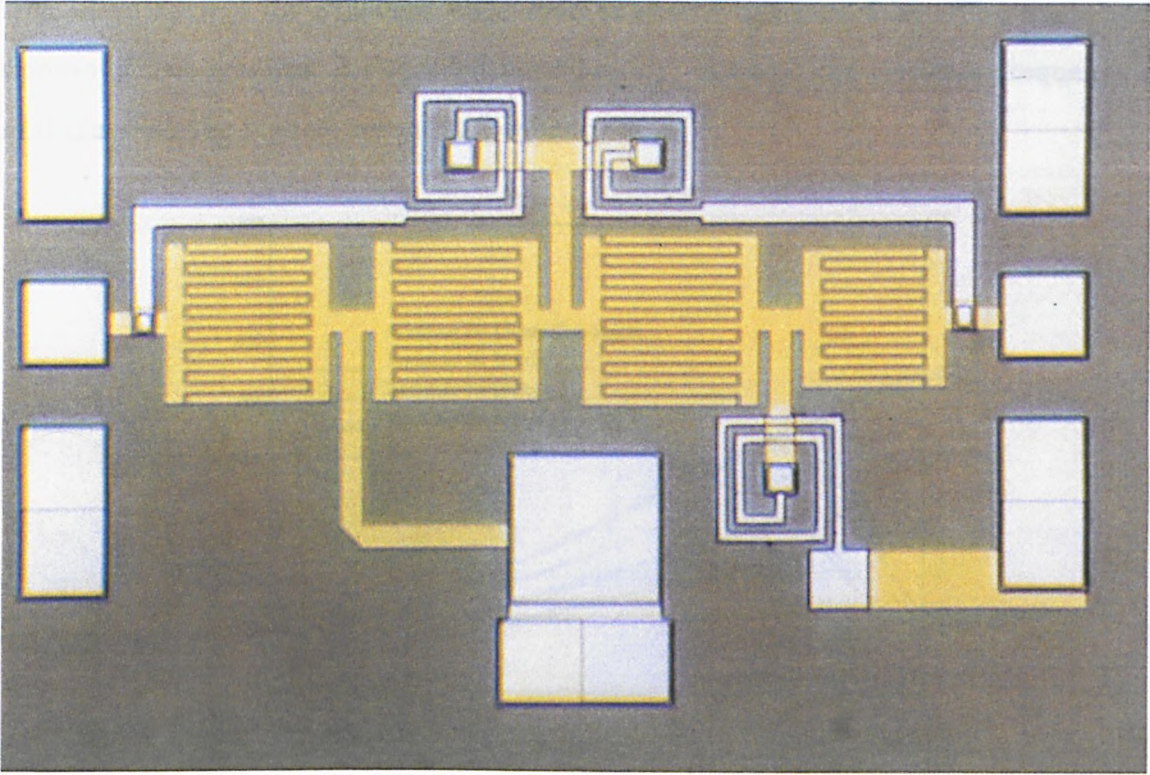


Figure 5.26: *Photomicrograph of cascaded bridged-T equalisers*

The optimised element values for this equaliser yield the response illustrated previously in figure 5.25. The variation in the element values as a percentage of the ideal component values are given in table 5.6.

In seeking to effect a match to the fibre target, the element values obtained after optimisation for the GaAs MMIC realisation are considerably different from the initial ideal values. With the GaAs element parasitics it is not always possible to replicate the ideal group delay response without considerable degradation of the magnitude characteristics.

Equalisers have been designed in this way to compensate for fibre spans of 150, 200, 250 and 300km comprising of 3, 4, 4 and 5 cascaded single sections respectively, with that for 200km being evaluated via GaAs MMIC realisation. The remaining equalisers have been evaluated using ideal lumped element components. The group delay characteristics of the four ideal element based equalisers are illustrated in figure 5.27.

The magnitude and group delay characteristics of the optimised GaAs MMIC equalisers designed to correct for a 200km fibre span is shown in figure 5.28. The magnitude response of the equaliser is degraded considerably, worst at the resonant frequency of the stage with the highest resonant frequency ω_{res} .

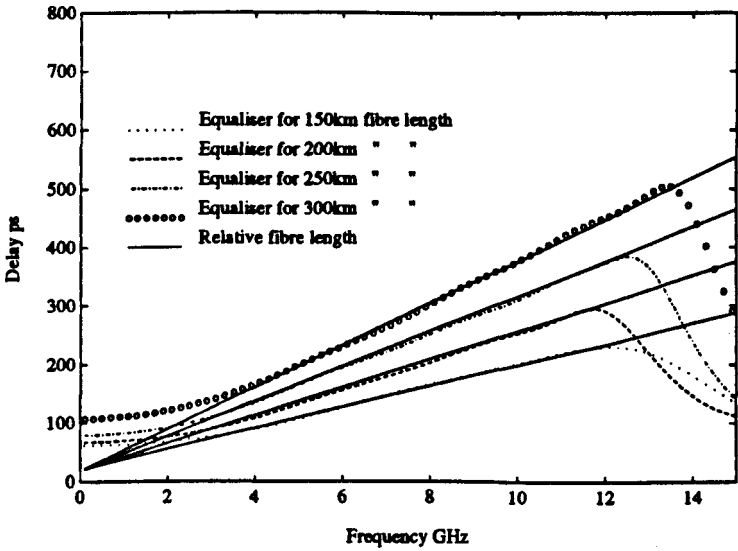


Figure 5.27: Group delay responses of four ideal element equalisers designed to correct for fibre spans of 150, 200, 250 and 300km

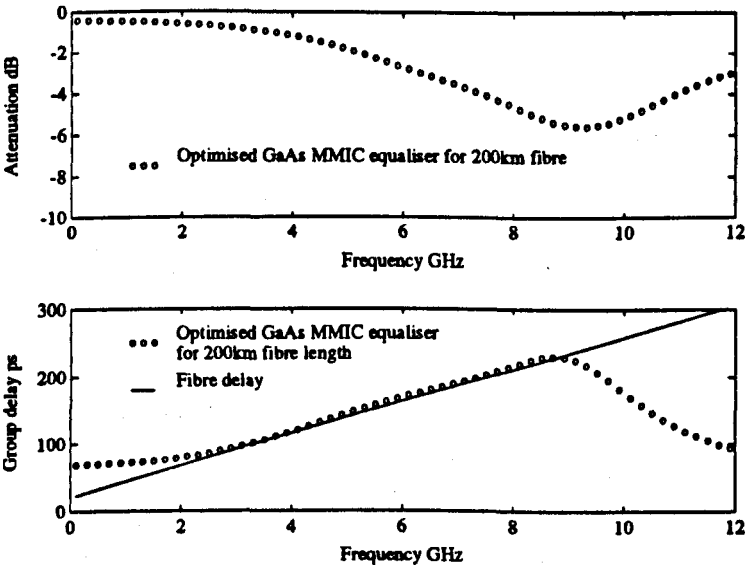


Figure 5.28: Magnitude (top) and group delay (bottom) responses of an optimised GaAs MMIC equaliser to compensate for the dispersion produced by 200km of single mode fibre

	Element L(nH) C(pF)	Ideal	GaAs	% change in value after optimisation
Section 1	L ₁	1.357	1.608	18
	L ₂	0.386	0.3547	8
	C _{1a}	0.3084	0.2406	22
	C _{1b}	0.3084	0.2131	31
	C ₂	4.511	19.380	300
Section 2	L ₁	0.525	0.590	12
	L ₂	0.612	0.764	24
	C _{1a}	0.490	0.279	43
	C _{1b}	0.490	0.157	68
	C ₂	0.268	0.148	45

Table 5.6: Percentage change in the component values after optimisation of the two-section cascaded equaliser

5.6 Summary

This chapter has introduced a commercial gallium arsenide GaAs foundry process, highlighting the processes and layout requirements for the fabrication of MMICs. The models of the GaAs elements provided by the foundry have been found to allow for accurate modelling of the MMIC realisations.

While alternative microwave technologies have resulted in physically bulky solutions to the problem of dispersion compensation the GaAs MMIC fabrication process has been utilised to realise compact circuits, with dimensions on a millimetre level, that can correct for the dispersion produced by a standard monomode fibre when operating in the 1.55µm window.

All-pass GaAs MMIC networks designed to correct for the dispersion produced by specified fibre lengths have been devised and fabricated. A single section equaliser based on a bridged-T transformation of the second order lattice network has been

used to correct for the dispersion produced by a fibre span of 100km. The maximum correctable bandwidth of this equaliser is limited, as only the linear region of the group delay characteristics of the equaliser is used. This equaliser has been fabricated and a comparison effected between the predicted and measured results has shown very good agreement.

The problem of achieving larger equalised bandwidths has been addressed by means of cascading a number of single section equalisers with staggered individual group delay responses. In this way an optimised equaliser has been designed offering a 10GHz equalised bandwidth for a fibre span of 100km. Additional equalisers designed for larger fibre reaches have been presented.

The realisation of pseudo-lumped element networks with this technology offers a particular advantage over the alternative electrical domain equalisation strategies in that the GaAs MMIC equalisers may be fully integrated with other receiver circuitry if so desired.

The use of a MMIC equaliser as an integral component of a coherent transmission system is assessed in the following chapter. The influence of various modulation schemes on the electrical dispersion power penalty for an equalised transmission system is examined.

Chapter 6

System Performance Implications of Equalisation

6.1 Introduction

The concept of using all-pass networks as phase equalisers was introduced in the previous chapter and taken to the stage where such networks were realised as gallium arsenide (GaAs) monolithic microwave integrated circuits (MMICs). The physical size and the possibility of integration with other receiver circuitry make this approach an attractive option when compared to the alternative microstrip or waveguide IF equalisation strategies.

In this chapter the system performance benefits of dispersion equalisation are assessed by determining the inter symbol interference (ISI) observed in the eye pattern. GaAs MMIC equaliser performance is assessed for linear and non-linear modulation schemes.

A comparison is affected here between the potential of the ideal GaAs and microstrip equalisers in terms of the bit-rate distance product.

Equaliser performance is further assessed for optically chirped signals. As a measure of robustness, system performance is evaluated for fibre spans exceeding the target length of the original equaliser design.

6.2 Modulation Formats

Both linear and non-linear modulation formats are assessed, chosen specifically to emulate the results reported by Elrefaie et al. The linear scheme explored is binary amplitude shift keying (ASK) and the non-linear schemes are continuous-phase frequency shift keying (CPFSK) and minimum shift keying (MSK). The results presented by Elrefai et al. show that the linear ASK modulated waveform is degraded by the fibre chromatic dispersion the least, whereas at the other extreme CPFSK is degraded the most.

6.2.1 Amplitude Shift Keying (ASK)

In amplitude shift keying, the modulated output results from the carrier being switched on and off in sympathy with the data stream. This can be generalised to take into consideration the possibility of having M discrete amplitude levels. A two-level ASK modulated wave form is illustrated in figure 6.1.

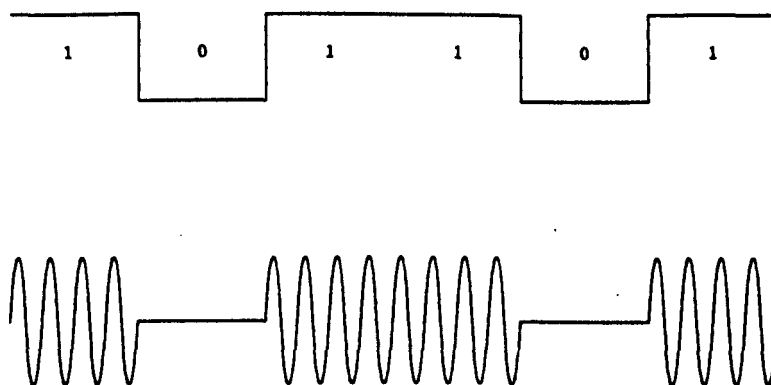
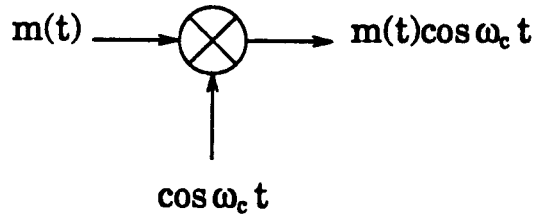


Figure 6.1: ASK waveform

The modulation process is essentially the multiplication, in the time domain, of the unipolar message, $m(t)$, with the carrier, ω_c .



The demodulation process for ASK is the multiplication of the received signal with the carrier.

$$\begin{aligned}
 m(t) \cdot \cos \omega_c t \times \cos \omega_c t &= m(t) \cos^2 \omega_c t \\
 &= \frac{m(t)}{2} \{1 + \cos 2\omega_c t\}
 \end{aligned} \tag{6.1}$$

The high frequency components can be filtered out by a low-pass filter to recover the message. With heterodyne detection the demodulation method requires a local oscillator frequency (f_{lo}) that is offset from the carrier such that the received signal is translated to the IF as shown by

$$\begin{aligned}
 m(t) \cdot \cos \omega_c t \times \cos \omega_{lo} t &= \frac{m(t)}{2} \{ \cos(\omega_c - \omega_{lo})t + \underbrace{\cos(\omega_c + \omega_{lo})t}_{\text{Filtered}} \} \\
 \text{yielding} \quad &\underbrace{\frac{m(t)}{2} \cos(\omega_c - \omega_{lo})t}_{\text{IFSignal}}
 \end{aligned} \tag{6.2}$$

In the case of homodyne detection f_{lo} is set equal to the carrier frequency.

The power spectrum of an ASK modulated signal relative to the carrier frequency is illustrated in figure 6.2

Most of the signal power is contained within the main lobe with nulls of the power spectrum occurring at the signalling rate b_r . The power spectrum of ASK decreases at a rate proportional to f^{-2} away from the carrier frequency. The bandwidth of the main

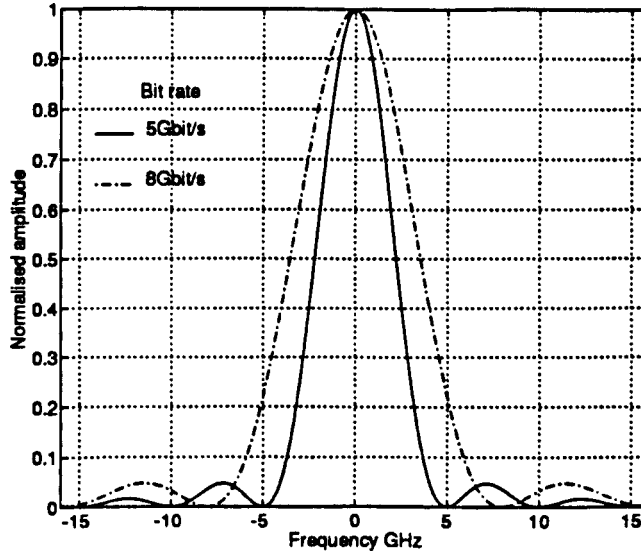


Figure 6.2: ASK power spectrum for 5 & 8Gbit/s signalling rates

lobe (B_l) is taken at the full-width-half-maximum (FWHM) point. The transmission bandwidth B_T can then be estimated to be

$$B_T \approx b_r \approx B_l \quad (6.3)$$

The performance of a modulation format is assessed in terms of its *spectral efficiency*; the ratio of the bit-rate to the transmission bandwidth given by

$$\frac{b_r}{B_T} \approx \log_2 M \quad \text{bps/Hz} \quad (6.4)$$

where M is the number of discrete amplitude levels for an M -level ASK signal. The spectral efficiency (or modulation “speed”) of ASK is quite poor, $b_r/B_T \approx 1\text{bps/Hz}$ when $M=2$.

6.2.2 Continuous-Phase FSK (CPFSK) and Minimum Shift Keying (MSK)

In the pre-fibre days of the twisted wire transmission medium, bandwidth limitations resulted in research into alternative modulation schemes of superior spectral efficiency to that offered by amplitude modulation. This resulted in the non-linear modulation schemes such as CPFSK and MSK, of which the latter has since been used for domestic satellite, military tactical radio and underwater communication systems [88]. As the name suggests CPFSK is an offshoot of the conventional Frequency Shift Keying, while MSK as shall be shown later is a special case of CPFSK.

With ASK the amplitude of the carrier was switched between two levels ($M = 2$) depending on the data stream. For FSK the amplitude is kept constant but the frequency is varied in sympathy with the data as shown in figure 6.3.

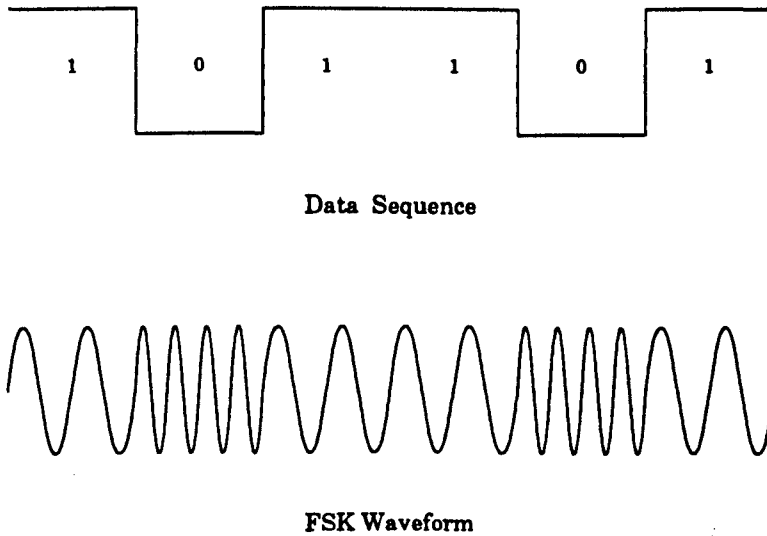


Figure 6.3: Data sequence and corresponding FSK waveform

The instantaneous frequency at any time may be written as

$$f_i = f_c + \Delta f a_n \quad (6.5)$$

where $a_n = \pm 1$ (the data sequence) and Δf is the maximum frequency deviation given

by

$$\Delta f = \beta_m f_m \quad (6.6)$$

β_m is referred to as the modulation index while $f_m = 1/b_r$ is the frequency of the modulating message $m(t)$.

If a FSK modulated signal is generated by means of switching two unlocked oscillators, then the phase of the signal may be randomly distributed over a 2π range, having no correlation to the modulating signal and taking any random value at the switching transitions. This can lead to sharp transitions at every bit change resulting in generation of high frequency spectral components. FSK has a resulting power spectrum with a main lobe possessing a transmission bandwidth of $B_T \approx b_r$. The nulls in the power spectrum occur at $3/2b_r$ and have a fourth order roll-off as compared to a second order roll-off for ASK.

The use of a single oscillator can overcome the obstacles of phase discontinuity, as the phase is maintained while frequency deviating the oscillator. It is the continuous phase form of FSK that is called CPFSK. A continuous-phase frequency shift keying modulated signal is expressed as

$$x_{CPFSK}(t) = \cos \left\{ \omega_c t + \phi + \left[\Delta\omega \int_0^t x(\lambda) d\lambda \right] \right\} \quad \text{for } t \geq 0 \quad (6.7)$$

where ϕ is the phase of the previous bit, ω_c is the carrier frequency in rad.s^{-1} and the term in the inner parenthesis is the frequency modulated data sequence with $\Delta\omega$ being the frequency deviation. CPFSK is a memory based scheme in that the phase shift of the k^{th} bit depends on the previous bit. In this way a continuous phase is maintained for all t at the expense of circuit complexity.

To maintain phase continuity, for a message signal of a non return-to-zero (NRZ) bit period T_b the central carrier frequency must be

$$f_c = N \frac{1}{4T_b} \quad (6.8)$$

where N is an integer and the separation between the upper f_h and lower f_l modulated frequencies is

$$f_h - f_l = N \frac{1}{2T_b} \quad (6.9)$$

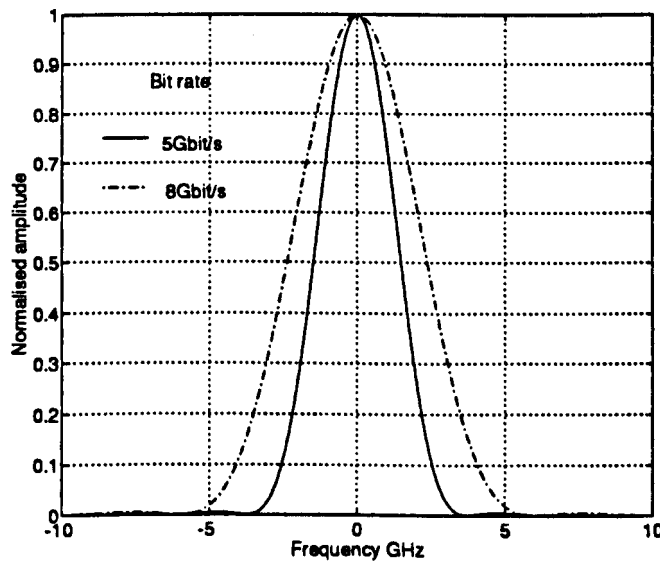


Figure 6.4: MSK power spectrum for 5 & 8 Gbit/s signalling rates

If $N = 1$, the spacing between f_h and f_l is the minimum for maintaining phase continuity. This is therefore referred to as Minimum Shift Keying (MSK) - a special case of CPFSK. The minimum frequency separation in conjunction with phase continuity gives MSK an improved spectral efficiency as compared to FSK and ASK. The power spectrum of MSK is illustrated in figure 6.4.

The power spectrum at base band is obtained from the expression

$$G_{msk} = \frac{16}{\pi^2 b_r} \left[\frac{\cos(2\pi f/b_r)}{(4f/b_r)^2 - 1} \right]^2 \quad (6.10)$$

The nulls occur at $(3/4)b_r$ for the spectrum which has a fourth order roll-off resulting in minuscule spillover beyond the main lobe. The transmission bandwidth for MSK is taken as $B_T \approx b_r/2$ resulting in a spectral efficiency of

$$\frac{b_r}{B_T} \approx 2 \text{ bps/Hz}$$

twice that of FSK. MSK is therefore often referred to as Fast FSK. Approximately 99% of the energy is contained within the transmission bandwidth, however the MSK power spectrum has a main lobe which is larger than the main lobe of modulation schemes such as Quadrature and Offset Quadrature Phase Shift Keying, QPSK and OQPSK respectively. The improvement in spectral efficiency, fast power spectrum roll-off and ease of demodulation are some of the properties that make MSK an attractive alternative.

Generation of MSK/CPFSK

As MSK is a special case of CPFSK then by showing the method of generating MSK the generation of a CPFSK modulated signal follows by varying N in equations 6.8 and 6.9.

Figure 6.5 illustrates the process for generating a MSK signal. The input data stream (A) of bit period T_b is divided into its odd (B) and even (C) parts. The odd stream (B_o) comprises of all the odd bits $b_{1,3,5,\dots}$, whereas the even stream (B_e) contains all the even bits $b_{2,4,6,\dots}$. All the bits in the odd and even stream are held for a period of $2T_b$. The staggered even and odd streams are multiplied by the waveforms $\sin 2\pi \left(\frac{t}{4T_b}\right)$ and $\cos 2\pi \left(\frac{t}{4T_b}\right)$ as shown in (D), which are generated at the transmitter. A criteria for continuous phase is that the waveforms in (D) have zero crossings corresponding to their respective bit edges. That is $\sin 2\pi \left(\frac{t}{4T_b}\right)$ has a zero crossing at the end of every even bit interval while $\cos 2\pi \left(\frac{t}{4T_b}\right)$ has a zero crossing at the end of every odd bit interval. The generated products are as shown in (E) and (F). By generating the quadrature carriers $\cos \omega_c t$ and $\sin \omega_c t$ the MSK transmitted signal is then

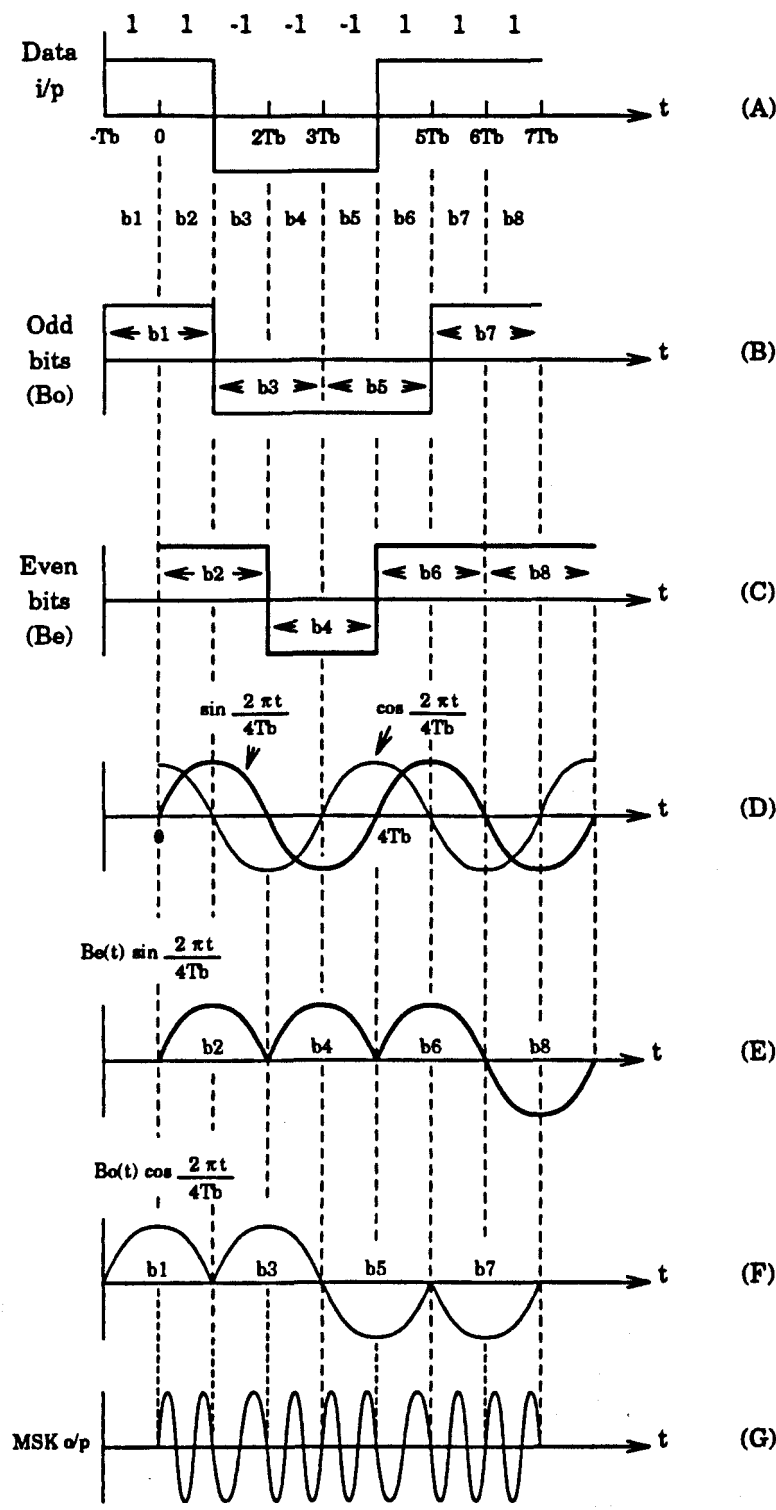


Figure 6.5: MSK waveform generation

$$x_{MSK}(t) = \left[B_e(t) \sin 2\pi \left(\frac{t}{4T_b} \right) \right] \cos \omega_c(t) + \left[B_o(t) \cos 2\pi \left(\frac{t}{4T_b} \right) \right] \sin \omega_c(t) \quad (6.11)$$

as shown in (G). The upper and lower modulating frequencies together with the carrier frequency are evaluated using the expressions given by equations 6.8 and 6.9 with the condition that $N = 1$.

The more compact power spectrum of MSK results from the smoother transitions in the pulse shapes as those defined in (E) and (F).

The simplistic model of a MSK transmitter is illustrated in figure 6.6.

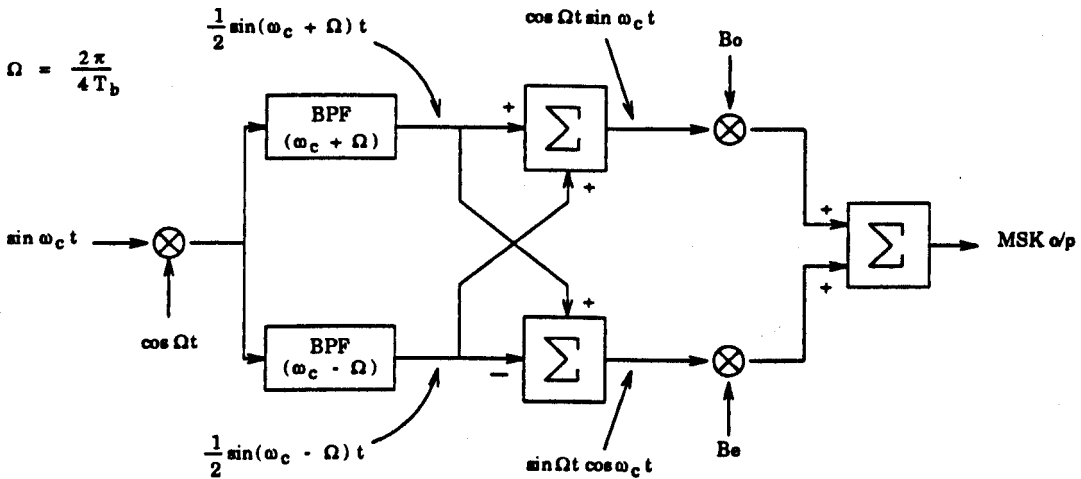


Figure 6.6: MSK transmitter

6.3 System Modelling

In this section the basic system models for the linear and the non-linear modulation formats are presented. These models are used to simulate a coherent transmission system. To simplify matters, all the models have been translated to their baseband equivalents.

The transmission medium, the fibre, is characterised in the frequency domain by the baseband equivalent expression

$$h_{fibre}(f) = \exp \left\{ j2\pi^2 \tilde{\beta} f^2 L + j\frac{4}{3}\pi^3 \ddot{\beta} f^3 L + \dots \right\} \quad (6.12)$$

where $\tilde{\beta} = -20 \times 10^{-27} \text{ s}^2/\text{m}$ [15ps/km/nm] and $\ddot{\beta} = 8.1 \times 10^{-40} \text{ s}^3/\text{m}$ [0.08ps/km/nm/nm] are the second and third derivatives of the propagation constant β respectively and L is the fibre length. The linear phase term is omitted since it does not introduce distortion. The fibre is modelled as a bandpass filter with a flat amplitude response and linear group delay.

The block diagrams for ASK and MSK/CPFSK transmission systems are shown in figures 6.7 and 6.8.



Figure 6.7: Block diagram of an ASK transmission system

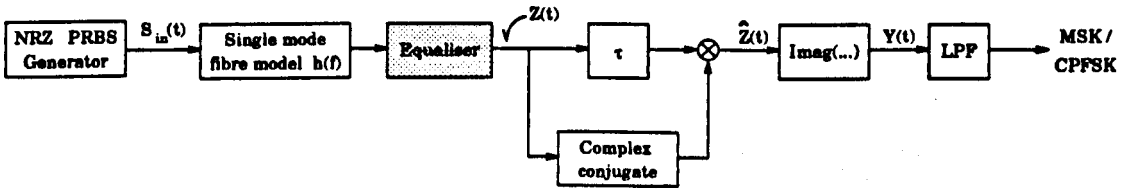


Figure 6.8: Block diagram of a MSK transmission system

The fibre input signal linearly modulated (ASK) onto the optical carrier is given by:

$$S_{in(ask)}(t) = \sum_n a_n F(t - nT_b) \quad (6.13)$$

Here T_b is the bit period, $F(t)$ is the signal pulse waveform, taken to be of unit amplitude within the bit period and zero elsewhere, and a_n is 0 or 1. The corresponding

frequency domain baseband expression for the output of the fibre is given by

$$z(f) = \left\{ \int_{-\infty}^{\infty} S_{in(ask)}(t) e^{-j2\pi ft} dt \right\} . h_{fibre}(f) \quad (6.14)$$

In a heterodyne detection system the received signal is mixed with a local oscillator frequency f_{lo} , generating sum and difference frequencies, the difference ($f_{if} = f_s - f_{lo}$) being the desired IF. The equaliser response, centred on f_{if} , may be translated to a baseband equivalent:

$$eq(f) = eq_{if}(f - f_{if}) \quad (6.15)$$

Dealing with a linear modulation scheme, the final processed output is then the real (\Re) part of the inverse Fourier transform of the product of $z(f)$ and $eq(f)$ as given by

$$Y(t) = \Re[\mathcal{F}^{-1}\{z(f).eq(f)\}] \quad (6.16)$$

Similarly, from equation 6.7 the complex equivalent baseband modulated signal for MSK and CPFSK at the fibre input is given by [89]

$$S_{in(msk,cpfsk)}(t) = \exp \left\{ j2\pi \Delta f \int_{-\infty}^t \sum_n a_n F(t' - nT_b) dt' \right\} \quad (6.17)$$

This baseband expression relates to the inphase and quadrature waveforms (E & F) as depicted in figure 6.5. In this case $a_n = \pm 1$, and Δf is $0.5/T_b$ for CPFSK and $0.25/T_b$ for MSK. The baseband expression at the output of the fibre is given by

$$z(f) = \left\{ \int_{-\infty}^{\infty} S_{in(msk,cpfsk)}(t) e^{-j2\pi ft} dt \right\} . h_{fibre}(f)$$

The inverse Fourier transform of $z(f)$ is given by

$$Z(t) = \int_{-\infty}^{\infty} z(f)e^{j2\pi ft}df \quad (6.18)$$

$Z(t)$ is delayed and multiplied together with its undelayed complex conjugate in order to model a frequency discriminator, resulting in

$$\begin{aligned} \hat{Z}(t) = & \{\Re[Z(t-\tau)]\Re[Z(t)] + \Im[Z(t-\tau)]\Im[Z(t)]\} \\ & + j \{\Im[Z(t-\tau)]\Re[Z(t)] - \Re[Z(t-\tau)]\Im[Z(t)]\} \end{aligned} \quad (6.19)$$

The delay τ is chosen to be smaller than the bit period and \Re and \Im represent the real and imaginary parts of the complex signal.

Only the imaginary part of $\hat{Z}(t)$ is used as this contains the information. The reason behind only using the imaginary component of the signal can be supported by considering the model of the frequency discriminator, that is multiplying the delayed signal with its undelayed complex conjugate, as shown previously in figure 6.8. If at some time (t)

$$Z(t) = e^{j\omega_i t}$$

where ω_i is the instantaneous frequency at time (t), then the output of the multiplier will be

$$\hat{Z}(t) = e^{-j\omega_i t} \cdot \underbrace{e^{j\omega_i t} \cdot e^{-j\omega_i \tau}}_{\text{delayed signal}}$$

results in $e^{-j\omega_i \tau}$ since $e^{j(\omega_i t - \omega_i t)} = 1$ with the complex conjugate of $Z(t)$ given by $e^{-j\omega_i t}$. The phase is equivalent to $\omega_i \tau$ then using the appropriate trigonometric identity the signal may then be represented as

$$\hat{Z}(t) = \cos(\omega_i \tau) - j \sin(\omega_i \tau)$$

With the delay τ chosen to be smaller than the bit period, the cosine term tends to 1, while $\sin(\omega_i\tau) \Rightarrow \omega_i\tau$. Therefore the phase information is contained in the imaginary portion of $\hat{Z}(t)$.

The lowpass 2nd order Butterworth filter with a 3dB cut-off frequency equal to $0.65/T$ is used as a receiver shaping filter, giving zero ISI for rectangular input pulses [40].

6.4 Performance Assessment of Equalised Systems

The transmission systems furnishing both the linear and non-linear modulation formats are assessed with the GaAs implementations of the single section equaliser and with the wideband staggered cascaded section equaliser. Their performance is evaluated by means of the “electrical dispersion” power penalty P_{disp} given by the extent of the eye closure

$$P_{disp} = 20 \log \frac{a}{b} \quad (6.20)$$

where a is the eye opening without any fibre present and b is the eye opening of the system under test for a given fibre length.

The optical source here is assumed to be spectrally pure such that any phase noise and chirp may be neglected. Optical sources such as those mentioned earlier in chapter two support the assumption of noise free spectrally pure laser sources, as their linewidth is relatively smaller than the signalling bandwidth. By using an external integrated optical modulator of the Mach-Zehnder type, fabricated on titanium-lithium niobate, chirp can be neglected [90, 91, 92]. The assumption that the phase noise may be eliminated is also supported by the results reported by Iwashita and Matsumoto [93] where the authors evaluated the linewidth requirements for differentially detected CPFSK. In their findings the authors reported a bit error rate of 10^{-9} with an averaged received optical power of -49.9dBm for a $1.55\mu\text{m}$ 400Mbit/s transmission over 290km of single mode fibre for linewidths ranging from 600kHz - 1MHz. These results suggest that for

near giga-bit transmission rates non-negligible linewidths can be accommodated while maintaining a receiver sensitivity approximating the theoretical shot noise limit. For the experiment reported by Iwashita and Matsumoto the maximum laser linewidth as a percentage of the bit-rate is 0.25%, however, if the bit-rate is increased to 5Gbit/s, then a laser with a linewidth of 12.5MHz can be tolerated. It is reasonable to assume then that the effects of the phase noise can be ignored for high bit-rate systems.

The PRBS is a non-return-to-zero code of length 2^5-1 such that the effect of chromatic dispersion alone may be measured by means of the ISI. A super-Gaussian pulse with $m = 3$ is used to approximate the output of the modulator representing a "1".

In a practical system a much longer PRBS sequence would be required to test the system, however, in this case the short PRBS length is not a deficiency as the shape of the eye is unaffected.

6.4.1 Performance of the single section equaliser

The single section equaliser is assessed for a 5Gbit/s modulation rate. Table 6.1 illustrates the performance of the equaliser in correcting for the dispersion produced by a 100km transmission.

Modulation format	Power penalty with no equalisation (dB)	Power penalty with equalisation (dB)	Improvement (dB)
ASK	0.34	0.29	0.05
MSK	0.43	0.18	0.25
CPFSK	1.12	0.08	1.04

Table 6.1: System performance of the single section equaliser for various modulation formats

The influence of equalisation for a 5Gbit/s transmission rate is not that dramatic, however table 6.1 does illustrate its effect with the various modulation formats. ASK suffers the least from fibre chromatic dispersion suggesting larger allowable un-equalised

transmission spans for a given dispersion power penalty than that possible with MSK or CPFSK. The equaliser offers a greater degree of improvement for the non-linear schemes than for ASK.

The equaliser, having been designed to correct for the dispersion produced by a 100km fibre span is evaluated for larger fibre spans to obtain a measure of its robustness.

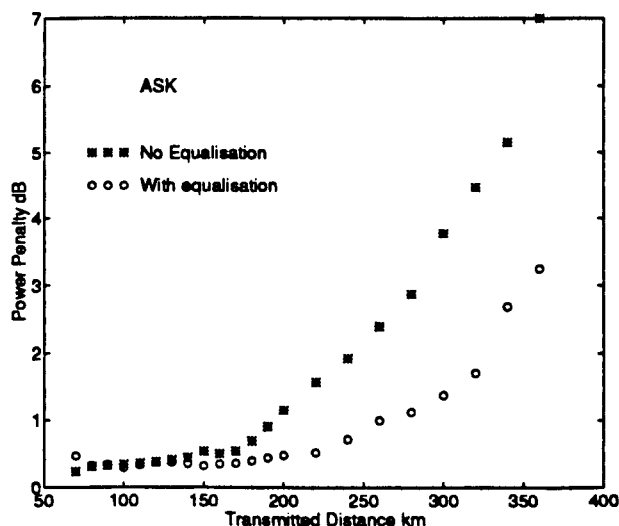


Figure 6.9: Dispersion power penalty improvement with single section equaliser for a 5Gbit/s ASK modulated system

Figure 6.9 depicts the performance of the GaAs MMIC single section equaliser out to a fibre length of 350km where it offers an improvement of over 3.5dB at a 5Gbit/s modulation rate. For fibre lengths in the range of 100-200km, the dispersion power penalty is ≈ 1 dB and the equaliser has little effect. However, at larger fibre lengths the ASK modulated signal is degraded substantially and rapidly with increasing distance. At 350km the dispersion degrades the performance of the unequalised transmission system by about 7dB. The eye pattern for both the unequalised and the equalised signals after a 350km transmission are shown in figure 6.10.

Although MSK is a more spectrally efficient modulation scheme than ASK, the four state signal space representation of the message makes it more sensitive to system degradations. Similarly CPFSK modulated signals are degraded. With two level CPFSK the frequency separation between the two modulating frequencies is larger than it is

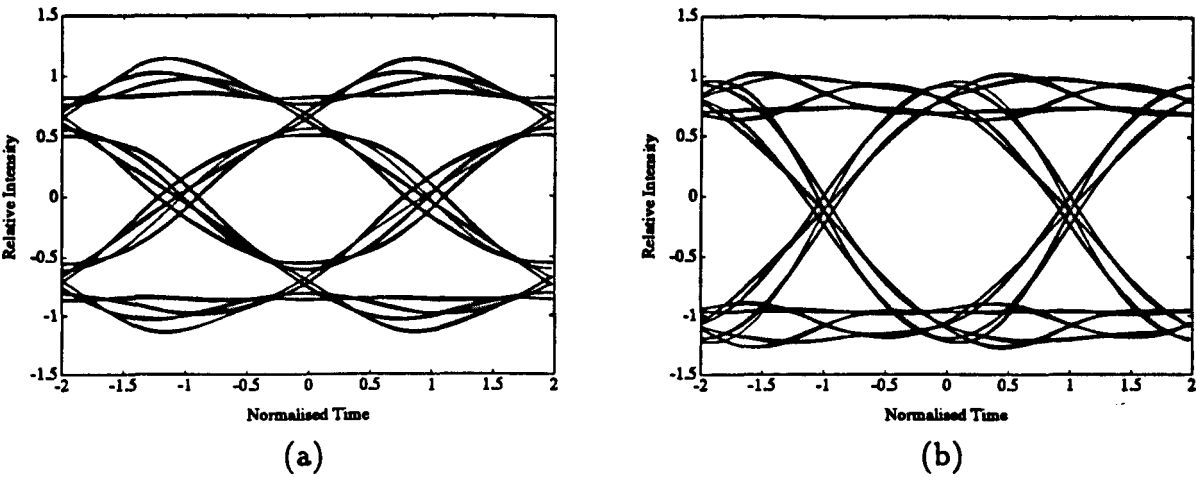


Figure 6.10: Eye patterns for a) unequalised and b) equalised ASK modulated signals at 5Gbit/s over 350km

for MSK. This large frequency difference results in a larger differential delay time between the two frequencies degrading CPFSK modulated signals to a greater extent than MSK. The extent of degradation is illustrated in figure 6.11. The maximum attainable transmission distance is taken as being the distance at which the un-equalised system performance is degraded by 2dB.

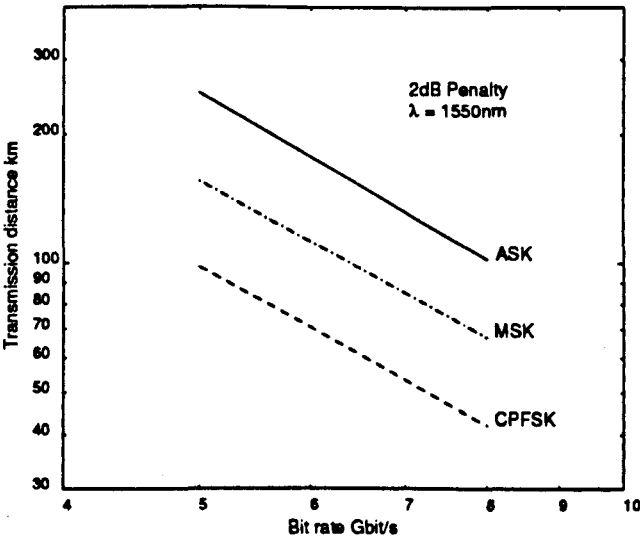


Figure 6.11: Dispersion limitations for ASK,MSK and CPFSK modulated systems operating at $1.55\mu\text{m}$ with $15\text{-}17\text{ps/km-nm}$ of chromatic dispersion

For the non linear modulation formats the modulation rate used is again 5Gbit/s, equivalent to the equalised bandwidth of the single section equaliser. Generally with

FM transmission, the transmission bandwidth is set according to *Carlson's rule* which suggests a transmission bandwidth of $\approx 15\text{GHz}$ for a 5Gbit/s modulation rate, much wider than the equalised bandwidth provided by the single section equaliser. However, with MSK as 99% of the power is contained within the main lobe, the transmission bandwidth at the -3dB point is taken to be $\approx b_r/2$ with the nulls of the main lobe having a $1.5b_r$ separation. Bearing this in mind, the following results for MSK and CPFSK are calculated with the assumption that the majority of the signal power is contained within the main lobe of bandwidth approximately equal to that of the equaliser.

The equaliser performance is assessed for transmission lengths exceeding 100km for MSK modulated signals. The MSK system dispersion power penalty with increasing distance is plotted in figure 6.12.

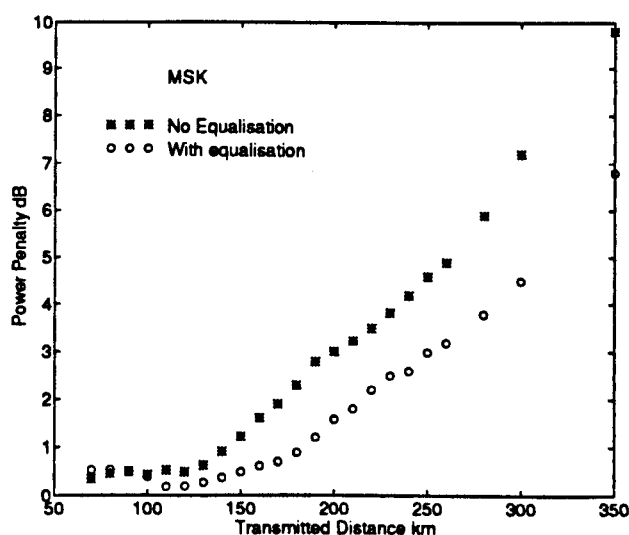


Figure 6.12: Dispersion power penalty improvement with single sectioned equaliser for a 5Gbit/s MSK modulated system

With equalisation and after 250km transmission through single mode fibre the dispersion power penalty resulting in a MSK system is reduced to 3dB , an improvement of over 1.5dB . The eye patterns for the unequalised and equalised systems at this distance are illustrated in figure 6.13.

The CPFSK modulated system is the most sensitive of the three compared. The dispersion penalty rapidly increases degrading the system performance with increasing

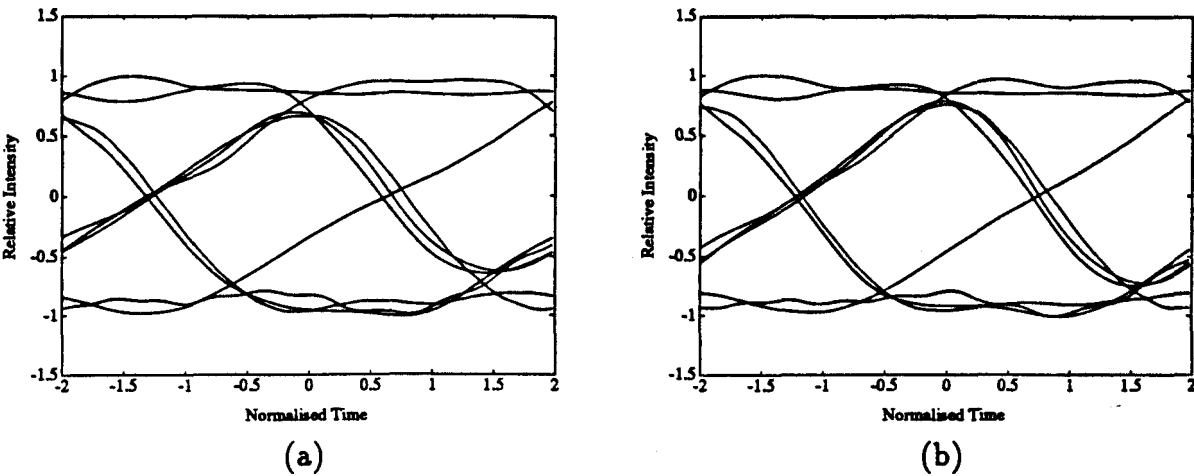


Figure 6.13: Eye patterns for a) unequalised and b) equalised MSK modulated signals at 5Gbit/s over 250km

distance. For a 5Gbit/s modulation rate a fibre length of 120km is sufficient to degrade the system performance by 3dB. The dispersion power penalty as a function of the transmitted distance is illustrated in figure 6.14.

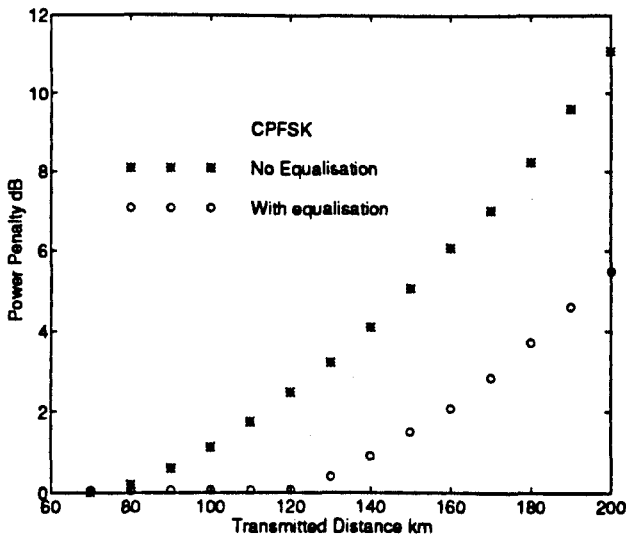


Figure 6.14: Dispersion power penalty improvement with single sectioned equaliser for a 5Gbit/s CPFSK modulated system

The affect of the equaliser on CPFSK modulated signals is shown in figure 6.15 by the eye patterns produced for a 5Gbit/s transmission over 160km of standard monomode fibre. An improvement of the eye is evident although the pulse shape is not fully recovered.

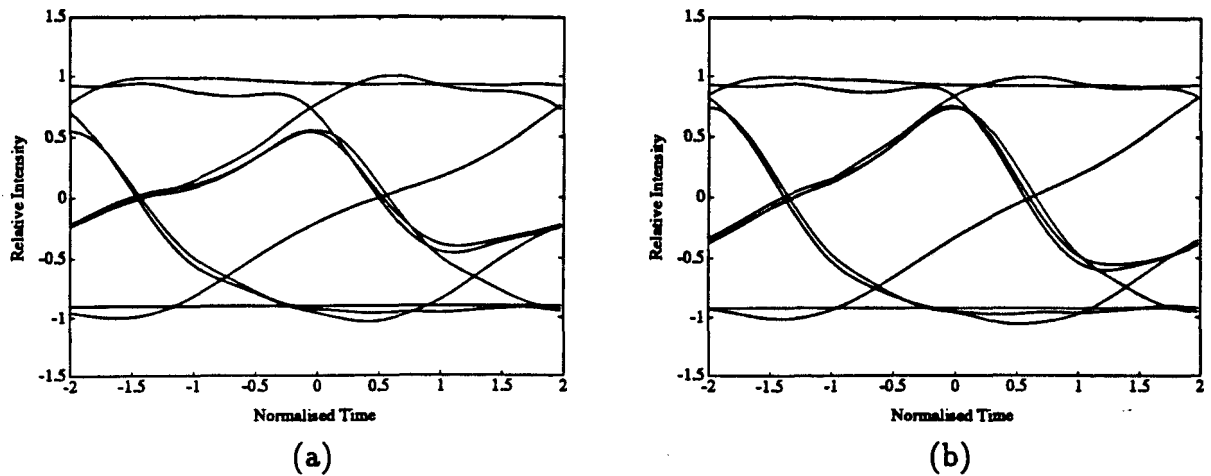


Figure 6.15: Eye patterns for a) unequalised and b) equalised CPFSK modulated signals at 5Gbit/s over 160km

The performance of all the modulation systems considered is depicted in figure 6.16. The severity of the degradation experienced by CPFSK modulated signals is clearly pronounced.

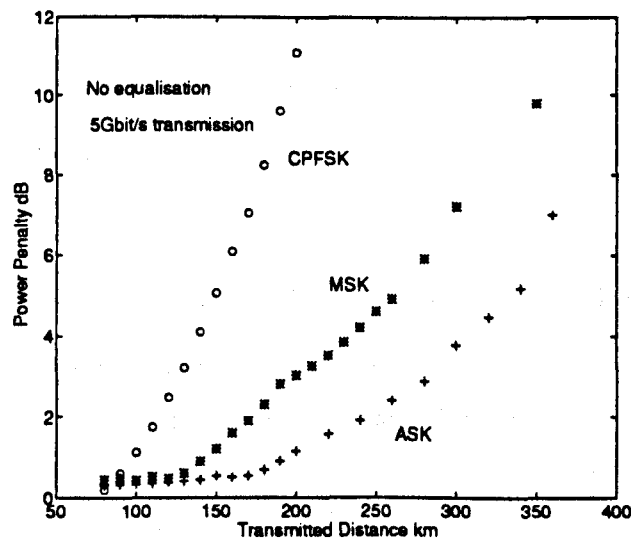


Figure 6.16: Dispersion power penalty for ASK, MSK and CPFSK systems for a 5Gbit/s modulation rate

6.4.2 Performance of the cascaded staggered section equaliser

The GaAs cascaded staggered section equaliser introduced in section 5.5 is evaluated here. The larger equalised bandwidth allows for its performance to be assessed with a higher bit-rate of 8Gbit/s. The results for the electrical dispersion power penalty obtained with and without equalisation are presented in table 6.2.

Modulation format	Power penalty with no equalisation (dB)	Power penalty with equalisation (dB)	Improvement (dB)
ASK	2.0	0.6	1.4
MSK	4.72	0.95	3.77
CPFSK	15	3.5	11.5

Table 6.2: System performance of the cascaded staggered section equaliser for various modulation formats

The effect of the equaliser is again more pronounced for the non-linear schemes than for ASK.

The non-linear modulation schemes are more severely impaired by the fibre chromatic dispersion at such high bit-rates. The equaliser performance is more pronounced with CPFSK where it offers an improvement of over 11dB.

For 8Gbit/s transmission over an unequalised system, the fibre length required to give rise to a 2dB dispersion power penalty has been reported by Elrefaie et al. as being \approx 40km for CPFSK, \approx 70km for MSK and \approx 100km for ASK.

The performance of the wideband equaliser is evaluated once again over a range of fibre spans. Eye diagrams of the individual systems are evaluated and presented in figures 6.17, 6.18 and 6.19.

High bit-rate transmission drastically degrades the performance of CPFSK. The equaliser at this high bit-rate is pushed extremely hard to recover the signal shape. The ISI at a fibre span of 100km is so severe that even with the equaliser the eye is degraded by

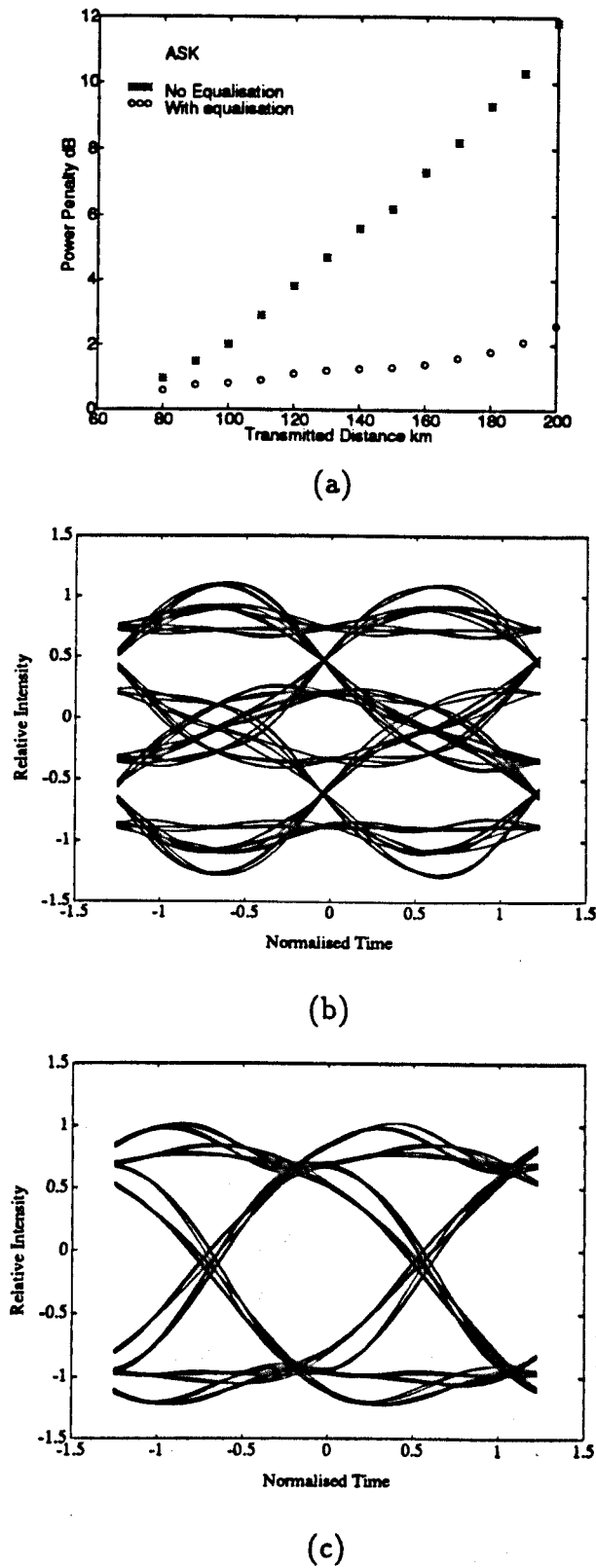


Figure 6.17: Performance assessment of the wideband equaliser at 8Gbit/s for an ASK system; a) dispersion power penalty with variation in distance, b) eye without equalisation at 200km and c) eye of equalised system at 200km

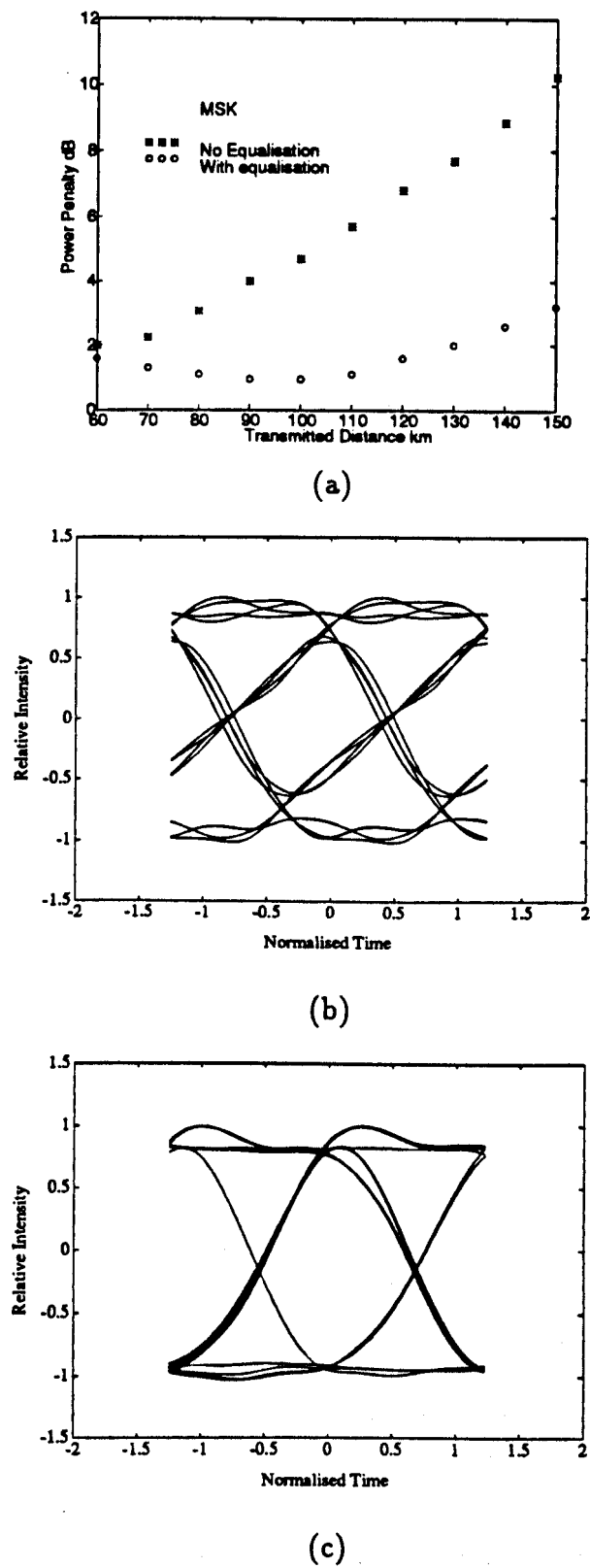


Figure 6.18: Performance assessment of the wideband equaliser at 8Gbit/s for a MSK system; a) dispersion power penalty with variation in distance, b) eye without equalisation at 100km and c) eye of equalised system at 100km

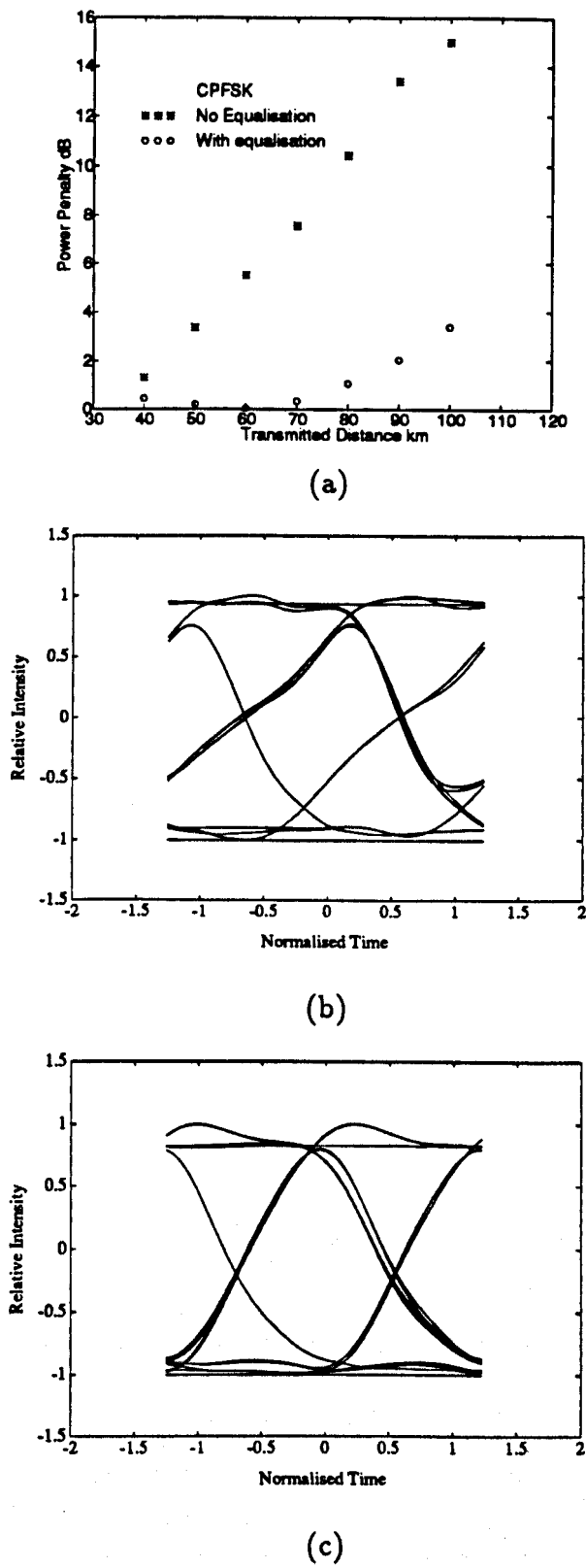


Figure 6.19: Performance assessment of the wideband equaliser at 8Gbit/s for a CPFSK system; a) dispersion power penalty with variation in distance, b) eye without equalisation at 50km and c) eye of equalised system at 50km

ISI. This illustrates the sensitivity of the non-linear modulation formats specifically to multigigabit signalling rates. For the more spectrally efficient MSK the signal can be recovered with the equaliser offering a reduction in the dispersion power penalty of up to 4dB at 100km. Better performance of the equaliser is attained for the linear ASK scheme. Even at a fibre span of 200km the improvement afforded by the equaliser is in excess of 9dB as shown in figure 6.17. The equalisers have shown the potential of correcting for fibre spans both greater and less than they were designed for (100km). Figure 6.18a illustrates this effect best, where optimum equalisation occurs at 100km. Fluctuations in the fibre length relative to the optimum fibre length lead to an increase in the equalised power penalty.

The performance of the single section equaliser may now be compared with that of the wideband cascaded staggered section equaliser. The comparison illustrates the improvement obtained with the wideband equaliser due to the additional bandwidth available and is shown in figure 6.20.

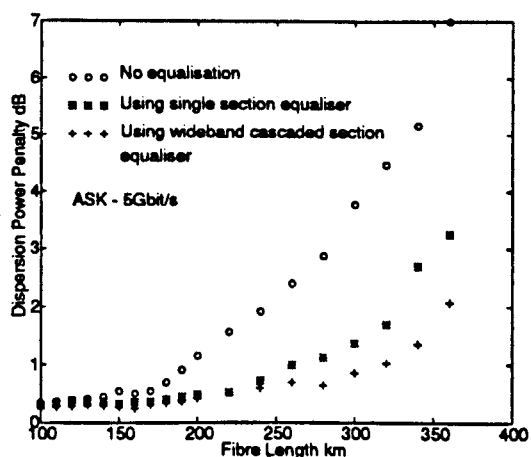


Figure 6.20: Comparison of performances between the single section equaliser and the cascaded staggered section wideband equaliser

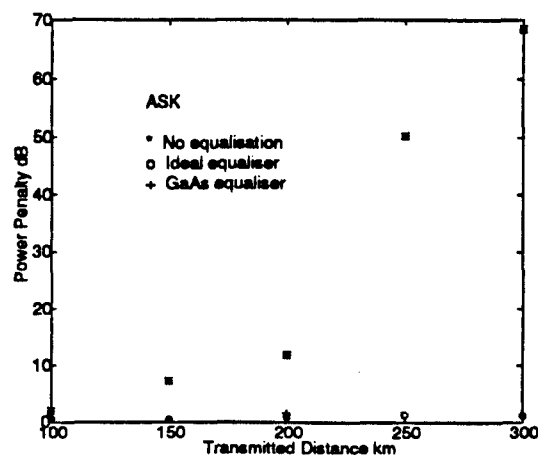
For a 5Gbit/s modulation rate the wideband equaliser offers an improvement over the single section equaliser of over 1dB at fibre spans in excess of 340km. At the lower fibre spans where the dispersion effects are limited the improvement offered by the equalisers is relatively small but at larger fibre spans becomes more pronounced as does the extent of the dispersion.

6.4.3 Performance of higher order equaliser

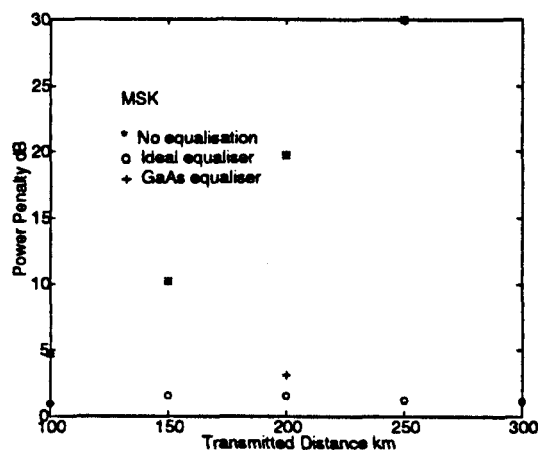
The performance of the four additional equalisers presented in section 6.21, designed to correct for larger fibre spans are evaluated here. The equalisers are designed to correct for 150, 200, 250 and 300km fibre spans and comprise of a cascade of 3, 3, 4 and 5 single sections respectively. The group delay characteristics of the equalisers are as those shown previously in figure 5.27. The equaliser designed to correct for the dispersion produced by 200km of fibre was realised on GaAs. The dispersion power penalty of these equalisers for the various modulated systems is presented in figure 6.21, together with the dispersion power penalty of the wideband equaliser discussed in the previous section. For the non-linear modulated systems the dispersion power penalty at large fibre spans degrades the system to such an extent that the eye opening is unrecognisable.

The equalisers perform very well for ASK modulated systems affording a very small corrected dispersion power penalty. For the non-linear modulation systems the equalisers make a dramatic improvement to the system performance, as in the case of ASK, however, there is a small remnant dispersion power penalty of $\approx 1\text{-}2\text{dB}$ for MSK and $\approx 3\text{-}6\text{dB}$ for CPFSK. Operating the wideband equaliser in systems of fibre spans other than 100km as demonstrated previously, has suggested that it can offer improvement for fibre lengths less than the design length (100km). In this way the higher order equalisers may be used to correct for fibre spans slightly less than they were designed for, to attain a better eye opening and thereby reduce the remnant dispersion power penalty, or alternatively a higher order equaliser could be designed to correct specifically a shorter fibre length. Of the four additional equalisers, the compensator designed to correct for the dispersion produced by a 200km fibre length was further realised on GaAs. The response of this equaliser is also compared to the ideal target in figure 6.21. The match in performance between the GaAs MMIC and the ideal equaliser (200km) is close. The least squares optimisation method was used in attaining the match between the GaAs MMIC equaliser and the target.

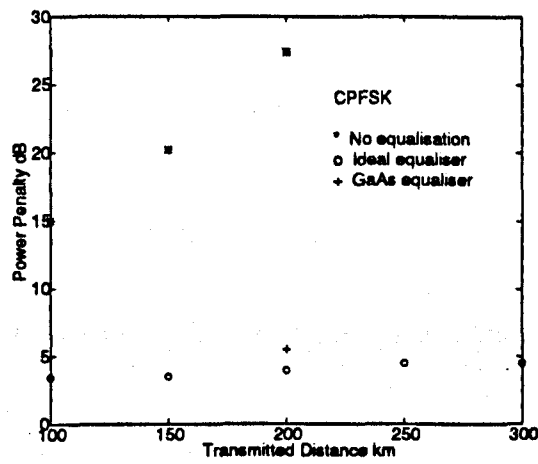
The ideal element higher order equalisers presented here can now be compared to the



(a)



(b)



(c)

Figure 6.21: Performance evaluation of the higher order equalisers

Fibre length (km)	Cascaded Staggered Section Power Penalty (dB)	Microstrip Equaliser Power Penalty (dB)
100	0.6	0.42
150	0.41	0.71
200	0.88	0.7
250	1.2	1.85
300	1.15	2.00

Table 6.3: Comparison in performance of microstrip and cascaded staggered section equaliser types

microstrip based equalisers. Table 6.3 draws a comparison between the two types of equalisation strategy for an ASK modulated system operating at 8Gbit/s. The microstrip line equaliser is altered in length appropriately depending on the fibre span. The microstrip line design is based on a RT/duroid substrate of permittivity $\epsilon_r = 10.5$ of height $h = 625\mu m$, while the actual line is of thickness $t = 35\mu m$ and width $w = 535.32\mu m$. The width is chosen such that the characteristic impedance of the line is $Z_o = 50\Omega$.

The larger fibre spans illustrate the equalisation capabilities of the cascaded staggered section equalisers as compared to the microstrip type. For the relatively smaller fibre spans (100-200km) both the equalisation strategies offer practically the same amount of improvement in the dispersion penalty. As the cascaded type equaliser is matched much more closely to the fibre group delay target over a larger linear range, it affords a better improvement in the dispersion power penalty than does the microstrip equaliser for the larger fibre spans, in addition to being physically smaller.

This work shows that application of GaAs MMIC equalisers to a practical systems will offer an instant benefit, either by extending the transmission distance or by affording an improvement in the dispersion power penalty.

6.4.4 Equalisation of chirped systems

To this stage all the results presented have been for chirp free systems. This has been a valid assumption as the modulators proposed and utilised in field demonstrations of coherent systems have been of the external type. That is to say that the laser is used as a continuous wave optical source and the message signal is modulated onto the optical carrier by means of loss or electro-optic intensity modulators for amplitude modulated systems. Operating in the continuous wave manner the laser cavity undergoes no intensity fluctuations and is therefore chirp free. The modulated message signal is not subject to any loss-induced patterning.

External modulators can introduce slight chirping in a similar manner to the laser diode due to the subtle variations in the refractive index of the modulator. By appropriate choice of modulator type the chirp may be eliminated [91, 94] or varied to achieve extended transmission distances by means of pulse compression. The bitrate distance products for chirped optical pulses have been illustrated in figure 3.1. The external modulator type most commonly used for intensity modulated systems is the Mach-Zehnder Interferometer type [90, 95, 96]. This modulator can be realised as essentially chirp free as both the guide arms of the interferometer are physically similar, with the propagation constants of the two arms changing by the same amount but of opposite polarity thereby eliminating phase modulation. When this "balanced" arrangement is not employed the chirp factor for the Mach-Zehnder modulator is expressed as [92]

$$\vartheta = \frac{\eta_1 + \eta_2}{\eta_1 - \eta_2} \quad (6.21)$$

where η_1 and η_2 is the index change per volt (including sign) for the Mach-Zehnder modulator arms. The modulator output instantaneous field is given by

$$E = E_o \cos \left(\frac{\pi V(t)}{2V_\pi} \right) \quad (6.22)$$

where $V(t)$ is the drive (modulating) voltage, V_{π} is the modulator switch voltage and E_o is the amplitude of the electric field at the input of the modulator. The instantaneous phase of the modulated output signal is given by

$$\varphi = \vartheta \frac{\pi V(t)}{4V_{\pi}} \tag{6.23}$$

Using the above model for the external modulator the performance of the wideband equaliser can be determined for a chirped system. Figure 6.22 illustrates the degradation caused by chirp limiting the maximum allowable transmission span for an ASK modulated system operating at a 5Gbit/s transmission rate. The dispersion limited transmission was chosen to be equivalent to that which resulted in a 2dB eye closure with the chirp factor limited to a range between ± 2 [94]. From the results in figure 6.22 it is apparent that the assumption made earlier ignoring the influence of the residual chirp from an external modulator was valid, as the profile of the dispersion limited transmission distance is practically flat for the range of values of chirp. Similarly this profile is replicated by the equalised output which is tolerant to the chirp affording an increment in the dispersion limited transmission span of nearly twice that obtained with no equalisation.

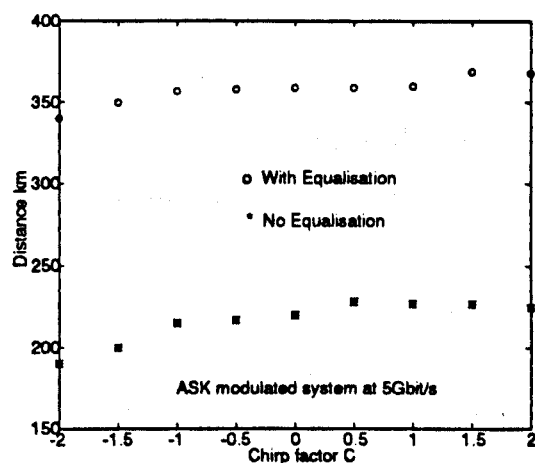


Figure 6.22: Equaliser performance for a chirped ASK system

6.5 Summary

This chapter has detailed the performance of the GaAs MMIC equalisers for systems employing both linear (ASK) and non-linear (MSK and CPFSK) modulation formats. The underlying principles behind the modulation and demodulation of these signal formats have also been outlined.

The performance of the equalisers devised in the previous chapter have been evaluated. The single section equaliser was evaluated for the various modulated systems at 5Gbit/s and showed a pronounced improvement in the eye. For the higher bit-rate transmission (8Gbit/s) the cascaded staggered section equaliser was used which again exhibited the potential of recovering the signal shape. The GaAs MMIC equalisers, having been designed to correct for a modest 100km fibre span were evaluated for transmission spans in excess of this distance. The equalisers have demonstrated their flexibility and robustness for the larger spans by affording marked improvements.

Higher order equalisers targeted specifically at correcting for the fibre chromatic dispersion produced by larger fibre spans have also been assessed. These have demonstrated a performance on a par with their microstrip counterparts.

The equalisers have been devised for transmission systems that have been assumed to be chirp free. The system implications of using the equalisers to correct for chirped ASK modulated transmission have also been investigated and this has shown the equaliser to be tolerant to the slight residual chirp from external modulators.

Chapter 7

Conclusions

The research presented in this thesis has addressed the issue of fibre chromatic dispersion and its implications for very high bit-rate transmission over long haul coherent heterodyne systems. Equalisation of the dispersion in the electrical domain has been previously reported using waveguide and microstrip structures. These structures have been physically large and consequently limited in their application to practical long haul systems. Here, variation of the microstrip parameters to optimise dispersion compensation has been explored, appropriate for intermediate length systems. A novel approach has been developed here based on GaAs MMIC technology and this has been used to realise very compact post detection electrical domain equalisers for correction of fibre dispersion.

7.1 Research Outcomes

The outcomes of this research programme fall into three main areas:

1. Microstrip technology.
2. GaAs MMIC equaliser realisation.
3. System implications with equalisation.

7.1.1 Microstrip Technology

There have been many reported models describing the dispersive characteristics of microstrip. Some of the more commonly used models were compared with each other and were found to deviate considerably as parameters were varied. All the models were compared with practical microstrip realisations and a model was identified that behaved in sympathy with the practical realisation. A model offering a good match with practical realisations over a large frequency range was found and all subsequent analyses of the microstrip equaliser group delay responses were based on this model.

The influences of the microstrip constituent material and physical geometry on the group delay characteristics of the equaliser were investigated such that the actual size of the equaliser might be reduced and the fibre span extended. All parameters were found to allow manipulation of the group delay characteristics, some more than others.

The implications for in-line transparent amplification on the tolerable residual delay dispersion were addressed and evaluated in terms of eye diagrams. Cascading individually optimised equalisers can be used to correct for a long haul link provided the microstrip parameters are chosen appropriately.

The main achievements in this area may be summarised as follows:

- Investigation of the microstrip dispersion models to obtain a good match with practical microstrip realisations.
 - The investigation of the influence of microstrip constituent material and physical geometry on the group delay characteristics of microstrip delay equaliser for application in long haul systems.
 - Evaluation of the system implications of the residual delay dispersion for transparent amplified systems.
-

7.1.2 GaAs MMIC Realisation

A novel approach to realising post detection equalisation was implemented using GaAs MMIC technology. A pseudo-lumped-element GaAs MMIC phase equalising network was realised offering an equalised bandwidth of 5GHz, correcting for the dispersion produced by 100km transmission over standard monomode fibre of 15-17ps/km-nm dispersion. The equaliser was derived from a simple second order all-pass lattice configuration transformed into a bridged-T single section network. The model of the equaliser was compared to the practical results showing very good agreement over a large frequency range for both the magnitude and group delay responses.

Equalisers with larger equalising bandwidths were devised and evaluated. These higher order networks were realised by cascading the single section networks each with staggered group delay characteristics.

The higher order equalisers have been shown to offer the possibility of equalising for larger fibre spans, thereby making them appropriate for application in long haul systems.

The main achievements in this area may be summarised as follows:

- Design and realisation of pseudo-lumped-element phase correcting networks on gallium arsenide.
 - Design and evaluation of higher order networks offering extended equalised bandwidth realised by means of cascading single sections.
 - Design and evaluation of higher order networks designed specifically for larger fibre spans.
-

7.1.3 System Implications of Equalisation

The GaAs MMIC equalisers were evaluated for application to transmission systems employing linear (ASK) and non-linear (MSK/CPFSK) modulation formats for high bit-rates. The single section and wideband cascaded staggered section equalisers offered marked improvement, more so with the non-linear schemes as these were shown to be degraded the most by dispersion. A comparison was effected between the single section and wideband cascaded staggered section equalisers.

The implications of using higher order GaAs MMIC equalisers to correct for a larger fibre span (200km) were assessed. All higher order equalisers offered marked improvements in the system performance stressing the instant improvement available with a heterodyne detection.

The robustness and flexibility of the equalisers were investigated by evaluating them for fibre spans greater than that for which they had been originally designed. The equalisers demonstrated resilience in degrading gracefully, satisfactorily correcting for the dispersion resulting from fibre spans three times greater than the original design.

The wideband equaliser was also evaluated for a mildly chirped system. The equaliser was tolerant to the small amount of chirp resulting from the slight mismatch in the Mach-Zehnder modulator arms.

GaAs MMIC equalisers offer the benefit of potential for full scale integration with receiver circuitry.

The main achievements in this area may then be summarised as follows:

- Evaluation of system implications of equalisation using linear and non-linear modulation formats for high bit-rates.
 - Evaluation of system implications using higher order equalisers designed for larger fibre spans.
-

- Determination of the robustness of the equalisers for extended fibre spans and mildly chirped systems.

7.2 Summary of Thesis

Chapter 2 reviewed coherent and direct detection systems, highlighting the advantages offered by the coherent schemes for future applications. The system device requirements were addressed and a comparison effected between homodyne and heterodyne systems. In the latter part of the chapter the issue of fibre chromatic dispersion was considered together with its implications for long haul systems.

The various approaches to equalisation of the fibre chromatic dispersion were noted and described in chapter 3. The methods fall into two broad categories; 1) optical domain equalisation - employing pre-detection strategies and 2) electrical domain equalisation - employing post-detection strategies. The optical domain strategies ranged from pre-chirping the laser diode at the transmitter to using etalon based equalisers prior to detection. The electrical domain equalisers, specifically relevant to heterodyne detection, due to the preservation of the phase with translation of the signal to the IF, were of the microstrip and waveguide types.

Chapter 4 extended the principle of microstrip equalisation further. The various documented models of microstrip dispersion characteristics were evaluated and compared with measurements of physical microstrip realisations to determine a model affording a good match with the practical results. This model was used for all further analyses reported in the thesis. The effects of varying the microstrip constituent material and physical geometry on the group delay characteristics were investigated. The chapter concluded by examining the system implications of the residual delay resulting from using cascaded microstrip sections to equalise for long haul transmission.

A new approach for realising fibre dispersion correcting networks was introduced in chapter 5, exploiting GaAs MMIC technology to realise pseudo-lumped-element equalis-

ers. A single section GaAs MMIC equaliser was designed and fabricated. Comparison of the practical responses with the theoretical prediction resulted in very good agreement, thereby validating the models defining the network. The equaliser offered an equalised bandwidth of 5GHz. Higher order equaliser networks were explored and designed by cascading the single section equalisers, each with a staggered group delay response. Wideband equalisers were designed in this manner ($\approx 10\text{GHz}$). Equalisers were also designed to correct for the fibre dispersion produced by larger fibre spans.

Chapter 6 is devoted to the system implications of equalisation. Linearly (ASK) and non-linearly (MSK/CPFSK) modulated systems were considered in evaluating the equaliser performance. Both the single section and the higher order wideband cascaded staggered section equalisers were used demonstrating a marked improvement in the dispersion power penalty. The performance of the single section equaliser was assessed for 5Gbit/s systems, where as the higher order equaliser performance was assessed for 8Gbit/s. The equalisers having been designed to correct for a given fibre length were examined for larger fibre lengths demonstrating their robustness and tolerance to variations in the fibre length. The equalisers designed specifically for larger fibre spans were evaluated demonstrating the potential of GaAs MMIC equalisers. The performance of the wideband cascaded staggered section equaliser was further assessed for a mildly chirped system, showing tolerance to slight chirp.

In conclusion, this research programme has addressed the issue of fibre chromatic dispersion and its implications for coherent systems including multi-section amplified links. As a novel alternative to the present equalisation methods we have devised, fabricated and demonstrated the effectiveness of GaAs MMIC fibre chromatic dispersion equalisers for application in heterodyne optical fibre systems, affording significant reductions in dispersion penalty of the detected signal at bit-rates of up to 8Gbit/s for a range of fibre lengths.

An important feature of this approach is that the use of GaAs MMIC technology allows dispersion compensation to be integrated, if desired, with other receiver electronics thereby providing a practicable and convenient solution to fibre group delay

equalisation in heterodyne optical communications. When applied to a practical system this equalisation strategy offers an instant benefit by reducing the dispersion power penalty, thereby allowing larger achievable transmission spans. Further to this, the results show that the fibre length for which the equaliser is designed does not have to be closely matched to the actual fibre length to offer significant improvement.

7.3 Suggestions for Further Work

There are further areas of research stemming from this research that are worthy of further investigation. These are summarised briefly here.

- The equalisers developed here are not adaptive but the possibility of using active GaAs inductors[97] may deserve consideration to achieve a degree of on-chip tuning.
 - The system implications of equalisation may usefully be investigated further considering, for example, optical sources of non-negligible linewidths, the influence of amplified spontaneous emission (ASE) for optically amplified systems and fibre non-linearities.
 - The applicability of dispersion equalised heterodyne systems to achieve “up-lift” of existing installed fibre links to single-span multigigabit/s operation deserves exploration in the light of the developments reported here. This is perhaps especially appropriate for unrepeatable submarine telecommunications.
 - The use of GaAs MMIC technology to effect approximate post detection compensation for dispersion in homodyne and direct detection systems could now valuably be explored.
-

References

- [1] S.Yamazaki, K.Fukuchi, T.Ono, and T.Ogata. 'Estimation on Maximum Transmission Distance for 2.5Gbit/s Coherent FDM Optical Repeater Systems'. *IEEE Photonics Technology Letters*, 5(5):534-536, 1993.
- [2] C.R.Batchellor, B.T.Debney, A.M.Thorley, T.J.B.Swanenburg, G.Heydt, F.Auracher, J.Patillon, and P.Lagasse. 'The RACE 1010 CMC Demonstrator'. In *Proceeding of EFOC/LAN '91, London*, pages 338-342, June 1991.
- [3] C.R.Batchellor, B.T.Debney, and A.M.Thorley. 'Coherent Multichannel Communications for High Capacity Reconfigurable Networks'. *GEC Journal of Research*, 10(2):73 - 79, 1993.
- [4] Y.Hayashi. 'Implementation of a Practical Coherent Trunk System'. In *OSA/IEEE Digest of Conference on Optical Fibre Communication, OFC'93*, pages 191 - 192, February 1993.
- [5] J.Winters, R.D.Gitlin, and S.Kasturia. 'Reducing the Effects of Transmission Impairments in Digital Fibre Optic Systems'. *IEEE Communications Magazine*, pages 68-76, June 1993.
- [6] T.L.Koch and U.Koren. 'Semiconductor Lasers for Coherent Optical Fibre Communications'. *IEEE Journal of Lightwave Technology*, 8(3):274 - 293, 1990.
- [7] T.Kimura. 'Coherent Optical Fibre Transmission'. *IEEE Journal of Lightwave Technology*, 5(4):414 - 428, 1987.
- [8] M.J.Creaner, R.C.Steele, G.R.Walker, N.G.Walker, J.Mellis, S.Al.Chalabi, I.Sturgess, M.Rutherford, J.Davidson, and M.C.Brain. 'Field Demonstration of

- 565 Mbit/s DPSK Coherent Transmission System Over 176 km of Installed Fibre'. *Electronic Letters*, 24(22):1354 – 1356, 1988.
- [9] T.Imai, Y.Hayashi, N.Ohkawa, T.Sugie, Y.Ichihashi, and T.Ito. 'Field Demonstration of 2.5 Gbit/s Coherent Optical Transmission Through Installed Submarine Fibre Cables'. *Electronic Letters*, 26(17):1407 – 1409, 1990.
- [10] J.R.Barry and E.A.Lee. 'Performance of Coherent Optical Receivers'. In *Proceedings of the IEEE*, pages 1369 – 1394, August 1990.
- [11] T.Okoshi and K.Kikuchi. *Coherent Optical Fibre Communications*. KTK Scientific Publishers, 1988.
- [12] N.A.Olsson. 'Semiconductor Optical Amplifiers'. In *Proceedings of the IEEE*, pages 375 – 382, March 1992.
- [13] M.J.N.Sibley. *Optical Communications*. Macmillan Education Ltd., 1990.
- [14] B.Wandernoth. '20 Photon/Bit 565 Mbit/s PSK Homodyne Receiver Using Synchronisation Bits'. *Electronic Letters*, 28(4):387 – 388, 1992.
- [15] M.Brain. 'Coherent Optical Networks'. *British Telecom Technology Journal*, 7(1):50 – 57, 1989.
- [16] J.M.Senior. *Optical Fibre Communications: Principles and Practice (Second edition)*. Prentice Hall, 1992.
- [17] E.Lichtman. 'Bit-Rate Distance Product Limitations Due to Fibre Nonlinearities in Multichannel Coherent Optical Communication Systems'. *Electronic Letters*, 27(9):757 – 759, 1991.
- [18] R.G.Waarts, A.A.Friesem, E.Lichtman, H.H.Yaffe, and R.P.Braun. 'Nonlinear Effects in Coherent Multichannel Transmission Through Optical Fibres'. In *Proceedings of the IEEE*, pages 1344 – 1368, August 1990.
- [19] A.R.Chraplyvy. 'Limitations on Lightwave Communications Imposed by Optical-Fibre Nonlinearities'. *IEEE Journal of Lightwave Technology*, 8(10):1548 – 1557, 1990.
-

- [20] L.G.Kazovsky, C.Barry, M.Hickey, C.A.Noronha (Jr), and P.Poggiolini. 'WDM Local Area Networks'. *IEEE Magazine of Lightwave Telecommunication Systems*, 3(2):8 - 15, 1992.
 - [21] H.Tsushima, S.Sasaki, K.Kuboki, S.Kitajima, R.Takeyari, and M.Okai. '1.244Gbit/s 32 Channel 121km Transmission Experiment Using Shelf-Mounted Continuous-Phase FSK Optical Heterodyne System'. *Electronic Letters*, 27(25):2336 - 2337, 1991.
 - [22] T.Lee. 'Recent Advances in Long-Wavelength Semiconductor Lasers for Optical Fibre Communication'. In *Proceedings of the IEEE*, pages 253 - 276, March 1991.
 - [23] K.Iwatsuki, H.Okamura, and M.Saruwatari. 'Wavelength-Tunable Single-Frequency and Single-Polarisation Er-Doped Fibre Ring-Laser With 1.4kHz Linewidth'. *Electronic Letters*, 26(24):2033 - 2035, 1990.
 - [24] W.B.Sessa, R.E.Wagner, and P.C.LI. 'Frequency Stability of DFB Lasers Used in FDM Multi-Location Networks'. In *OSA/IEEE Digest of Conference on Optical Fibre Communication, OFC'92*, pages 202 - 203, February 1992.
 - [25] G.P.Agrawal and N.K.Dutta. *Long-Wavelength Semiconductor Lasers*. Van Nostrand Reinhold Co. Inc., 1986.
 - [26] H.Bissessur, C.Starck, J.Y.Emery, F.Pommereau, C.Duchemin, J.G.Provost, J.L.Beylat, and B.Fernier. 'Very Narrow-Linewidth (70kHz) 1.55 μ m Strained MQW DFB Laser'. *Electronic Letters*, 28(11):998 - 999, 1992.
 - [27] T.Kunii, Y.Matsui, H.Horikawa, T.Kamijoh, and T.Nonaka. 'Narrow Linewidth (85kHz) operation in Long Cavity 1.55 μ m MQW DBR Laser'. *Electronic Letters*, 27(9):691 - 692, 1991.
 - [28] R.Wyatt and W.J.Devlin. '10kHz Linewidth 1.5 μ m InGaAsP External Cavity Laser With 55nm Tuning Range'. *Electronic Letters*, 19(3):110 - 112, 1983.
 - [29] S.P.Smith, F.Zarinetchi, and S.Ezekiel. 'Narrow-Linewidth Stimulated Brillouin Fibre Laser and Applications'. *Optics Letters*, 16(6):393 - 395, 1991.
-

- [30] C.Rolland, L.E.Tarof, and A.Somani. 'Multigigabit Networks: The Challenge'. *IEEE Magazine of Lightwave Telecommunication Systems*, 3(2):16 – 26, 1992.
 - [31] I.Garrett and G.Jacobsen. 'Theoretical Analysis of Heterodyne Optical Receivers for Transmission Systems Using (Semiconductor) Lasers of Nonnegligible linewidth'. *IEEE Journal of Lightwave Technology*, LT-4(3):323 – 334, 1986.
 - [32] L.G.Kazovsky, R.Welter, A.F.Elrefaie, and W.Sessa. 'Wide-Linewidth Phase Diversity Homodyne Receivers'. *IEEE Journal of Lightwave Technology*, 6(10):1527 – 1536, 1988.
 - [33] I.Garrett, G.Jacobsen, E.Bodtker, R.J.S.Pedersen, and J.X.Kan. 'Weakly Coherent Optical Systems Using Lasers With Significant Phase Noise'. *IEEE Journal of Lightwave Technology*, 6(10):1520 – 1526, 1988.
 - [34] S.H.Rumbaugh, M.D.Jones, and L.W.Carlson. 'Polarisation Control for Coherent Fibre-Optic Systems Using Nematic Liquid Crystals'. *IEEE Journal of Lightwave Technology*, 8(3):459 – 465, 1990.
 - [35] N.G.Walker and G.R.Walker. 'Polarisation Control for Coherent Communications'. *IEEE Journal of Lightwave Technology*, 8(3):438 – 458, 1990.
 - [36] R.Noé, H.J.Rodler, A.Ebberg, G.Gaukel, B.Noll, J.Wittmann, and F.Auracher. 'Comparison of Polarisation Handling Methods in Coherent Optical Systems'. *IEEE Journal of Lightwave Technology*, 9(10):1353 – 1366, 1991.
 - [37] L.G.Kazovsky. 'Phase and Polarisation-Diversity Coherent Optical Techniques'. *IEEE Journal of Lightwave Technology*, 7(2):279 – 292, 1989.
 - [38] R.J.Hoss. *Fibre Optic Communications Design Handbook*. Prentice-Hall, 1990.
 - [39] P.S.Henry. 'Lightwave Primer'. *IEEE Journal of Quantum Electronics*, 21(12):1862 – 1879, 1985.
 - [40] A.F.Elrefaie, R.E.Wagner, D.A.Atlas, and D.G.Daut. 'Chromatic Dispersion Limitations in Coherent Lightwave Transmission Systems'. *IEEE Journal of Lightwave Technology*, 6(5):704 – 709, 1988.
-

- [41] K.Iwashita and N.Takachio. 'Chromatic Dispersion Compensation in Coherent Optical Communications'. *IEEE Journal of Lightwave Technology*, 8(3):367 - 375, 1990.
 - [42] G.P.Agrawal. *Nonlinear Fibre Optics*. Academic Press, Inc., 1989.
 - [43] K.Iwashita, K.Nakagawa, Y.Nakano, and Y.Suzuki. 'Chirp Pulse Transmission Through A Single-Mode Fibre'. *Electronic Letters*, 18(20):873 - 874, 1982.
 - [44] T.Saito, N.Henmi, S.Fujita, M.Yamaguchi, and M.Shikada. 'Prechirp Technique for Dispersion Compensation for a High-Speed Long-Span Transmission'. *IEEE Photonics Technology Letters*, 3(1):74 - 76, 1991.
 - [45] N.Henmi, T.Saito, M.Yamaguchi, and S.Fujita. '10Gbit/s, 100km Normal Fibre Transmission Experiment Employing a Modified Prechirp Technique'. In *OSA/IEEE Digest of Conference on Optical Fibre Communication, OFC'91*, page 54, February 1991.
 - [46] T.L.Koch and R.C.Alferness. 'Dispersion Compensation by Active Predistorted Signal Synthesis'. *IEEE Journal of Lightwave Technology*, 3(4):800 - 805, 1985.
 - [47] A.D.Ellis, S.J.Pycock, D.A.Cleland, and C.H.F.Sturrock. 'Dispersion Compensation in 450km Transmission System Employing Standard Fibre'. *Electronic Letters*, 28(10):954 - 955, 1992.
 - [48] L.Mollenauer. 'Solitons: The Future of Fibre Communications'. *Physics World*, pages 29 - 32, 1989.
 - [49] D.Marcuse. 'An Alternative Derivation of The Gordon-Haus Effect'. *IEEE Journal of Lightwave Technology*, 10(2):273 - 278, 1992.
 - [50] L.Mollenauer, E.Lichtman, G.T.Harvet, M.J.Neubelt, and B.M.Nyman. 'Demonstration of Error Free Soliton Transmission Over More Than 15,000km at 5Gbit/s, Single-Channel, and Over 11,000km at 10Gbit/s in a Two-Channel WDM'. In *OSA/IEEE Conference on Optical Fibre Communication (Postdeadline Papers)*, OFC'92, pages 351 - 354, February 1992.
-

- [51] M.Nakazawa, K.Suzuki, H.Kubota, and Y.Kimura. '10Gbit/s - 1200km Single-Pass Soliton Data Transmission Using Erbium-Doped Fibre Amplifiers'. In *OSA/IEEE Conference on Optical Fibre Communication (Postdeadline Papers)*, OFC'92, pages 355 - 358, February 1992.
 - [52] J.M.Dugan, A.J.Price, M.Ramadan, D.L.Wolf, E.F.Murphy, A.J.Antos, D.K.Smith, and D.W.Hall. 'All-Optical, Fibre-Based 1550nm Dispersion Compensation in a 10 Gbit/s, 150 km Transmission Experiment over 1310nm Optimised Fibre'. In *OSA/IEEE Conference on Optical Fibre Communication (Postdeadline Papers)*, OFC'92, pages 367 - 370, February 1992.
 - [53] C.D.Poole, K.T.Nelson, J.M.Wiesenfeld, and A.R.McCormick. 'Broad-band dispersion compensation using the higher-order spatial-mode in a two-mode fibre'. In *OSA/IEEE Conference on Optical Fibre Communication (Postdeadline Papers)*, OFC'92, pages 363 - 366, February 1992.
 - [54] C.D.Poole, C.D.Townsend, and K.T.Nelson. 'Helical-Grating Two-Mode Fibre Spatial-Mode Coupler'. *IEEE Journal of Lightwave Technology*, 9(5):598 - 604, 1991.
 - [55] A.W.Snyder and J.D.Love. *Optical Waveguide Theory*. Chapman and Hall, 1983.
 - [56] N.A.Olsson, G.P.Agrawal, and K.W.Weht. '16Gbit/s, 70km Pulse Transmission by Simultaneous Dispersion and Loss Compensation with 1.5 μ m Optical Amplifiers'. *Electronic Letters*, 25(9):603 - 605, 1993.
 - [57] P.Cochrane. 'Future Directions in Long Haul Fibre Optic Systems'. *British Telecom Technical Journal*, 8(2), April 1990.
 - [58] B.Wedding. 'New Method for Optical Transmission Beyond Dispersion Limit'. *Electronic Letters*, 28(14):1298 - 1300, 1992.
 - [59] L.J.Cimini, L.J.Greenstein, and A.A.M.Saleh. 'Optical Equalisation for High-Bit-Rate Fibre-Optic Communications'. *IEEE Photonics Technology Letters*, 2(3):200-202, 1990.
-

- [60] L.J.Cimini, L.J.Greenstein, and A.A.M.Saleh. 'Optical Equalisation to Combat The Effects of Laser Chirp and Fibre Dispersion'. *IEEE Journal of Lightwave Technology*, 8(5):649-659, 1990.
 - [61] A.H.Gnauck, L.J.Cimini (Jr), J.Stone, and L.W.Stulz. 'Optical Equalisation of Fibre Chromatic Dispersion in a 5Gbit/s Transmission System'. *IEEE Photonics Technology Letters*, 2(8):585-587, 1990.
 - [62] A.H.Gnauck, C.R.Giles, L.J.Cimini (Jr), J.Stone, L.W.Stulz, S.K.Korotky, and J.J.Veseka. '8Gbit/s - 130km Transmission Experiment Using Er-Doped Fibre Preamplifier and Optical Dispersion Equalisation'. *IEEE Photonics Technology Letters*, 3(12):1147-1149, 1991.
 - [63] J.Winters. 'Equalisation in Coherent Lightwave Systems Using Microwave Waveguides'. *IEEE Journal of Lightwave Technology*, 7(5):813 - 815, 1989.
 - [64] P.J.Tu. 'A Computer-Aided Design of a Microwave Delay Equaliser'. *IEEE Trans. on Microwave Theory Tech.*, MTT-17(8):626 - 634, 1969.
 - [65] G.L.Matthaei, L.Young, and E.M.T.Jones. *Microwave Filters, Impedance-Matching Networks and Coupling Structures*. McGraw-Hill, 1964.
 - [66] J.Winters and R.D.Gitlin. 'Electrical Signal processing Techniques in Long Haul Fibre Optic Systems'. *IEEE Trans. on Communications*, 38(9):1439 - 1453, 1990.
 - [67] J.Nakagawa and T.Okoshi. 'Precise Compensation of Fibre Group-Delay in Coherent Optical Fibre Communications'. In *SPIE - Int. Symp. OE/Fibres*, September 1992.
 - [68] T.C.Edwards. *Foundations for Microstrip Circuit Design*. John Wiley & Sons Ltd., 1988.
 - [69] R.K.Hoffmann. *Handbook of Microwave Integrated Circuits*. Artech House Inc., 1987.
 - [70] H.A.Wheeler. 'Transmission-Line Properties of a Strip on a Dielectric Sheet on a Plane'. *IEEE Trans. on Microwave Theory Tech.*, MTT-25(8):631 - 647, 1977.
-

- [71] E.Hammerstad and O.Jensen. 'Accurate Models for Microstrip Computer-Aided Design'. *IEEE MTT-S Int. Microwave Symp. Digest*, pages 407 – 409, 1980.
 - [72] W.J.Getsinger. 'Microstrip Dispersion Model'. *IEEE Trans. on Microwave Theory Tech.*, MTT-21(1):34 – 39, 1973.
 - [73] H.J.Carlin. 'A Simplified Circuit Model for Microstrip'. *IEEE Trans. on Microwave Theory Tech.*, MTT-21(9):589 – 591, 1973.
 - [74] E.Yamashita, K.Atsumi, and T.Hirahata. 'Microstrip Dispersion in a Wide-Frequency Range'. *IEEE Trans. on Microwave Theory Tech.*, MTT-29(6):610 – 611, 1981.
 - [75] M.Kirschning and R.H.Jansen. 'Accurate Model for Effective Dielectric Constant of Microstrip with Validity up to Millimetre-Wave Frequencies'. *Electronic Letters*, 18(6):272 – 273, 1982.
 - [76] J.L.Medina, A.Serrano, and F.J.Mendieta. 'Microstrip Effective Dielectric Constant Measurement and Test of CAD Models up to 20GHz'. *Microwave Journal*, 35(3):82–93, 1993.
 - [77] J.J.O'Reilly and M.S.Chaudhry. 'Microstrip Compensation of Fibre Chromatic Dispersion in Optically Amplified Coherent Systems'. In *IEE Colloquium on Microwave Optoelectronics*, November 1990.
 - [78] E.H.Fooks and R.A.Zakarevičius. *Microwave Engineering Using Microstrip Circuits*. Prentice Hall, 1990.
 - [79] A.Bar-Lev. *Semiconductors and Electronic Devices*. Prentice-Hall, 1984.
 - [80] A.B.Williams and F.J.Taylor. *Electronic Filter Design Handbook*. McGraw-Hill, 1988.
 - [81] F.Kuo. *Network Analysis and Synthesis*. John Wiley & Sons Ltd., 1966.
 - [82] J.E.Storer. *Passive Network Synthesis*. McGraw-Hill, 1957.
-

- [83] A.Mateescu. 'Phase Corrector Circuit Computation by a Graphical- Analytical Method'. *Telecommunicatii (Rumania)*, 10(7):312 – 317, 1966.
 - [84] M.W.Medley. *Microwave and RF Circuits: Analysis, Synthesis and Design*. Artech House, 1993.
 - [85] Z.Hajoč. 'The Design of Delay Lines With The Aid of All-pass Networks'. *Slaboproudý Obz. (Czechoslovakia)*, 45(2):59 – 65, 1984.
 - [86] M.S.Chaudhry and J.J.O'Reilly. 'Chromatic Dispersion Compensation in Heterodyne Optical Systems Using Monolithic Microwave Integrated Circuits'. In *OSA/IEEE Digest of Conference on Optical Fibre Communication, OFC'92*, page 179, February 1992.
 - [87] M.S.Chaudhry and J.J.O'Reilly. 'Equalisation of Fibre Chromatic Dispersion for Very High Bit Rate Transmission Using Monolithic Microwave Integrated Circuits'. In *OSA/IEEE Digest of Conference on Optical Fibre Communication, OFC'93*, pages 132–133, February 1993.
 - [88] S.Pasupathy. 'Minimum Shift Keying: A Spectrally Efficient Modulation'. *IEEE Communications Magazine*, pages 14 – 22, July 1979.
 - [89] J.Proakis. *Digital Communications*. McGraw-Hill, 1983.
 - [90] T.Namiki, N.Mekada, H.Hamano, T.Yamane, M.Seino, and H.Nakajima. 'Low-Drive-Voltage TiLiNbO_3 Mach-Zehnder Modulator Using a Coupled Line'. In *OSA/IEEE Digest of Conference on Optical Fibre Communication, OFC'90*, page 34, 1990.
 - [91] F.Koyama and K.Iga. 'Frequency Chirping in External Modulators'. *IEEE Journal of Lightwave Technology*, 6(1):87 – 93, 1988.
 - [92] A.Djupsjobacka. 'Residual Chirp in Integrated-Optic Modulators'. *IEEE Photonics Technology Letters*, 4(1):41 – 43, 1992.
-

- [93] K.Iwashita, T.Matsumoto, C.Tanaka, and G.Motosugi. 'Linewidth Requirement Evaluation and 290km Transmission Experiment for Optical CPFSK Differential Detection'. *Electronic Letters*, 22(15):791 – 792, 1986.
 - [94] F.Koyama and K.Iga. 'Frequency Chirping of External Modulation and its Reduction'. *Electronic Letters*, 21(23):1065 – 1066, 1985.
 - [95] H.Ohta, H.Miyamoto, K.Tabuse, and Y.Miyagawa. 'TiLiNbO₃ Mach-Zehnder Modulator Using a Burried Travelling Wave Electrode'. In *OSA/IEEE Digest of Conference on Optical Fibre Communication, OFC'90*, page 222, 1990.
 - [96] H.Sano, H.Inoue, S.Tsuji, and K.Ishida. 'InGaAs/InAlAs MQW Mach-Zehnder Optical Modulator for 10Gbit/s Long-Haul Transmission Systems'. In *OSA/IEEE Digest of Conference on Optical Fibre Communication, OFC'90*, page 223, 1990.
 - [97] C.J.Gulliford. *Implementation and Design of GaAs Active Inductor MMIC*. M. Sc. Thesis, University of Wales, Bangor, 1993.
-